


Master Thesis

# Gas flow behaviour in the deep lung under high-frequency jet ventilation and high frequency oscillation

carried out for the purpose of obtaining the degree of

Master of Science (MSc or Dipl.-Ing. or DI)

submitted at TU Wien, Faculty of Mechanical and Industrial Engineering, by

Veronika Lederer

Mat.Nr.: 01027722

under the supervision of

Univ.-Doz. Univ. Lektor Dr.med. Alexander Aloy

in cooperation with

Privatdoz. Dipl.-Ing. Dr.techn. Christoph Reichl

Institute of Fluid Mechanics and Heat Transfer

Vienna, 21.6.2022

TECHNISCHE UNIVERSITÄT WIEN

*Affidavit*

I declare in lieu of oath, that I wrote this thesis and performed the associated research myself, using only literature cited in this volume. If text passages from sources are used literally, they are marked as such.

I confirm that this work is original and has not been submitted elsewhere for any examination, nor is it currently under consideration for a thesis elsewhere.

I acknowledge that the submitted work will be checked electronically-technically using suitable and state-of-the-art means (plagiarism detection software). On the one hand, this ensures that the submitted work was prepared according to the high-quality standards within the applicable rules to ensure good scientific practice "Code of Conduct" at the TU Wien. On the other hand, a comparison with other student theses avoids violations of my personal copyright.

*City and Date* *Signature*

# Danksagung

Zu allererst möchte ich mich bei meinen beiden Betreuern für die Zeit und Geduld bedanken, mich in die Welt der maschinellen Beatmung und Strömungssimulation einzuführen. Bei Alexander Aloy, dass du trotz turbulenten Zeiten unser Projekt weiter vorangetrieben hast und für deine ansteckende Passion für die Erforschung der Vorgänge in der Lunge. Sowie bei Christoph Reichl, für die viele Unterstützung bei der technischen Realisation dieser Arbeit. Besonders dafür, dass ich mich jederzeit an dich wenden konnte, wenn ich nicht mehr weitergekommen bin.

Einen großer Dank gebührt auch meiner Familie, die mich immer wieder während der gesamten Studienzeit aufgebaut und an mich geglaubt haben. Sie haben mich in vielerlei Hinsicht bis zum Schluss unterstützt. Leider können nicht mehr alle diesen Abschluss mit mir feiern.

Auch meine Freunde dürfen nicht unerwähnt bleiben. Sie haben sich immer wieder meinen Problemen angenommen und gemeinsam an einer Lösung gearbeitet.

Des Weiteren möchte ich mich auch bei all meinen Studienkollegen und Studienkolleginnen in den vielen Jahren bedanken. Die gemeinsame Lernzeit, Zusammenarbeit, Diskussionen und vielen Erklärungen haben viel dazu beigetragen, dass ich dieses Studium nun erfolgreich absolvieren konnte.

Der abschließende Dank gilt meiner Chefin sowie meinen Arbeitskolleginnen und -kollegen, dafür dass sie mir für mein Studium immer den Rücken frei gehalten haben.

Vielen Dank euch allen!

# Abstract

Although superimposed high-frequency jet ventilation, SHFJV for short, has already achieved good clinical success, there has been little theoretical work on the method and no simulations have yet been performed using computational fluid dynamic simulations. SHFJV is an electrically controlled ventilation method in which a high-frequency gas flow is superimposed on a low-frequency gas flow. This creates a low-pressure plateau in addition to a high-pressure plateau, resulting in continuous delivery of small volumes of gas to the lungs during ventilation. Clinical studies have shown that this method leads to a faster recruitment of collapsed alveoli, thus improving patient oxygenation.

In this work, a user-defined function (UDF) was created to control the application of ventilator-generated gas at the inlet. At the same time, a second function was used to mimic the physiological characteristics of the lungs, which allowed the gas flows in the lungs to be influenced. To calculate the flow patterns, the commercial software Fluent from ANSYS Inc. was used, and the Menter-SST-k-$\omega$ model was used as the turbulence model. An important part of working with simulation analysis is the validation of the system. Especially the functions that were programmed in the UDF had to be created and verified in single steps. The main simulations were performed on several symmetric single bifurcation geometries with a different number of lung tubes, allowing a progression of results along these so-called generations and estimating magnitudes for deeper lung regions.
For comparison, the ventilation with a high-frequency oscillating ventilator was additionally mimicked, which has already been studied by many research groups. Parameters such as the Womersley number and the tidal volume served as basis.

# Kurzfassung

Obwohl die überlagerte Hochfrequenzjetbeatmung, kurz SHFJV, bereits einen guten klinischen Erfolg verzeichnet, gibt es zu der Methode nur wenige theoretische Arbeiten und es wurden bisher auch keine Simulationen mittels nummerischer Strömungsmechanik durchgeführt. Bei der SHFJV handelt es sich um eine elektrisch kontrollierte Beatmungmethode bei der ein niederfrequenter Gasstrom von einem hochfrequenten Gasstrom überlagert wird. Dadurch entsteht zusätzlich zu einem Hochdruckplateau auch ein Niederdruckplateau, wodurch kontinuierlich kleine Gasvolumina während der Beatmung in die Lunge appliziert werden. Klinische Studien haben gezeigt, dass dieser Vorgang zu einer schnelleren Rekrutierung von kollabierten Lungenbläschen führt und damit die Oxygenierung bei Patienten verbessert wird.

In dieser Arbeit wurde in einer benutzerdefinierte Funktion (UDF) eine Funktion erstellt, welche die Zufuhr des vom Beatmungsgerät erzeugten Gases am Einlass vorgibt. Gleichzeitig wurde mit einer zweiten Funktion die physiologischen Eigenschaften der Lunge nachgestellt, wodurch die Strömungen in der Lunge beeinflusst werden konnten. Um die Strömungsverläufe zu berechnen, wurde mit der kommerziellen Software Fluent von ANSYS Inc. gearbeitet. Das Menter-SST-k-$\omega$ Modell kam dabei als Turbulenzmodell zum Einsatz. Ein wichtiger Teil bei der Arbeit mit Simulationsanalysen ist die Validierung des Systems. Vor allem die Funktionen, die in der UDF programmiert wurden, mussten in einzelnen Schritten erstellt und kontrolliert werden. Die Hauptsimulationen wurden an mehreren symmetrischen Einzelverzweigungsgeometrien mit einer unterschiedlichen Anzahl an Lungenröhren durchgeführt, wodurch ein Verlauf der Ergebnisse entlang dieser sogenannten Generationen ermöglicht wurde und Größenordnungen für tiefere Lungenbereiche geschätzt werden konnten.
Zum Vergleich wurde zusätzlich die Beatmung mit einem Hochfrequenzoszillationsventilator nachgestellt, welche bereits von vielen Forschungsgruppen untersucht wurde. Parameter wie zum Beispiel die Womersley Zahl und das Tidalvolumen dienten dabei als Grundlage.

# List of Figures

# List of Tables

# Nomenclature

### Abbreviations

| | |
|---|---|
| ARDS | acute respiratory distress syndrome |
| BIPAP | Biphasic Positive Airway Pressure |
| CFD | Computational Fluid Dynamics |
| CHFJV | Combined High Frequency Jet Ventilation |
| CMV | Controlled Mechanical Ventilation |
| E | Expiration |
| FDM | Finite Difference Method |
| FEM | Finite Element Method |
| FVM | Finite Volume Method |
| HF | High Frequency |
| HFJV | High Frequency Jet Ventilation |
| HFOV | High Frequency Oscillation Ventilation |
| HFPV | High Frequency Percussive Ventilation |
| I | Inspiration |
| LF | Low Frequency |
| MAP | Mean Airway Pressure |
| PCV | Pressure Controlled Ventilation |
| PEEP | Positive End Expiatory Pressure |
| SHFJV | Super imposed High Frequency Jet Ventilation |
| ts | Time step |
| UDF | User Defined Function |
| VCV | Volume Controlled Ventilation |
| z | Generation |

### Greek Symbols

| | | |
|---|---|---|
| $\alpha$ | Womersley number | |
| $\Delta$ | Delta | |
| $\eta$ | Dynamic viscosity | kg/ms |
| $\nu$ | Kinematic viscosity | $m^2/s$ |
| $\rho$ | Density | $kg/m^3$ |

### Latin Symbols

| | | |
|---|---|---|
| $\dot{m}$ | Mass Flow Rate | kg/s |
| $\dot{V}$ | Volume Flow | $m^3/s$ |

| | | |
|---|---|---|
| $A$ | Area | $m^2$ |
| $d$ | Diameter | $m$ |
| $d'_0$ | Diameter at Origin | $m$ |
| $E$ | Energy | J |
| $f$ | Factor | |
| $f$ | Frequency | Hz |
| $m$ | Mass | kg |
| $n$ | Number of Elements | |
| $p$ | Pressure | Pa |
| $Re$ | Reynolds number | 1 |
| $V$ | Volume | L |
| $V$ | Volume | $m^3$ |
| $v$ | Velocity | m/s |
| $z$ | Generation | |

**Subscripts**

| | |
|---|---|
| f | Fluid |
| in | Inlet |
| kin | Kinetic |
| max | Maximum |
| out | Outlet |
| T | Tidal |
| t | Tube |
| u | Units |

# Contents

# 1 Introduction

In everyday clinical practice, there are often situations in which patients have to be ventilated mechanically. There are two options for this: with negative or positive pressure. Negative pressure therapy achieved good clinical results, but this device was not able to establish itself due to limited handling with patients. [1] For positive pressure therapy, on the other hand, there is now a wide range of different ventilation devices available. Important parameters for mechanical ventilation are the ratio of inspiratory to expiratory (I:E) time, plateau pressure, positive end-expiratory pressure (PEEP), and mean airway pressure as well as peak pressure for some techniques. From the lungs side, compliance and airway resistance also have an important influence. [2] In addition to conventional methods, high-frequency ventilation techniques (HFJV), like superimposed high-frequency jet ventilation (SHFJV), are applied. [3] While in conventional mechanical ventilation (CMV) the applied inspiratory volume is usually 10-15 mL/kg, in HFJV it is only 1-3 mL/kg. The ventilation frequency also differs greatly between the two techniques from 0.2-0.4 Hz for CMV and 1-15 Hz for HFJV. [2, 3] In SHFJV, both low and high frequencies are combined and applied simultaneously. [4]
To understand how ventilators perform, clinical studies are conducted on patients or animals and, whenever possible, experimental measurements are taken. However, these experiments are very limited due to the small tubes in the lungs and the sensitivity to higher frequencies.

For the investigation of fluid mechanics, computational fluid dynamics has been developed over the last 50 years. In the meantime, this method is being used in many engineering fields. [5] The use for the medical field established itself only in the last years. Due to the complexity of real medical devices, the models are presented in a relatively simple and idealized form. [6]
In general, the problems in the engineering field can be divided into two areas: the calculation of flow-around problems and the calculation of flow-through problems. The simulation of gas flows in the lung is a flow-through problem. [7] Apart from the fact that not all flows can be analyzed experimentally, there are other reasons that make CFD so popular. For one thing, the costs are usually much lower, they are faster to

perform than experimental analyses, and for another, solutions are found for complex problems that would otherwise not be possible. [5]
Since the analytical solution is often not known, the basic equations of the fluid mechanics problem are solved in CFD programs using suitable numerical methods. Consequently, the results of a CFD simulation is an approximation and must be questioned and verified. [5, 8]

## 1.1 Task

The superimposed high-frequency jet ventilator is already used in clinics, but there have been few theoretical and no computational fluid dynamic studies on it. The aim of this thesis is to reconstruct the airflow generated by the ventilation device and create multiple symmetrical single bifurcation models of the lung with up to eight generations. Special attention is given to the physiological characteristics of the lung in terms of compliance and capacity of the air volume.
Subsequently, the gas flow entering the lungs is calculated using computational fluid dynamics. In addition, the flow behavior in deeper lung regions is estimated using the different geometry sizes and the resulting kinetic energy is calculated. I have already written a project paper on part of this work and some basic passages overlap or coincide.

# 2 Theoretical background

## 2.1 Respiratory system

The respiratory system can be divided into the upper and lower respiratory tract. The upper respiratory tract includes the pharynx, oral cavity and larynx. [9] The trachea and lungs form the lower parts. [10] In the course of this thesis, only the lower area will be considered further.

A cycle of spontaneous respiration, consists of two processes: inhalation and exhalation. One of the ways the thorax expands, during inhalation, is by pulling the diaphragm toward the abdominal cavity. This increases the volume of the inside of the lungs and creates a negative pressure in the lungs that draws air in through the airways. In general, air always flows from the point of higher pressure to the one of lower pressure. [3, 10, 11] During exhalation, the opposite effect occurs. The volume of the lungs is reduced by relaxation of the thorax, in part by the restoring force of the tissue. This creates excess pressure in the lungs and the air is expelled. [3, 10] The total capacity of the lung air volume is 6 liters. Of this, approximately 0.5 L is exchanged per breath. During deep breaths, 2.5 L can be inhaled and 1.5 L exhaled. Approximately 1.5 L of air remains in the lungs as residual volume. [3]
One attribute that strongly influences this cycle is the ease with which the lung expands and contracts. This is often altered by disease. [10]

### 2.1.1 Geometry of the lung

The detailed structural studies of the lung dates back to an article by Weibel and Gomez [12], who contributed significantly to the understanding of airflow in the lungs. This work is still considered a benchmark for research used today.
The lungs consist of a system of tubes, also called the bronchial system or bronchial tree, through which the air flows. These airways are divided into generations, which form a new generation by the branching of the bronchi into two smaller bronchi. There

are 23 generations up to the alveoli, the smallest unit in the bronchial system. The first and largest generation (gen 0) is formed by the trachea, a single tube at the beginning of the system. After that the tubes for each generation become smaller and smaller. [10]

Weibel and Gomez [12] presented the following equations in their paper. Over the generations (z) the number of elements (n) increases according to the formula 1.

$$n(z) = 2^z \tag{1}$$

Up to the tenth generation, the diameters (d) can be calculated using the formula 2, where $d'_0$ is the diameter at the origin. After that the diameter decreases much more. The diameter is the most important parameter related to the respiratory flow. [10]

$$d(z) = d'_0 * 2^{-z/3} \tag{2}$$

Although the trachea is the longest tube with the largest diameter, it has the smallest total cross-sectional area at 3 $cm^2$. According to Weibel, a healthy lung consists of 300 million alveoli and, according to newer calculations, they have a total surface area of 140 $m^2$. Consequently, the total cross-sectional area increases very strongly in the course of the generations. Due to the many branching, the velocity of incoming air in the airways decreases dramatically and almost comes to a standstill. Thus, it can be said that the bronchi have more of an air-conducting function between generation 0 and 16. While between generation 17 to 23 a respiratory zone is present. [10, 12, 13]

As can be seen in Figure 1a, the larger airways are supported by cartilage plates. These gradually decrease so that bronchioles less than 1 mm in diameter are no longer stabilized. This functional section, between generation 16 and 23, is also referred to as the pulmonary acinus, see 1b. These airways are kept open by a strong traction of the lung tissue. If there is over pressure in the alveoli, the lung tissue compresses this pressure and causes the alveoli to collapse. [13] This effect can be achieved, for example,

by diving with held breath [14], or more commonly as a side effect by mechanical ventilation in anesthesia. [15, 16]

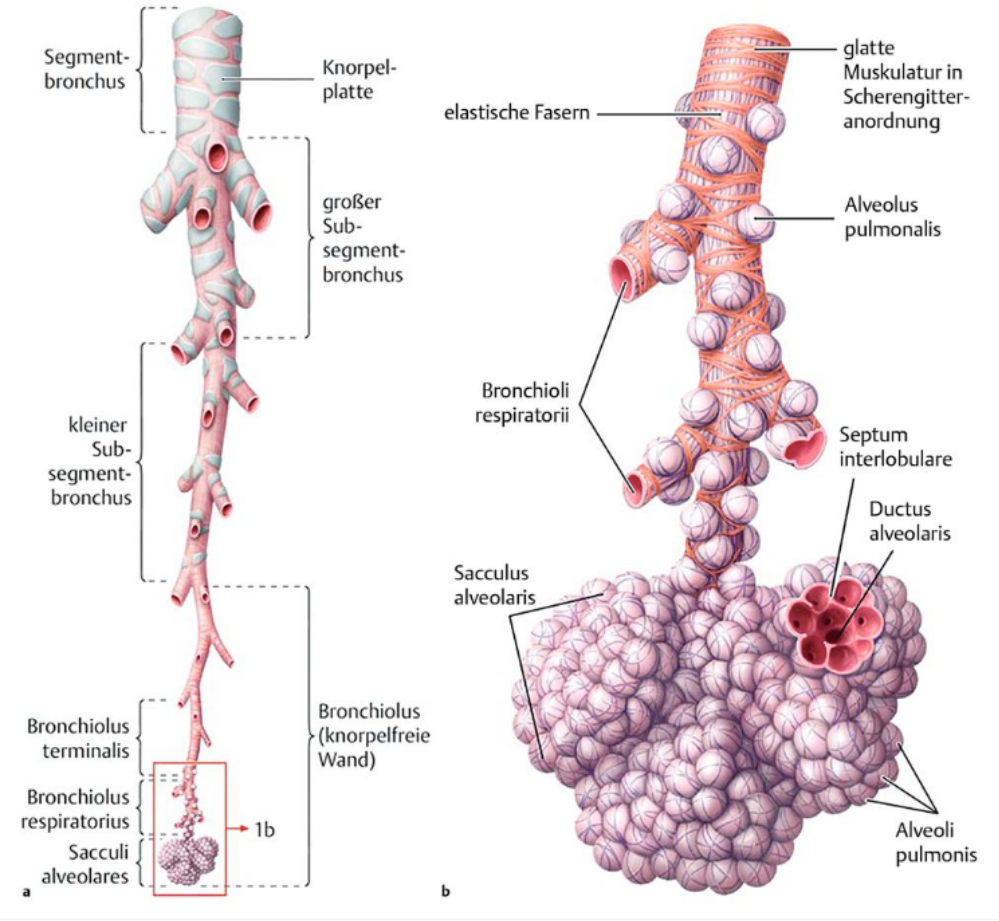


Figure 1: *Anatomical lung structure with conducting airways (a) and respiratory zone (b)*

Before going into more detail about ventilation techniques, some term definitions are essential for understanding mechanical ventilation, as Mora Carpio and Mora [11] point out in their publication.

- "Ventilation: Exchange of air between the lungs and the air (ambient or delivered by a ventilator), in other words, it is the process of moving air in and out of the lungs. Its most important effect is the removal of carbon dioxide (CO2) from the body, not on increasing blood oxygen content. Ventilation is measured as minute ventilation in the clinical setting, and it is calculated as respiratory rate (RR) times tidal volume (Vt). In a mechanically ventilated patient, the CO2 content

of the blood can be modified by changing the tidal volume or the respiratory rate."

- "Oxygenation: Interventions that provide greater oxygen supply to the lungs, thus the circulation. In a mechanically ventilated patient, this can be achieved by increasing the fraction of inspired oxygen (FiO 2%) or the positive end-expiratory pressure (PEEP)."

- "PEEP: The positive pressure that will remain in the airways at the end of the respiratory cycle (end of exhalation) is greater than the atmospheric pressure in mechanically ventilated patients."

- "Tidal volume: Volume of air moved in and outside the lungs in each respiratory cycle."

- "FiO2: Percentage of oxygen in the air mixture that is delivered to the patient."

- "Flow: Speed in liters per minute at which the ventilator delivers breaths."

- "Compliance: Change in volume divided by change in pressure. In respiratory physiology, total compliance is a mix of lung and chest wall compliance as these two factors cannot be separated in a patient."

## 2.2 Mechanical Ventilation

Although the first recognized mechanical ventilation was already performed in the 16th century, it took until the 20th century for mechanical ventilation methods to become established. [17] The first successful ventilator was the iron lung. This was a negative pressure machine, a metal tank in which the patient's body was enclosed. Despite its clinical success, it did not catch on because patient care was very difficult. Therefore, subsequently, mainly ventilators working with positive pressure were developed. [1] The basic principle is to use pressure to transport a volume of gas into the lungs. In general,

two types are distinguished volume-controlled and pressure-controlled ventilation. In volume-controlled method, a tidal volume, is set and the inflation pressure is adjusted mechanically. Thus, the velocity (flow) is constant. If, on the other hand, the inflation pressure is controlled, the flow increases sharply at the beginning and then decreases fast. [2] This kind of ventilators will now be discussed in more detail.

If the patient can control their own breathing, it is referred to as spontaneous ventilation. Total support is when the patient is unable to breathe and is 100% dependent on ventilation. This is also referred to as controlled or mandatory mechanical ventilation (CMV), which can be either volume- (VCV) or pressure-controlled (PCV). More often, patients require a mixed form of the two extremes. This partial support is called assisted mechanical ventilation. Meanwhile, controlled and assisted ventilation even exist in one mode, so that the patient can control the appropriate support, depending on the trigger effort. [17, 18]
According to Karcz et al. [17], "There are 4 phases during each ventilatory cycle: trigger phase (breath initiation), flow delivery phase, cycle phase (breath termination) and expiratory phase." In the first phase, breaths can be triggered, either by a machine timer set by the physician, a pressure change, or a flow change. Once the breath is initiated, a valve opens and gas flows into the lungs until a flow or pressure target or a set limit is reached. In the subsequent cycle phase, this target is maintained until a cycle-off criterion is reached. This can be, for example, a set inspiration time. Finally, the expiration follows, which depends on the elasticity of the lungs and the airway resistance. [1, 17]

### 2.2.1 Conventional mechanical ventilation (CMV)

Marino et al. [2] describes six basic conventional ventilation methods with its advantages and disadvantages. The first two methods belong to the total support mode, while the others belong to the partial support mode.
In volume-controlled ventilation (VCV), which is used most commonly in the United States, the inspiratory volume is kept constant in the form of the inspiration or tidal volume. It compensates for any changes in lung compliance or airway resistance, as

the ventilator automatically generates a higher pressure in response to changes, to keep the volume constant at the set values. Though, the risk of lung damage is increased by the higher airway pressure.
In pressure-controlled ventilation (PCV), mainly used in Europe on the other hand, the inflation pressure is kept constant during ventilation. As a result, the flow increases rapidly, but returns to zero at the end of the inspiration phase. This allows the peak alveolar pressure to be controlled and reduces the risk of lung damage. However, as soon as the lung mechanics change, there is a decrease in alveolar volume.
Intermittent mandatory ventilation (IMV or SIMV) was developed to enable spontaneous breathing by the patient between breaths from the machine. For this purpose, there are two parallel circuits in the respirator, which are connected with a one-way valve. The disadvantage of this method is an increased work of breathing and a reduced cardiac output.
Pressure-supported ventilation (PSV) is a more interactive form of pressure-controlled ventilation (PCV). Here, the patient can terminate the mechanical breath himself and thus gains control over the tidal volume and the inspiration time.
In contrast to PSV, assisted-controlled ventilation (ACV) allows the patient to initiate a breath. However, if this is not possible, timed or controlled breaths are delivered by the respirator.

The tidal volume during conventional ventilation therapy is about 75 - 150 % of a patient's natural respiratory volume. The reason therefore is the assumption that the anatomical dead space has to be overcome for gas exchange. [19] Because large amounts of gas are applied in a short time, there are increased turbulent flows in the lungs, which can impede diffusion in the alveolar membrane. [20]

Although strategies such as volume- and pressure-limited procedures, the use of PEEP, and low tidal volumes during mechanical ventilation have proven their effectiveness in recent years, not all patients respond to these therapies. This has led to the exploration of alternative approaches of ventilation. [20, 21]

### 2.2.2 High frequency ventilation (HFV)

High-frequency ventilation is not a stand-alone form of ventilation. [18] It can be combined with the conventional ventilation method or even replace it. [22] The prerequisite for this therapy is that the ventilator can deliver small tidal volumes due to high frequency rates. [23] Depending on the type of principle, frequencies from 60 to 1000 cycles per minute are used. [18] Therefore, this shallow form of ventilation is considered to be less harmful to the lungs. [19] High-frequency ventilation is generally divided into three sub types based on the frequencies used: high-frequency positive pressure ventilation (HFPPV), high-frequency jet ventilation (HFJV), and high-frequency oscillatory ventilation (HFOV). Common to all sub types are three basic elements: a generator to produce the high pressure, a breathing circuit linked to the patient, and a safety valve. [22]

#### 2.2.2.1 High-frequency oscillatory ventilation (HFOV)

High-frequency oscillatory ventilation differs fundamentally from conventional mechanical ventilation as it was invented to minimize hemodynamic effects. [24] An oscillator sets a bias flow, which supplies the lungs with fresh gas, in a permanent oscillation at a high frequency rate of 200 to 900 cycles/min ($\equiv 3 - 16Hz$). Parameter that effect the tidal volumes are the bias flow, frequency, size of the endotracheal tube and pressure amplitude. Compliance and mean airway pressure, in contrast, have smaller influence. [25] The correlation between the tidal volume and the frequency is inversely proportional. Thus, small tidal volumes are applied at high breathing frequencies. [18] The tidal volume has a great influence on gas exchange. [26] Due to the oscillatory motion of the gas, the inspiratory flow behavior is quite different from the steady-state case in CMV. [19] A high mean airway pressure is generated, which maintains lung recruitment [27] and thereby reduces the risk of lung injury. [2] This therapy does not involve the generating of high peak pressures or low end-expiratory pressures. [28] A side effect of the higher mean airway pressure, is reduced cardiac output and the intravascular volume must be increased. [2]

Since it is said to be a lung-protective ventilation which can improve the oxygenation [29], various studies document the application for the therapy of neonates and patients with acute respiratory distress syndrome (ARDS). [19, 21, 27, 30]

The literature review of Chang [31] identified the responsible mechanisms for gas transport in the lung during high-frequency oscillation. According to them, there are five modes that influence gas transport. These include direct alveolar ventilation, mixing by mass convection, convective transport due to asymmetries between respiratory velocity profiles, longitudinal dispersion, and molecular diffusion in the area of alveolocapillary membrane. These modes occur in different areas of the lung. A more detailed observation of a backflow in the airways has already been made by Nagels and Cater [32] using a large-eddy simulation. This flow occurs near the walls at low propulsion velocities. In their study, Choi et al. [19] specifically consider the phenomenon of counter-flow during flow reversal in HFOV. This effect is said to account for about 20 % of the gas mixing.

#### 2.2.2.2 High-frequency jet ventilation (HFJV)

High frequency jet ventilation is another alternative to conventional mechanical ventilation. [33] The special feature of this technique is that the gas flow is generated by a nozzle. The jet is turbulent after exiting the nozzle and causes mixing of the fluids, transporting them to the lungs. Along the branches of the lung, the velocity of the jet decreases. [3] Typical values for high-frequency jet ventilation are frequencies between 100 and 1000 cycles/min and a tidal volume of 2-4 mL/kg. [18]
There are several forms of high-frequency jet ventilation. Because small tidal volumes can accumulate carbon dioxide in the deep lung when high-frequency gas is applied alone, these techniques have been improved by simultaneous application of a jet impulse with a larger tidal volume. [34, 35] Now carbon dioxide can be eliminated without difficulty. Of these, there are two techniques, high-frequency percussive ventilation and superimposed high-frequency jet ventilation, which are referred to as combined high-frequency jet ventilation. [36]

#### 2.2.2.3 High-frequency percussive ventilation (HFPV)

High-frequency percussive ventilation combines two gas flows. A pressure-controlled part as used in conventional mechanical ventilation for inspiration and expiration and a continuous oscillatory component. [30] This method is flow-regulated, time-cycled [28], and pneumatically powered. [23] The ventilator generates a low-frequency respiratory cycle (> 30 cycles per minute) on which a high-frequency gas flow is superimposed (200-900 cycles/min). [37] This creates two pulsating pressure plateaus, one higher and one lower (PEEP).
A so-called phasitron triggers the pulsation of the air and creates a tidal volume that is supposed to be smaller than the anatomical death space. [38] HFPV can treat altered lung compliance and airway resistance almost immediately. [28]

This therapy method is intended as a rescue therapy when CMV does not achieve the goals in clinical situations. [39] It was shown that unlike conventional mechanical ventilation, HFPV improved gas exchange at lower peak airway pressure and low tidal volume. [40] Allan et al. [38] found out, that the dependence between the pulsating frequency and tidal volume is inverse. Because of the lower peak pressure, it also results in fewer lung injuries like the risk of barotrauma. [20] In literature, the use of HFPV is described for patients with early ARDS [41], burn patients [40], patients with severe COVID-19 pneumonia [42], cardiac patients, for barotrauma or undecompressed pneumothorax. [23] However, it is possible that HFPV induces hyperinflation. [41]

"The mechanism by which HFPV carries out gas exchange is suggested by various theories, including direct bulk flow, longitudinal dispersion of gas molecules at terminal airways and alveoli, Pendelluft air flow between neighboring lung regions thereby increasing dead space ventilation, laminar flow, cardiogenic mixing, and molecular diffusion." [28]

#### 2.2.2.4 Superimposed high-frequency jet ventilation (SHFJV)

Unlike the pneumatic form of high-frequency percussive ventilation, SHFJV is an electrically controlled jet technique. [33] It also combines two pulsating gas streams. Low-frequency jet ventilation is combined synchronously with high-frequency jet ventilation. [36, 43] The low-frequency jet ventilation produces a high slow pulsating pressure plateau, and the high-frequency fast jet ventilation produces a pulsating PEEP level at a lower pressure plateau. [3] The low frequency jet has a frequency of 12-20 cycles per minute, while the high frequency jet usually has more than 500 cycles per minute. [34].

The application of SHFJV is in the field of surgical surgeries and intensive care medicine. Due to physical effects of the jet, the method can also be used in open systems. [4]

In the clinical application of high-frequency ventilation techniques, rapid improvement in gas exchange, especially oxygenation, is often seen. In the context of the application of this technique, a computed tomographic study has shown that there is a more rapid recruitment (opening) of collapsed alveoli. [36, 41, 44] This recruitment is responsible for the rapid improvement in oxygenation. The ventilation flow-related effect of this causation is not known. There are few experimental studies comparing SHFJV with other jet ventilation modes. [45] In addition, no computational studies have been performed to clarify the flow mechanics in the airways, probably they are similar to the mechanisms found for HFOV.

## 2.3 Computational fluid dynamics (CFD)

The study of flow phenomena using computational fluid dynamics (CFD) started about 50 years ago and has been rapidly developed since then. [5] This method is based on equations from the middle of the 19th century by Navier and Stokes. [8] These equations can be used to perform calculations for laminar flow, laminar-turbulent transition and turbulent flow. Special wall functions are used for the calculations near the wall. For CFD simulation, there is no general approach to the problem, but the appropriate

method must be selected individually.[8]

In the next step, the fundamentals of computational fluid dynamics relevant for this work are considered in more detail. For further information on this topic, reference is made to the extensive literature. [5, 8, 46, 47]

### 2.3.1 Mathematical models of a flow

In fluid mechanics, the conservation of physical quantities such as mass, momentum and energy is important. This results in five conservation equations, which obtain a complete description of the flow processes. These are [8, 46]:

- Conservation of mass
- Conservation of momentum in x-direction
- Conservation of momentum in y-direction
- Conservation of momentum in z-direction
- Conservation law for energy

These so called Navier-Stokes equations (NSE) are non-linear partial differential equations of second order. There are three ways to describe the NSE: the scalar, vector, and divergence forms. The vector form, equation 3, is used for implementation in computer programs. Here $\vec{U}$ is the conservation vector, $\vec{E}$, $\vec{F}$, $\vec{G}$ are the flux vectors in the three directions and $\vec{Q}$ is a so-called source term. [46]

$$\frac{\partial}{\partial t}\vec{U} + \frac{\partial}{\partial x}\vec{E} + \frac{\partial}{\partial y}\vec{F} + \frac{\partial}{\partial z}\vec{G} = \vec{Q} \tag{3}$$

On the one hand, this equation contains temporal derivatives which indicate the change

of a variable in the volume element with time. On the other hand, spatial derivatives that indicate the flow behavior into and out of the volume element. As well as a term without derivatives, which describes the effect of a source on a volume element. To calculate the temporal derivative for a transient solution, as done in this thesis, a temporal central difference of 2nd order of accuracy is used. An important parameter for the calculation is the physical time step. This must be selected so that the temporal changes can be resolved and the result stored. [46] Whether the time step was selected according to the problem can be seen from the scaled residuals. The values for this must be at least smaller than 1.

The detailed derivation of the Navies-Stoke equation will not be discussed here, as it would go beyond the scope of this thesis. More information can be found in the external literature [5, 8, 46, 47].

Due to the fact that the five conservation equations have 17 unknown variables, there are additional equations necessary to solve the problem. These include boundary conditions and geometry. [46]
The computational cost of solving the complete Navier-Stokes-equation is very high, so today's CFD programs rely on Reynolds-averaged Navier-Stokes (RANS) equations, which have acceptable computing times. In these equations, the flow and turbulence variables are averaged and the effect of unresolved turbulence is approximated by an appropriate turbulence model. Thus, the accuracy of the solution depends on the turbulence model chosen. [5, 46]

### 2.3.2 Turbulence model

There are various approaches for the creation of turbulence models. These range from simple algebraic equations to second order differential equations. Two important modeling approaches are the Reynolds stress model and the eddy viscosity model, which will be discussed in more detail. In these models, the unknown Reynolds stresses are related to the known flow variables using the turbulence model. In eddy viscosity models the Reynolds stresses are replaced by eddy viscosity.

Not all eddy viscosity models are based on the RANS equations. There are also approaches to solve the NSE transiently using large-eddy simulation (LES) or direct numerical simulation (DNS). However, these are much more time consuming. [46]

Eddy viscosity models can be divided into three groups, depending on how many partial differential equations are required for the calculation. [8, 46]

- Zero equation models
  Here, an algebraic equation is used for approximation and no differential equation is used for the eddy transport. The Baldwin-Lomax-Model is a representative.

- One equation models
  One differential equation is used to calculate the transportation of turbulent kinetic energy. An example is the Spalart-Allmaras model.

- Two equation models
  These models are currently widely applied and use two differential equations for calculation of the eddy viscosity.
  The most commonly applied two equation models used for turbulent flows at the moment include the standard-k-$\epsilon$-, RNG-k-$\epsilon$-, Realizable-k-$\epsilon$-, Wilcox-k-$\omega$- and Menter-SST-k-$\omega$-model. [5] The parameter k refers to the turbulent kinetic energy, $\epsilon$ to the turbulent dissipation rate and $\omega$ to the specific dissipation rate. [48] The turbulence model chosen for the simulations performed in this work is the Menter-SST-k-$\omega$-model. In this model, the two model equations are used in a hybrid approach. On the one hand the k-$\omega$-model, which can be used to calculate the mean turbulence and flow magnitude well near the wall, and on the other a k-$\epsilon$-model, which is used more effectively in the outside region. Thus, the advantages of both models are used and the respective disadvantages are well compensated. [5]

### 2.3.3 Reynolds number

The distinction as to whether a flow is laminar or turbulent is made on the basis of the Reynolds number. The limit value for flows in tubes or ducts is $\mathrm{Re}_{krit} = 2320$. Lower values are referred to as laminar flow and higher values as turbulent flow. The transition between laminar and turbulent flow occurs via several intermediate states. [8, 47] The Reynolds number for this work was calculated using formula 4 with the diameter of the trachea (18mm) and the density and dynamic viscosity at 15 °C and 1 bar.[49] An approximate value of 10 m/s was used for the velocity.

$$Re = \frac{\rho_{air} * v * d_{lung}}{\eta_{air}} = \frac{1.225 \frac{kg}{m^3} * 10 \frac{m}{s} * 0,018m}{18.0075 * 10^{-6} \frac{kg}{ms}} = 12245 >> Re_{krit} \tag{4}$$

Friction affects the boundary layer, a thin layer near the wall and occurs in both laminar and turbulent flow. This becomes apparent by the fact that the velocity near the wall is zero. [8, 47] The profile of the different flow types can be seen in figure 2.

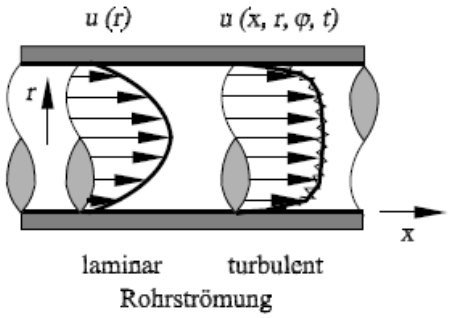


Figure 2: *Flow profile in a tube for laminar (left) and turbulent (right) flow [47]*

### 2.3.4 Sequence of a computational fluid dynamics calculation

In Figure 3, the workflow of a computational fluid dynamics calculation is graphically summarized. The graph was created by Lecheler [46] for another simulation program called ANSYS CFX, which uses separate programs for preprocessing, solvering and

postprocessing. With ANSYS FLUENT the sequence is identical. However, the three processing steps are performed directly within the simulator. More detailed descriptions of the individual process steps can be found in literature.

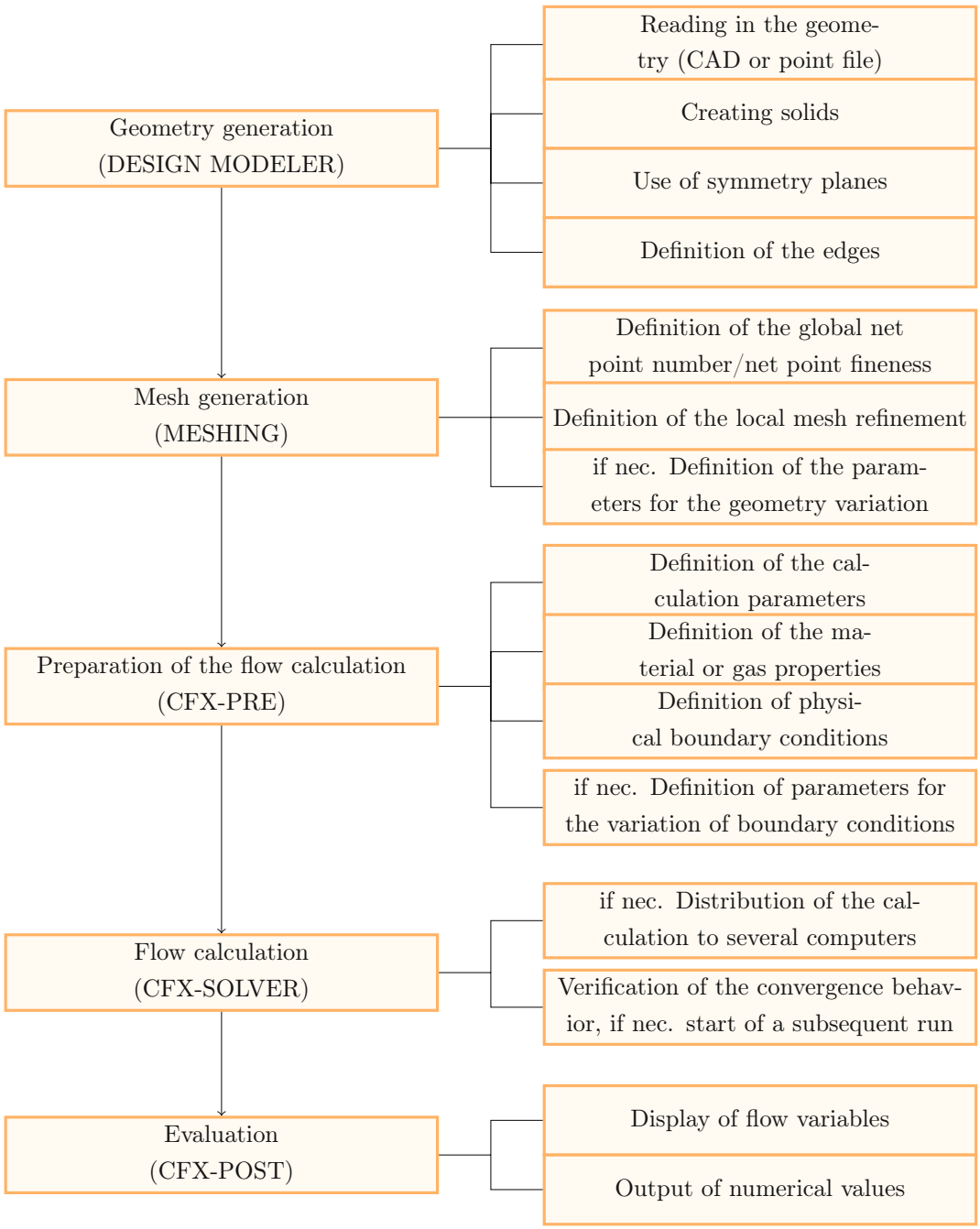


Figure 3: *Overview for a sequence of a CFD simulation in ANSYS CFX [46]*

# 3 Method

## 3.1 Geometry

The geometry of the model was created using the Design Modeler component of ANSYS software (2018 R0 and 2022 R1). Three different geometries were created. For the preliminary tests, a simple tube was chosen because the simulator's computing time for it is manageable and errors are easier visible. A circle with a diameter of 0.1 m and a tube length of 1 m was used as the shape of the cylindrical tube. Later this tube was scaled down to 0.02 m in diameter and a length of 0.12 m to adapt the dimensions to the trachea. For the main work, the lung was reconstructed as bifurcation model. For simplicity, the lungs was assumed to be symmetrical and the dimensions of the left half of the lung, according to Weibel's classification [3], were used for the model, see Table 1. The first lung model was mapped up to generation 4 with one symmetry axis through the trachea. In order to perform the calculations even deeper into the lung up to the $8^{th}$ generation, the geometry of the $4^{th}$ generation was split in half again, creating a second symmetry axis. Both geometries can be seen in Figure 4. According to Soni and Aliabadi [50], the branching angle between the lung branches was always chosen to be 70°. In reality, the branches that protrude from the plane are randomly distributed between 0 and 180°. For this simplified geometry, a rotation angle of 90° was almost always assumed for each new branch, except for the $7^{th}$ generation. Since the branches would have partially overlapped in the $8^{th}$ generation, some rotation angles in generation 7 were randomly chosen between -15 and -90°.
Furthermore, geometries of generation 1 to 4 were created analogous to symmetry of the $8^{th}$ geometry for additional experiments.

## 3.2 Mesh

For the calculation of the conservation equations, a numerical mesh is needed that fills the geometry. It is crucial for the accuracy of the solution. [46]
A mesh can be created with a finite difference method (FDM), finite volume method

Table 1 *Dimensions of the lung model geometry [3, 51]*

| Generation z | Name | Diameter [mm] | Length [cm] |
|---|---|---|---|
| 0 | Trachea | 18 | 12 |
| 1 | Mainstem bronchi | 12.2 | 4.76 |
| 2 | Lobar bronchi | 8.3 | 1.9 |
| 3 | Segmental bronchi | 5.6 | 0.76 |
| 4 | Subsegmental bronchi | 4.5 | 1.27 |
| 5 | Bronchi | 3.5 | 1.07 |
| 6 | Bronchi | 2.8 | 0.90 |
| 7 | Bronchi | 2.3 | 0.76 |
| 8 | Bronchi | 1.86 | 0.64 |

(FVM) or finite element method (FEM). In the FDM, the grid points are described using the neighboring points, which results in high computational accuracy, but is relatively inflexible. The FVM is the most commonly used method and describes the geometry with small volume cells in the form of hexahedra. For each of these volume cells, the conservation equations are used in integral form. It is a flexible but less accurate method. The lowest accuracy is achieved with the FEM, since the differentials are replaced by simpler equations that can be easily represented. Here, mostly tetrahedral elements are used, which allows a very good adaptation to complex geometries. [8, 46]

The mesh of the model was also created using ANSYS software. Like many other CFD programs, Ansys FLUENT uses the finite volume method because it has a good balance between flexibility and accuracy. [46]
To customize the mesh for CFD simulations, the physical preference has to be changed to CFD and FLUENT has to be selected as solver preference. The tube mesh was created using the algorithm of a sweep method (hexahedron) and inflation at the edge. The mesh of the lung, on the other hand, was modified by using inflation layers again, but an algorithm with tetrahedrons was chosen. Since the student version of Ansys has a limit for fluid physics of 512K cells/nodes [52], this had to be taken into account when creating the mesh. The meshes were varied by changing the element size, the curvature

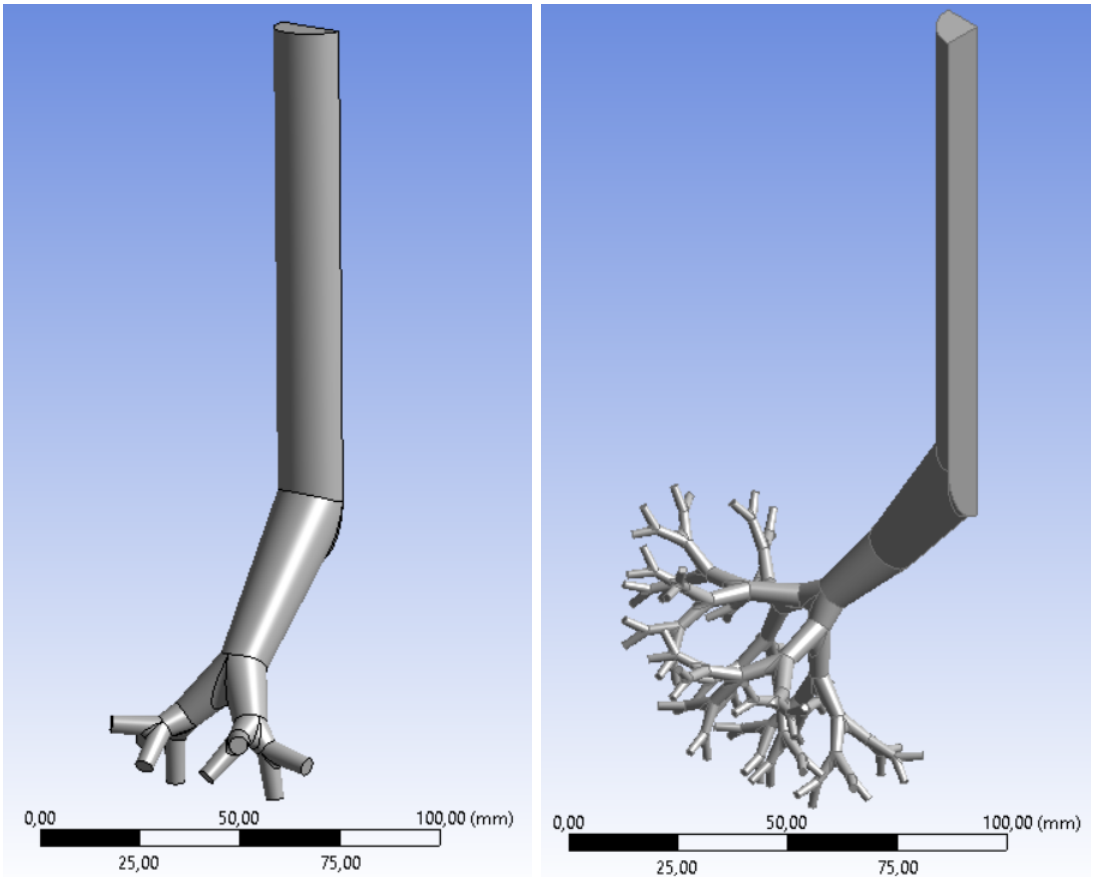


Figure 4: *The left image shows the geometry up to the $4^{th}$ generation with one symmetry axis and the right one the geometry up to the $8^{th}$ generation with two symmetry axes. The longest tube, trachea, is counted as generation 0.*

normal angle, the curvature minimum size and the defeature size. Table 2 summarizes the nodes and elements of the meshes, as well as the percent change of generation 4 and the amount of symmetry axis for each geometry. Since mesh dependency must be excluded, the geometry of generation 4 with one symmetry axis was meshed with three different element sizes and they were compared with each other before a mesh size was selected for further geometries. In the comparison of the three meshes, Figure 5, it can be seen that the number of elements increases especially in the area of the trachea (Gen0).

Table 2 *Nodes for all meshes*

| geometry | symmetry axis | nodes | cells | percent change |
|---|---|---|---|---|
| tube | 0 | 23000 | 21483 | |
| lung gen0 | 0 | 14978 | 38832 | |
| lung gen0 | 1 | 8423 | 21614 | |
| lung gen0 | 2 | 4401 | 10882 | |
| lung gen1 | 2 | 6681 | 16385 | |
| lung gen2 | 2 | 9520 | 23812 | |
| lung gen3 | 2 | 15052 | 39588 | |
| lung gen4 | 1 | 41248 | 109347 | -41.6% |
| lung gen4 | 1 | 67503 | 187229 | 100% |
| lung gen4 | 1 | 113359 | 329250 | 75,85% |
| lung gen4 | 2 | 34170 | 93841 | |
| lung gen8 | 2 | 176515 | 482603 | |

## 3.3 Boundary Conditions

In combination with the geometry, the boundary conditions specify the flow problem. [46] In the present work, the boundary conditions are used to model both the airflow emanating from a superimposed high-frequency jet ventilator and the response of the lung to this flow.

To adapt the simulation to the task, a user defined function (UDF) was written in C programming language and later linked to the software. The script consists of several parts, which defines the boundary conditions of the simulator. For the description of the respective condition a `DEFINE` macro must be written, which is provided by the software. In order to use the prerequisite macros, each UDF must start with the `include "udf.h"` command. Furthermore, the `include "math.h"` command is needed to use advanced mathematical operators.

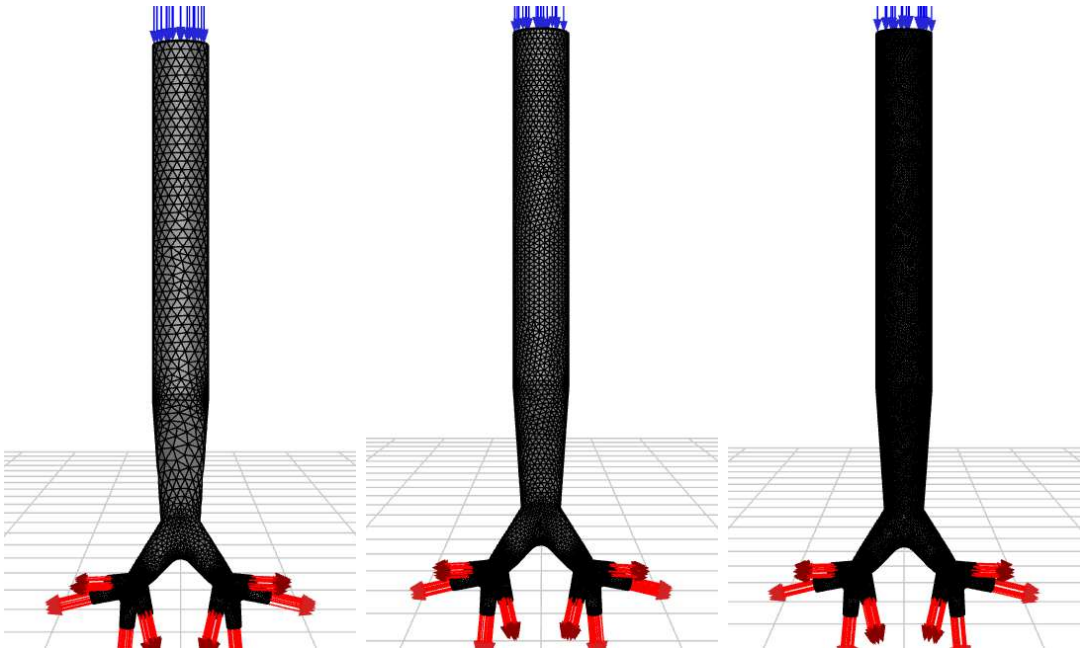

Figure 5: *Comparison of three different meshes on the same geometry. On the left, the mesh is shown with 109347 cells, in the middle with 187229 cells and on the right with 329250 cells. The arrows show the direction of the air flow from the beginning of the trachea (inlet) into deeper lung areas (outlet). Inlet arrows are shown in blue and outlet arrows in red.*

### 3.3.1 Description of the ventilation device

The super-imposed high frequency jet ventilator TwinStream from Carl Reiner GmbH served as template for the simulation on the inlet. The schematic structure of the device can be seen in figure 7. At the top of the figure, the device can be seen with a monitor 6 for setting the parameters and monitoring the workflow.

On the right side of the device, in the turquoise tube marked with one, a constant gas flow can be set. This is known as the bias flow and used for the permanent supply of fresh air as well as heating and humidifying this flow. While the bias flow adjusts the environment of the air, the gas flow on the left side, serves to ventilate the patient. The figure shows that both the low-frequency (orange line) and the high-frequency (green line) jets are directed into a second tube via a converter marked with two. As described earlier in chapter 2.2.2.4, the low frequency jet creates the upper pressure plateau and

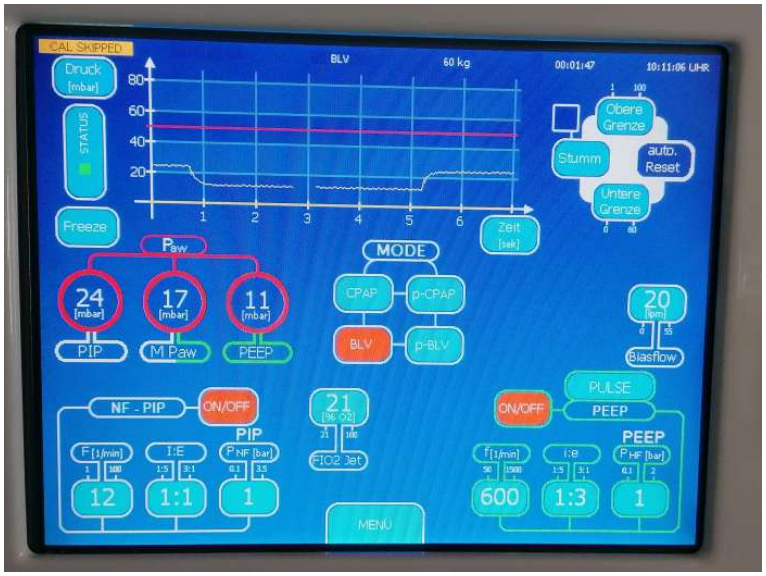


Figure 6: *Screen of the ventilator, all fields in light blue can be selected or changed. The orange fields mark what is currently actively selected.*

the high frequency jet creates the lower pressure plateau which corresponds to a PEEP. For a predefined unit of time, air flows through this tube into the lungs (inspiration). Then the air supply for the low frequency jet part is stopped and a constant pressure is maintained. After some time, the pressure is released so that the gas can flow back due to a restoring force of the lungs (expiration). The high-frequency jet is superimposed on both pressure plateaus and produces continuous pulsation toward the lungs. Both tubes are connected to an endotracheal tube with a Y-piece, which is cuffed in the trachea. The proximal tube system (2) on the left contains the so-called converter. In the p-BLV converter, two jet streams are combined by two injectors in one entrainment port. This results in greater entrainment and a higher pulsatile flow output. An air filter is connected to the left of the exhalation section of the converter. So the air flows in both directions in the white tube and in the converter, marked with two. [3, 53]
This flow behavior was attempted to be mimicked in the UDF. Since the constant bias flow is relatively small compared to the high and low frequency jet gas flow, it is not considered in this diploma thesis.

The effect of ventilation can be seen on a pigs lung in figure 8. Here, a collapsed lung without air supply can be seen on the left side, while on the right side the lung is

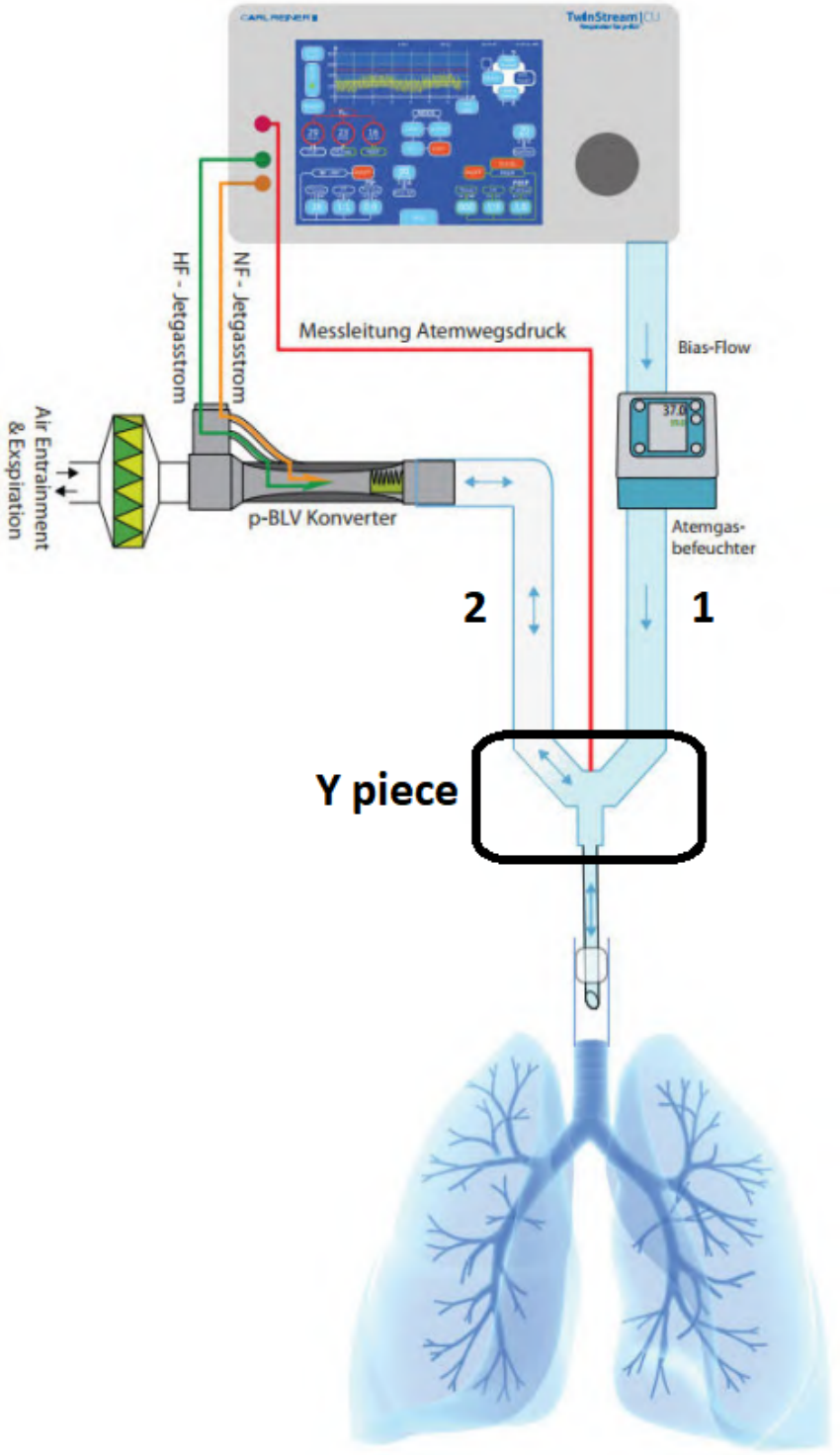


Figure 7: *Scheme of the super imposed high frequency jet ventilator TwinStream connected to a lung.*

expanded due to mechanical ventilation.

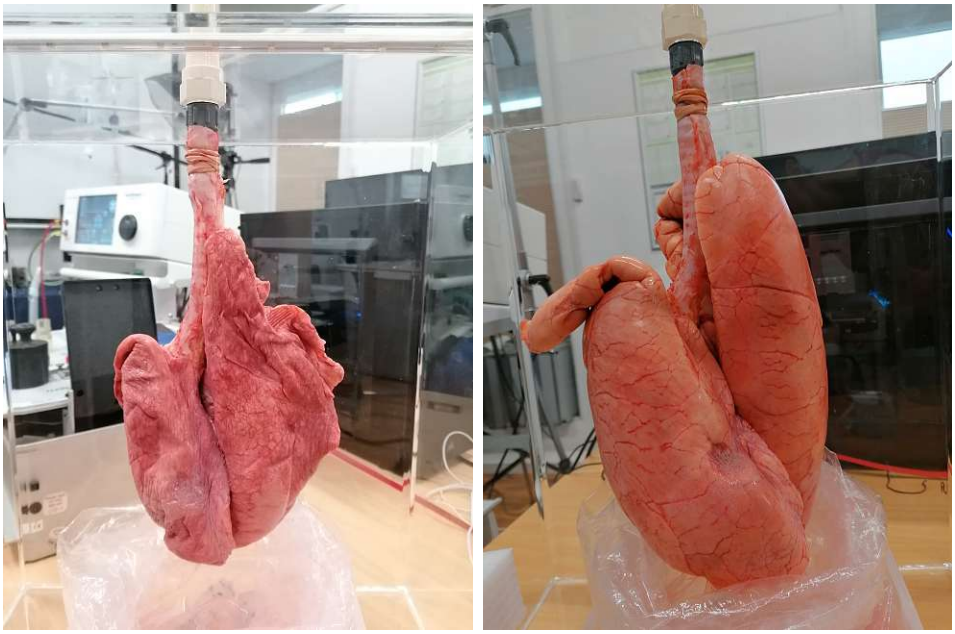

Figure 8: *On the left side, it can be seen how the pigs lung collapses without air supply. On the right side, a fully inflated lung at 1 bar ventilation pressure is shown.*

The individual components of the UDF, which are intended to describe the ventilation of the lungs with the aid of a ventilator, will now be considered in more detail. Explanatory information was taken from the ANSYS FLUENT UDF Manual [48].

```
DEFINE_PROFILE(pressure_inlet_square,thread,index)
```

This line defines the profile function which is used for the inlet boundary condition with the UDF name `"pressure-inlet-square"`. The other two arguments in the parenthesis are variables that are directly included in the function. Thread or t tells the program in which face the constraint will be applied. Index or i tells FLUENT solver on which variable the function should operate on.

```
face_t f
```

This term is a so called "face identifier" and explained by the manual of FLUENT [48] as a "face with index f that is on the thread pointed to by t."

```
real time = CURRENT_TIME;
real amplitude1 = 3000.0;
real amplitude2 = 0.01;
real pressure1 = 1500;
real pressure2 = 1800;
real offset = 1.5;
real rate = 3.5;
real frequency1 = 10;
real duration = 60/frequency1;
real frequency2 = 10;
```

With these commands the real values of the variables can be specified. A common pressure for the low frequency of 30 mbar or 3000.0 Pa was used as amplitude1. [3] The amplitude2 was set as the amplitude of the high frequency with 30 Pa. The parameters pressure1 and offset were chosen so that the curve, which is described by the equations below, starts at the origin of coordinates. A PEEP of 8 mbar was selected with adjusting pressure2. The rate was used to adjust the gradient of the function. This parameter could not be chosen too large, otherwise it would lead to inaccuracies in the calculation.
These values were found after a few tries. Frequency1 corresponds to the cycles per minute of the low frequency (LF). The duration of one LF cycle is calculated by $\frac{60}{frequency1}$. For Frequency 2, on the other hand, the unit is Hz, in this case 10 cycles per second for the high frequency jet.

```
begin_f_loop(f,thread)
end_f_loop(f,thread)}
```

As these command terms imply, they can be used to make a loop for all the faces and threads in the cells that are between the start and end command.

```
if ((time>=(0.0*(duration/2))) && (time<(1.0*(duration/2))))
F_PROFILE(f,thread,index)=pressure1+((tanh(rate*(time-(0.0*(duration/2)
```

```
+offset)))*amplitude1)/2)*(1-amplitude2*sin(2*3.1415926*frequency2*time));
if ((time>=(1.0*(duration/2))) && (time<(2.0*(duration/2))))
F_PROFILE(f,thread,index)=pressure2+((tanh(-rate*(time-(1.0*(duration/2)
+offset)))*amplitude1)/2.5)*(1-amplitude2*sin(2*3.1415926*frequency2*time));
```

With this operating function, the ventilation device is being imitated for LF and HF superimposed.
The if statement specifies the time span in which the following function is to be applied.
A common macro used within a `DEFINE_PROFILE` macro, is `F_PROFILE(f,thread,index)`. It is used to set a boundary condition value and is defined by the arguments face, thread and index. After the definition of the macro, the function that controls the gas flow at the inlet follows. In this case, the tangent hyperbolic was used to allow a more realistic on and off switching of the gas flow. The individual variables were used to modify the hyperbolic function according to the task.

```
DEFINE_PROFILE(pressure_inlet_square, thread, index)
{face_t f;
real amplitude1 = 3000.0;
real amplitude2 = 0.05;
real time = CURRENT_TIME;
real frequency1 = 12;
real duration = 60/frequency1;
real frequency2 = 10;
real pressure1 = 1500;
real pressure2 = 1800;
real offset = 1.5;
real rate = 3.5;

begin_f_loop(f,thread)
{if ((time>=(0.0*(duration/2))) && (time<(1.0*(duration/2)))) F_PROFILE(f,
thread,index)= pressure1+((tanh(rate*(time-(0.0*(duration/2)+offset)))
*amplitude1)/2)*(1-amplitude2*sin(2*3.1415926*frequency2*time));
if ((time>=(1.0*(duration/2))) && (time<(2.0*(duration/2)))) F_PROFILE(f,
thread,index)= pressure2+((tanh(-rate*(time-(1.0*(duration/2)+offset)))
*amplitude1)/2.5)*(1-amplitude2*sin(2*3.1415926*frequency2*time));
```

```
if ((time>=(2.0*(duration/2))) && (time<(3.0*(duration/2)))) F_PROFILE(f,
thread,index)= pressure2+((tanh(rate*(time-(2.0*(duration/2)+offset)))
*amplitude1)/2.5)*(1-amplitude2*sin(2*3.1415926*frequency2*time));
if ((time>=(3.0*(duration/2))) && (time<(4.0*(duration/2)))) F_PROFILE(f,
thread,index) = pressure2+((tanh(-rate*(time-(3.0*(duration/2)+offset)))
*amplitude1)/2.5)*(1-amplitude2*sin(2*3.1415926*frequency2*time));
if ((time>=(4.0*(duration/2))) && (time<(5.0*(duration/2)))) F_PROFILE(f,
thread,index) = pressure2+((tanh(rate*(time-(4.0*(duration/2)+offset)))
*amplitude1)/2.5)*(1-amplitude2*sin(2*3.1415926*frequency2*time));
if ((time>=(5.0*(duration/2))) && (time<(6.0*(duration/2)))) F_PROFILE(f,
thread,index) = pressure2+((tanh(-rate*(time-(5.0*(duration/2)+offset)))
*amplitude1)/2.5)*(1-amplitude2*sin(2*3.1415926*frequency2*time));
end_f_loop(f,thread)}
```

The course of the simulation can be represented graphically as follows in figure 9.

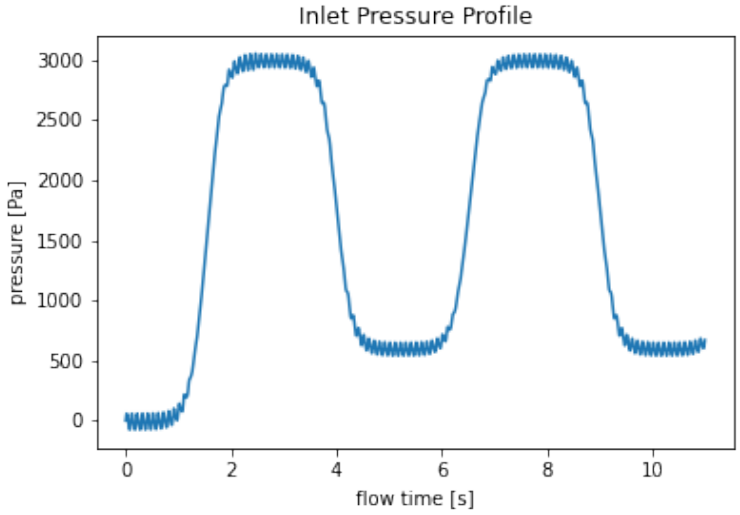


Figure 9: *Programmed pressure profile of the low and high frequency jet gas to mimic the input of the SHFJV applied at the beginning of the trachea.*

Since there is no literature about CFD simulation of superimposed high frequency jet ventilation, but about high frequency oscillation, a second function is programmed in the UDF, which simulates a typical HFO curve. Since the devices takes a short time to reach the desired parameters, a ramp was set at the beginning and then the oscillation was kept constant. The

mean breath pressure was set to 8 cm H2O (758 Pa) and a frequency of 10 Hz. In the UDF, this part is set up in the same way as that for the SHFJV.

```
DEFINE_PROFILE(pressure_inlet_sinus, thread, index)
{face_t f;
real amplitude1 = 785.0;
real amplitude2 = 0.05;
real time = CURRENT_TIME;
real frequency2 = 10;
real pressure1 = 392.5;
real offset = 1.5;
real rate = 3.5;

begin_f_loop(f,thread)
{ F_PROFILE(f,thread,index) = pressure1 + ((tanh(rate*(time-offset))
*amplitude1)/2)*(1-amplitude2*sin(2*3.1415926*frequency2*time));}
end_f_loop(f,thread)}
```

### 3.3.2 Description of the lung

First, the values which are going to be used in the UDF will be explained in more detail. The term compliance describes the ability of the lungs to expand and enlarge. Mathematically, this can be expressed by the volume change through the resulting pressure change. In medicine, the unit of compliance is often given in $L/cmH_2O$. [54] Thus, for further calculations the units must be converted to SI units, as done in formula 5.

$$f_u = 1[\frac{L}{cmH_2O}] = 1 * \frac{10^{-3}[m^3]}{98,0665[Pa]} = 1,0197 * 10^{-5}[\frac{m^3}{Pa}] \tag{5}$$

"The compliance of a normal human lung [...] varies with lung volume." [55] If, for example, a compliance of a healthy human lung with a value of 0.1 $\frac{L}{cmH_2O}$ is used, the resulting elastance

can be determined by means of formula 6. [11, 54]

$$Elastance = \frac{1}{Compliance * f_u} = 980665[\frac{Pa}{m^3}] \tag{6}$$

The elastance can also be represented by pressure per volume. Since a volumetric flow depends on the temperature, but not the mass flow, the volume was replaced in the formula 7 with mass per density. This allows the pressure to be expressed as a function of mass and is called reset pressure, equation 8. For $\rho$, an air density of 1.225 $\frac{kg}{m^3}$ at 15 °C was used, which is also predefined in ANSYS FLUENT.

$$Elastance = \frac{p}{V} = \frac{p}{m/\rho} \tag{7}$$

$$p = \frac{Elastance}{\rho} * m = \frac{980665}{1.225} * m = 800543 * m[Pa] \tag{8}$$

Since the influence of compliance on the simulation should also be taken into account, different values for the compliance have been used. All values used for the simulation are summarized in table 3.

Table 3 *Different parameters for the lung*

| Compliance $[\frac{L}{cmH_2O}]$ | Elastance $[\frac{Pa}{m^3}]$ | $p_{out}$ [Pa] |
|---|---|---|
| 0.2 | 490333 | 400272*m |
| 0.1 | 980665 | 800543*m |
| 0.05 | 1961330 | 1601086*m |
| 0.01 | 9806650 | 8005429*m |

In the preliminary tests, the entire lung is considered as a balloon in the UDF at the end of the tube, see Figure 10 (left image), which can be inflated until the inlet pressure is equal to the reset pressure. The reset pressure is then responsible for exhalation and equation 8 is put into the UDF. Once the lung geometry tests are performed, equation 8 is distributed between the individual outlets of the lung, according to the right picture in Figure 10. The

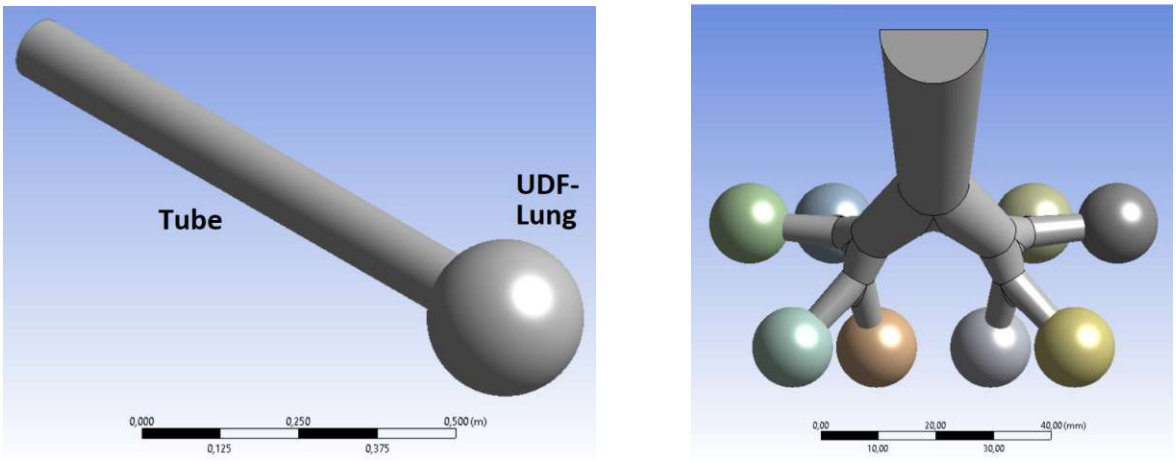


Figure 10: *These two images are to illustrate how balloons are programmed at the end of the tube (right) and lung (left) geometries using the UDF.*

UDF in this case represents the rest of the lung, in particular the alveoli at the end of the pulmonary branches. To make it easier to adapt the UDF to the geometry as well as the different compliances, another parameter called `factor` is added to the pressure_outlet formula, which can be adjusted accordingly.

It should also be mentioned that in this thesis the assumption was made that the bronchial branches do not move, as done in the work of Koullapis et al. [56].

```
DEFINE_PROFILE(pressure_outlet, thread, index)
{face_t f;
real time = CURRENT_TIME;

begin_f_loop(f,thread)
{ F_PROFILE(f,thread,index) = 800543.*factor*mass;}
end_f_loop(f,thread)}
```

### 3.3.3 General settings

The output information can also be controlled via the UDF, which is linked to the programm as function hook. In this part of the script, the first command `DEFINE_EXECUTE_`

`AT_END(calc_mass)` defines to the simulation program that it is a general macro that can be executed at the end of an iteration or a time step. The only argument "calc_mass" of this command is the name to describe it.
`DOMAIN *d` specifies the domain to which the function is to be applied. Domain needs a second command `d = Get_Domain(1)` to specify itself. If the number in the parenthesis is one, it is a single-phase flow. Command `real mass_flow_rate=0` specifies the starting point for the the mass flow rate. The next expression `real A[3]` describes the area of the normal vector, in this case a 3 dimensional space. This is followed by a local pointer that specifies which file is to be read or written. It is called `FILE *fp` and is needed for function `fp = fopen("mass.txt","a")`. This causes the program to open a file, in this case with the filenames "mass.txt", and append it to the new file, marked with "a". Later this command is closed with `fclose(fp)`

Here a loop is created with a so called `thread_loop_f(t,d)` which is defined "to loop over all face threads in a given domain." [48] The if command is used to describe where the script should be applied. The ID number 7 corresponds in this task to the outlet parameter in FLUENT's boundary conditions and might change. The real face area vector `face_t f` is transformed into a face thread by `F_AREA(A,f,t)`.
The basic idea for this part of the UDF is to create a new file in which both, mass flow rate and mass, are recorded for each time step. Thus, it must be specified how these two quantities are calculated. Exactly this was done in the next lines. The mass flow rate is calculated by the velocity times the area in all three directions times the density. All together the formula is: `mass_flow_rate+=(F_U(f,t)*A[0]+F_V(f,t)*A[1]+F_W(f,t)*A[2])*F_R(f,t)`. The mass is then equal to the mass flow rate times the time step: `mass+=mass_flow_rate*CURRENT_TIMESTEP`. The last two `if`-lines specify into which format the new file should be put. With the `RP_NODE"` command, only the calculated nodes are to be considered here. The `CX_Message ("mass_flow_rate=%g, mass=%g\n",mass_flow_rate,mass)` command defines in which format string the arguments of the command should be displayed, whereas `fprintf(fp,"%g,%g, %g\n",CURRENT_TIME,mass_flow_rate,mass)` specifies the direction of the function. The expression `%g` stands "for double data type" and `\n` indicates a new line.

```
DEFINE_EXECUTE_AT_END(calc_mass)
{ Domain *d;
 Thread *t;
 face_t f;
```

```
 d = Get_Domain(1);
 real mass_flow_rate=0;
 real A[3];
 FILE *fp;
 fp = fopen("mass.txt","a");

 thread_loop_f(t,d)
 {  if (THREAD_ID(t)==7)
  {   begin_f_loop(f,t)
       F_AREA(A,f,t);
       mass_flow_rate+=(F_U(f,t)*A[0]+F_V(f,t)*A[1]+F_W(f,t)*A[2])*F_R(f,t);
   end_f_loop(f,t) } }
mass+=mass_flow_rate*CURRENT_TIMESTEP;
if(RP_NODE) CX_Message("mass_flow_rate=%g, mass=%g\n",mass_flow_rate,mass);

if(RP_NODE) fprintf(fp,"%g,%g,%g\n",CURRENT_TIME,mass_flow_rate,mass);
fclose(fp);
```

Another piece of information that can be controlled by the UDF is the `DEFINE_INIT` condition. This determines what happens when the calculation is initialized. In this case, the initial mass should be set to zero so that there is no over-pressure in the lungs at the start of ventilation.

```
DEFINE_INIT(set_mass_zero,d)
 { mass=0; }
```

### 3.3.4 Parallel Processing

The computations of the large branching systems (Gen4 and Gen8) were performed in parallel on 32 processors to optimize computation time. All information for this part was taken from ANSYS Inc. [48, 57].

To solve problems with large numbers of cells more effectively, ANSYS FLUENT provides the option to perform a parallel calculation. For this purpose, the network and the data are

divided into several parts and are then assigned to different computing processes or nodes. All computing nodes are virtually connected to each other and are controlled by a host process. This host does not contain any data, but interprets the commands of the cortex, forwards them to the initial node (compute node-0) and reversed. This compute node-0 distributes the command to all other nodes. Figure 11 shows the connections for the parallel command transfer schematically.

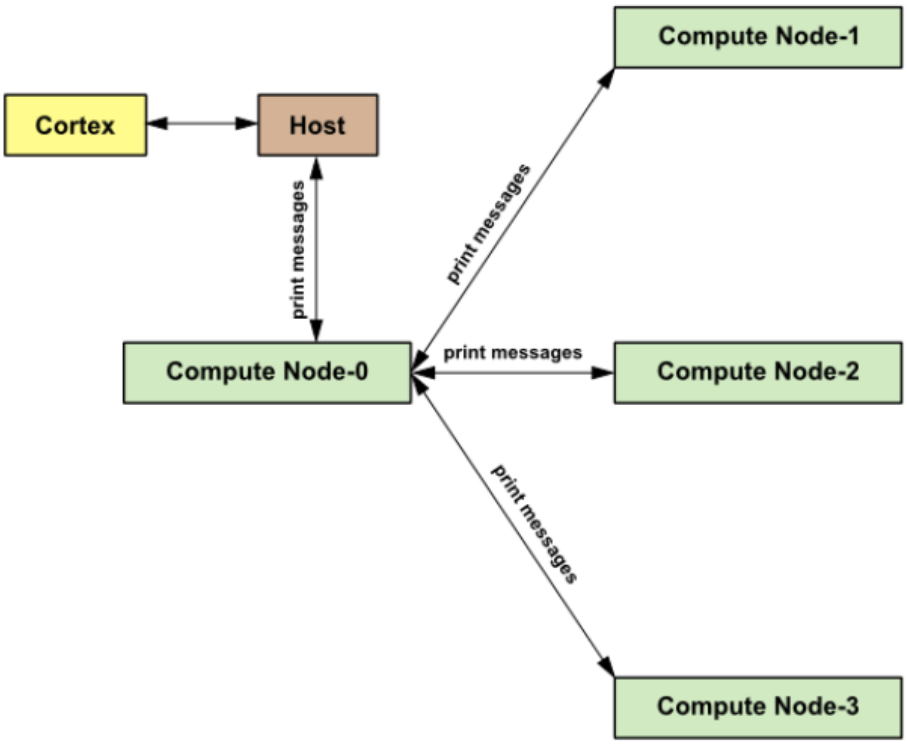


Figure 11: *Schematic illustration of how the commands are transported in a parallel calculation. [48]*

This type of calculation can already be selected when starting FLUENT in the so-called FLUENT Launcher. For the calculation itself, however, the user-defined function that was created for the serial computation must be adapted accordingly.
When parallelizing the UDF, it must be taken into account that there are three types of executables in parallel processing: Cortex, Host and Node. Since the cortex occurs in both serial and parallel computation, only the functions for host and node must be specified. This can be done by the macros `#if RP_HOST` or `#if RP_NODE` and is terminated with `#endif`. More often, however, the negative form, for example `#if !RP_HOST`, is used to exclude one operation. All other operations are performed this way.

As already mentioned, the host does not process any data, which is why it is excluded from all calculation functions. In contrast, the nodes are to combine the data into a message. Thus, the host must be activated for the creation of the files.
With `node_to_host_real_1` the program is informed that one real variable is to be sent from the compute node-0 to the host. However, not every outlet in the lung geometry is calculated from a single node or process. So to obtain the results of the real variables, a global summation has to be performed with the command `PRF_GRSUM1(x)`.

The parallelized UDF is listed here for only 1 of 64 outputs, and only the parts that were customized. The entire UDF is listed in the appendix of the thesis.

```
DEFINE_PROFILE(pressure_outlet1, thread, index)
{face_t f;
real frequency = 1.0;
real amplitude = 1.0;
real time = CURRENT_TIME;

begin_f_loop(f,thread)
{ #if !RP_HOST
  F_PROFILE(f,thread,index) = compliance*factor*mass1_sum;
 #endif }
end_f_loop(f,thread)}
-------------------------------------------------------------

DEFINE_EXECUTE_AT_END(calc_mass_at_end)
{ Domain *d;
 Thread *t;
 face_t f;
 real mass_flow_rate1=0;
 real mass_flow_rate1_sum=0;
 real A[3];

 #if !RP_NODE
  FILE *fp1;
  FILE *fp2;
```

```
 #endif

 d = Get_Domain(1);

 #if !RP_NODE
  fp1 = fopen("mass.txt","a");
  fp2 = fopen("massflow.txt","a");
 #endif

#if RP_NODE
 mass1_sum=PRF_GRSUM1(mass1);
 mass_flow_rate1_sum=PRF_GRSUM1(mass_flow_rate1);
#endif

 node_to_host_real_1(mass1_sum);

 #if !RP_NODE
  fprintf(fp1,"%g,",CURRENT_TIME);
  fprintf(fp1,"%g\n",mass1_sum);
  fclose(fp1);
  fprintf(fp2,"%g,",CURRENT_TIME);
  fprintf(fp2,"%g\n",mass_flow_rate1_sum);
  fclose(fp2);
 #endif
```

## 3.4 FLUENT Settings

For the simulation itself, ANSYS FLUENT has been used. This program is based on the finite volume method. Among other things, it can be used to calculate laminar and turbulent as well as steady or unsteady flows. [5] In this task, the calculation of the flows was unsteady (transient). For simplification, the moisture content in the air was not taken into account, and a rigid tube wall was assumed.

Before numerical solution processes can be started, some relevant boundary conditions must be predefined.

- General - Time: Transient
  At this point it can be defined whether the solution should be calculated stationary or non-stationary.

- Model: Viscous (SST k-omega), Production Limiter

- Materials

  1. Fluid: in compressible air

  2. Solid: aluminium

- Boundary Condition

  1. Inlet
     A pressure inlet has been chosen for this purpose. To recreate the applied gas flow of the respirator, Gauge Total Pressure is linked to the User Defined Function "pressure_inlet_square". Since there is a turbulent gas flow in the ventilation tube (Re $>$ 10000), the turbulence parameters must also be configured here. Therefore, the specification method was set to "Intensity and Hydraulic Diameter", with a turbulent intensity of 5 % and a hydraulic diameter in accordance to the diameter of the inlet face.

  2. Outlet

The backflow parameters were determined as follows: The reference frame is absolute, the direction specification method is normal to boundary and the pressure specification is total pressure. The Gauge Pressure was linked to UDF "pressure_outlet". The turbulence parameters were chosen as for the inlet, hence for the return flow a turbulence intensity of 5 % and a hydraulic diameter in accordance to the diameter of the outlet faces.

In FLUENT, not only the boundary conditions can be specified, but also the output data files. Under the item "Report File Definition" files have been programmed, which are to be saved by the simulation program. These were called "pressure" and "velocity" and contain in each case the flow time and the appropriate parameter at the inlet and outlet, which is indicated in the file name.

# 4 Results and Discussion

## 4.1 Preliminary tests - Validation of the system

Faizal et al. [58] affirms in his paper that "Model validation is a very important step in any simulation analysis to ensure the models are performing as expected or mimics the real condition.[...] Verification and validation of CFD results are required to determine the degree of accuracy that represents the real case scenario."
Consequently, an essential part of this thesis is the creation and verification of the user defined function (UDF) which defines the boundary conditions as explained in chapter 3.3. During the creation, the changes of the individual steps were controlled with a CFD simulation and the comparison with former simulation results. The preliminary tests were all performed on a simple tube, and only after the functionality of the system was confirmed, it was applied to the more complex geometry of the lung.

### 4.1.1 Adjusting the low frequency jet part

The tube in the pre-tests represents the tube 2 of the ventilator, as shown in 7. Thus, the inlet corresponds to the end that is closer to the converter and the outlet corresponds to the end that opens into the lungs.
At the beginning, a sine wave was programmed at the inlet with the `pressure_inlet_sinus` boundary condition and different amplitudes and frequencies were tested.
In the next step, the script for extracting the values for the mass was extended by the command "Execute at end". This command was tested with simulations of various constant velocity and pressure values at the inlet.
Then the pressure_outlet condition was added. Therefore, the pressure at the inlet was kept constant at 1 Pa again. The aim was to see how the pressure at the outlet changes when the factor of the mass changes on one hand and its power number on the other. The results were summarized in table 4. It can be seen in Figure 12 that both a larger factor in front of the mass and the power of the mass, reduce the amount of mass needed to achieve a balance between inlet and outlet pressure. After comparing the mass functions, the outlet pressure was set linearly to $p = 800543 * m$ as described in chapter 3.3.2.

Table 4 *Testing mass functions as pressure outlet*

| Outlet | Curve description |
|---|---|
| 10*m | mass first rises and then settles on a constant value after three oscillations |
| 100*m | similar to 10*m, several and faster oscillations are necessary |
| 1000*m | similar to 100*m, several and faster oscillations are necessary |
| $10*m^2$ | similar to 100*m, oscillations are wider and less |
| $10*m^{-1}$ | cannot be calculated. |
| $10*m^{\frac{1}{2}}$ | mass decreases over time and has a negative value → not realistic for this purpose |
| $10*m^{\frac{1}{3}}$ | mass decreases over time and has a negative value → not realistic for this purpose |

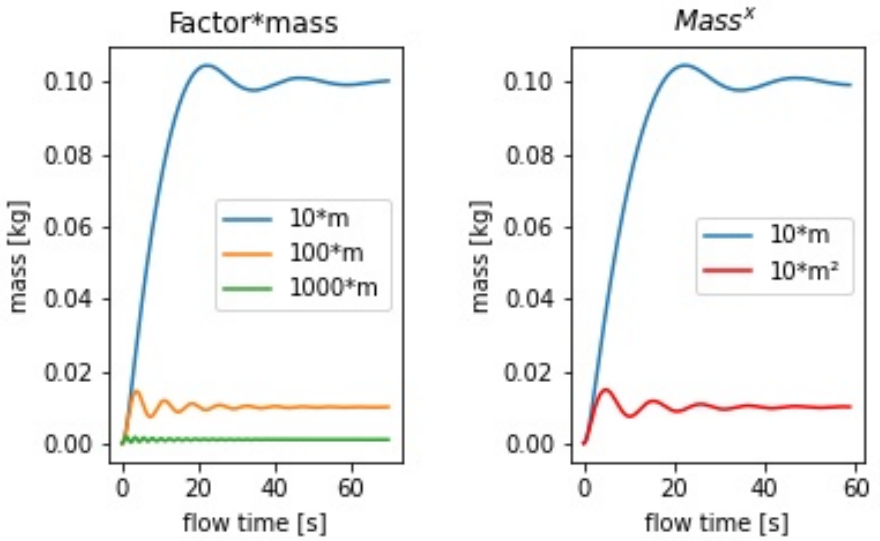


Figure 12: *These diagrams show the effect of different mass functions that can be set at the pressure outlet.*

Once the individual commands had been checked for functionality, they were adapted to the task step by step. Tables 5, 6 and 7 show all preliminary tests with the changed parameters.

In the next step, two functions were used in the UDF to mimic the on and off switching of the low frequency ventilation gas. Turning on the gas flow corresponds to inhalation and turning it off corresponds to exhalation. An inspiration to expiration ratio of 1:1 was chosen and kept for all simulations of this thesis. In a natural breathing cycle, the air is stopped briefly between inhalation and exhalation. This is mimicked by a constant pressure level. This can be seen in Table 5 in the column "inlet function" with f1 and f2. The gas flow was switched on at a constant pressure of 50000 Pa and off at 0 Pa.
Then, two further test on the tube were done to see how two different compliances relate to each other and if it makes a difference whether a constant or ideal gas is set for the material parameter "air" in FLUENT.

Table 5 *Changing compliance and variation between constant and ideal gas*

| name | inlet function | outlet $[Pa * kg]$ | gas | compliance $[m^3/Pa]$ |
|---|---|---|---|---|
| V004 | $f_1 = 50000$ $f_2 = 0$ | 800543m | constant | 0.1 |
| V005 | $f_1 = 50000$ $f_2 = 0$ | 8005429m | constant | 0.01 |
| V006 | $f_1 = 50000$ $f_2 = 0$ | 800543m | ideal | 0.1 |

Figure 13 shows that the mass flow into the lungs is significantly lower with poor compliance of 0.01 (V004) than with good compliance of 0.1 (V004). The mass flow rate shows the same curve for both, but the peak is lower, which results due to the lower increase of the mass.
In contrast, it can be seen that it makes almost no difference whether constant or ideal gas (V004 and V006) is used. Both the masses and the mass flow rate coincide, which is why constant gas was selected for the further calculations for "air" as material parameter.

The oscillation of the curve in all images of Figure 13 results from the sudden switching on and off of the pressure. To reduce this oscillation, the next step was to develop a function that enables a ramp-shaped pressure curve. This also corresponds more to the natural respiratory behavior. The lungs are not completely filled with air from one second to the next, but are

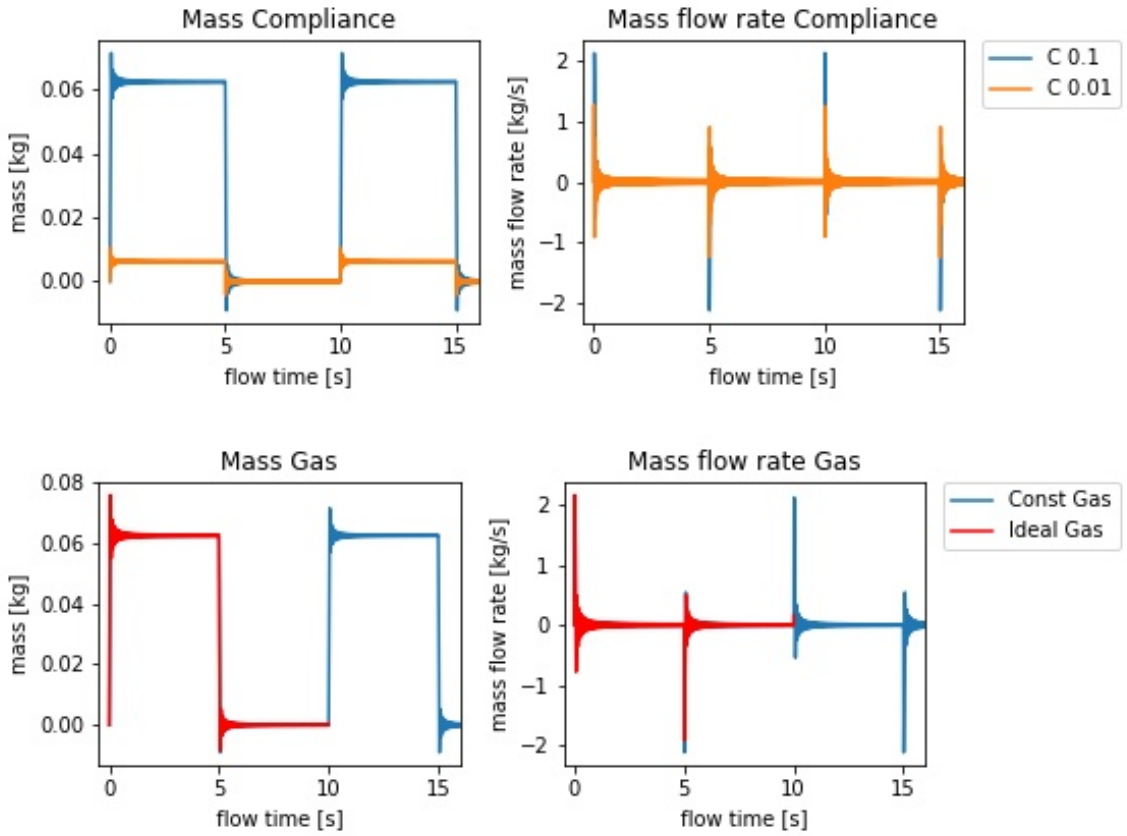


Figure 13: *The upper diagrams show the impact of the compliance on the mass and mass flow rate. The lower diagram, in contrast, the difference between constant and ideal gas. A clear difference between good and poor compliance can be seen in the mass plot. For constant and ideal gas, no significant difference could be found.*

continuously inflated during inhalation until a certain pressure is reached and continuously deflated during exhalation.
The tangential hyperbolic function was selected as pressure ramp to describe the low frequency jet of the ventilator. The suitable parameters for the corresponding course of the ramp as well as the desired pressure condition were found after some tests, see table 6. In the preliminary experiments a pressure of 50000 Pa was programmed at the inlet, due to the proximity to the converter.

After the requested function was programmed, the influence of the frequency on the curve was tested by looking at V010 and V011 in more detail. As expected, at a higher frequency of 0.5

Table 6 *Preliminary test parameter for the low frequency curve*

| name | inlet function | outlet $[Pa * kg]$ | duration per cycle $[s]$ |
|---|---|---|---|
| V007 | $f_1 = \frac{1000000*tanh(10*t)}{2}$; $f_2 = \frac{1}{tanh(10*t)}$ | 10.0 | |
| V008 | $f_1 = 50000 + \frac{(tanh(10*(t-0.5))*100000)}{2}$ $f_2 = \frac{1}{tanh(t)}$ $f_3 = 25000 + \frac{(tanh(10*(t))*50000)}{2}$ | 800543m | 10.0 |
| V009 | $f_1 = 25000 + \frac{(tanh(10*(t-0.5))*50000)}{2}$ $f_2 = 25000 + \frac{(tanh(-10*(t-0.5))*A)}{2}$ | 800543m | 10.0 |
| V010 | $f_1 = 25000 + \frac{(tanh(10*(t-0.5))*50000)}{2}$ $f_2 = 25000 + \frac{(tanh(-10*(t-1.5))*50000)}{2}$ | 800543m | 2.0 |
| V011 | $f_1 = 24997.75 + \frac{(tanh(10*(t-0.5))*50000)}{2}$ $f_2 = 24997.75 + \frac{(tanh(-10*(t-5.5))*50000)}{2}$ | 800543m | 10.0 |
| V012 | $f_1 = 24997.75 + \frac{(tanh(10*(t-0.5))*50000)}{2}$ $f_2 = 24997.75 + \frac{(tanh(-10*(t-5.5))*50000)}{2}$ | 800543m | 32.0 |
| V013 | $f_1 = 24997.8 + \frac{(tanh(5*(t-1))*50000)}{2}$ $f_2 = 24997.8 + \frac{tanh(-5*(t-(\frac{dur.}{2}+1)))*50000}{2}$ | 800543m | 10.0 |
| V013b | $f_1 = 24997.8 + \frac{(tanh(5*(t-1.5))*50000)}{2}$ $f_2 = 24997.8 + \frac{tanh(-5*(t-(\frac{dur.}{2}+1.5)))*50000}{2}$ | 800543m | 10.0 |
| V014 | $f_1 = 25000.0 + \frac{(tanh(10*(t-1))*50000)}{2}$ $f_2 = 25000.0 + \frac{tanh(-10*(t-(\frac{dur.}{2}+1)))*50000}{2}$ | 800543m | 10.0 |
| V026 | $f = 25000.0 + \frac{(tanh(5*(t-1.5))*50000)}{2}$ | 800543m | 10.0 |

Hz, the duration of one respiratory cycle is lower (2 seconds) than at a lower frequency of 0.1 Hz (10 seconds), which is graphically shown in Figure 14. A typical value for the respiratory rate is 10-12 cycles per minute. This corresponds to 0.17 - 0.2 Hz.[3] For the preliminary tests values between 6 and 16 cycles per minute and for the experiments on the lung 10 cycles per minute were used. The value which was used for which test is given in the corresponding tables.
The value of the velocity and of the pressure is not changed by the frequency.

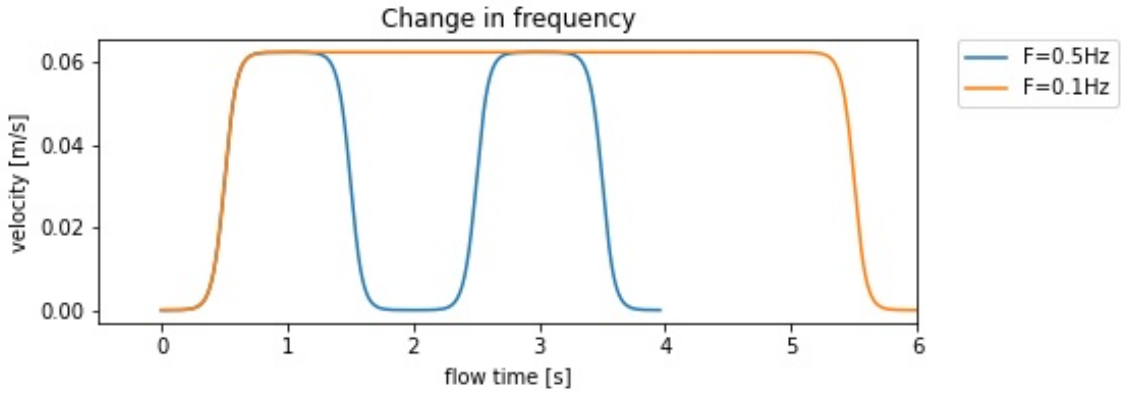


Figure 14: *By varying the frequency, the duration for one respiratory cycle can be adjusted. 0.1 Hz is a rather low value for a respiratory cycle, consequently, it was increased in a further step.*

The following Figure 15 shows the difference between two different offsets (V013 and V013b) and different rates (V013 and V014). These parameters are the numerical values in the tanh bracket of table 6. This part of the function is in words: tanh(rate(time-offset)).
It can be seen in the upper plots that for the pressure curve the offset shifts the entire curve along the x-axis, while the rate changes the rise and fall of the curve. At a smaller rate, the curve becomes slightly flatter, which increases the duration of the rise or fall. As can be seen in the lower graph of this figure, the change in offset does not have an impact on the velocity curve behaviour, but the rate does. Lower values of the rate correspond to a reduced velocity peak, were as higher values result in higher velocity maxima.

At this point, it was also checked whether the results change or stay the same during longer simulations. For this purpose, in experiment V013, the simulation was run for more than 100 s. In Figure 16 it can be seen that there were no changes in either the mass obtained or the resulting velocities. Based on this conclusion, the further simulations were stopped at earlier

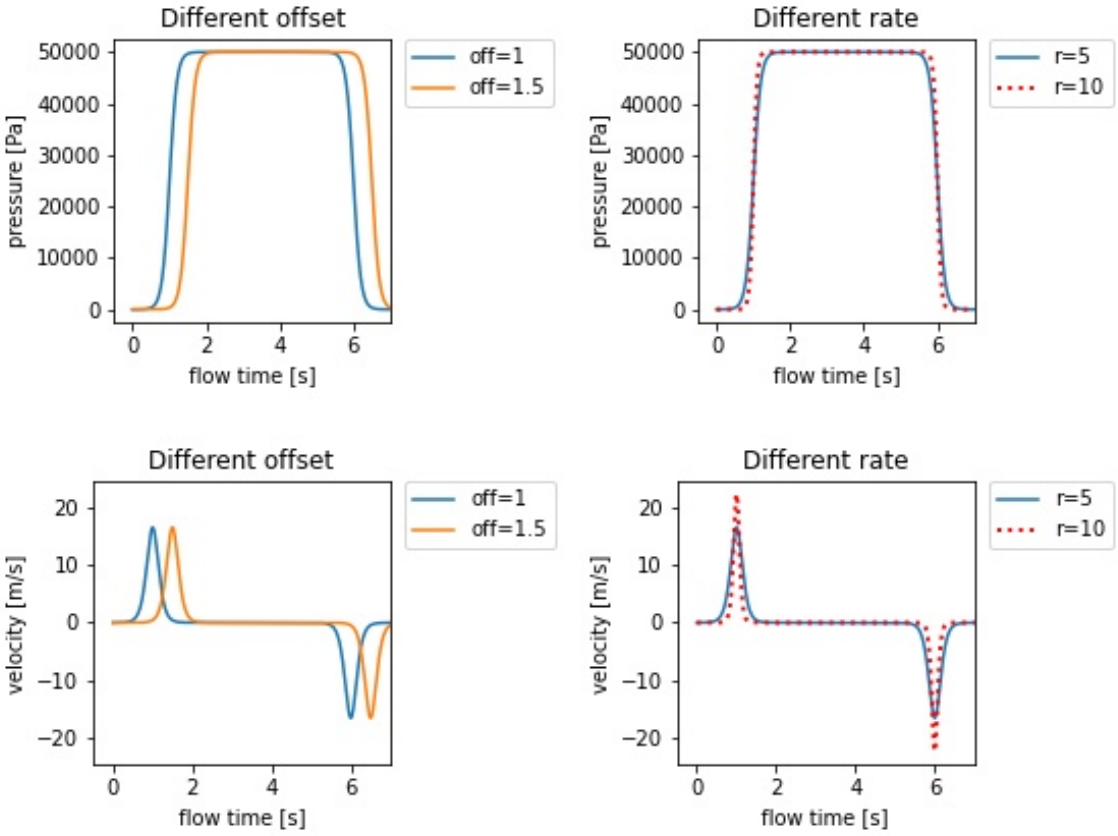


Figure 15: *The influence of the parameter "offset" on the pressure and velocity curve can be seen in the diagrams on the left. There is shift along the x-axis. The diagrams at the right side show the influence of the parameter "rate". Both, the pressure and the velocity curve can be varied with this parameter.*

times.

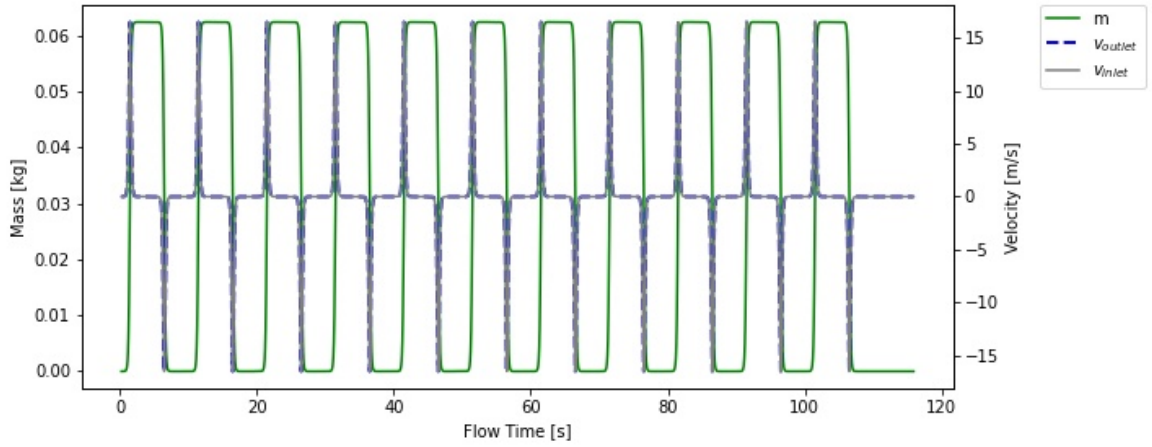


Figure 16: *By means of this result it can be shown that results are independent of simulation time.*

In ANSYS Fluent, different views can also be used directly to visualize the results. One of them is a so called Contour Plot, which presents the velocity in x-direction, in this case. Figure 17 serves to ilustrate at which points in time the contour plots represent the velocities. In addition, the diagram shows how high the velocity was at this point in time. Six time points were selected for demonstration purposes.

- 1: during the positive pressure ramp, which corresponds to inspiration.
- 2: at the beginning of the high pressure plateau
- 3: at the end of the high pressure plateau
- 4: during the negative pressure ramp, which corresponds to exhalation
- 5: at the beginning of the plateau without pressure
- 6: at the end of the plateau without pressure

In illustration 19 and 20 the x-axis of the coordinate system points to the left, thus the programmed lungs is located on the left side of the images, marked by an ellipse and the inlet

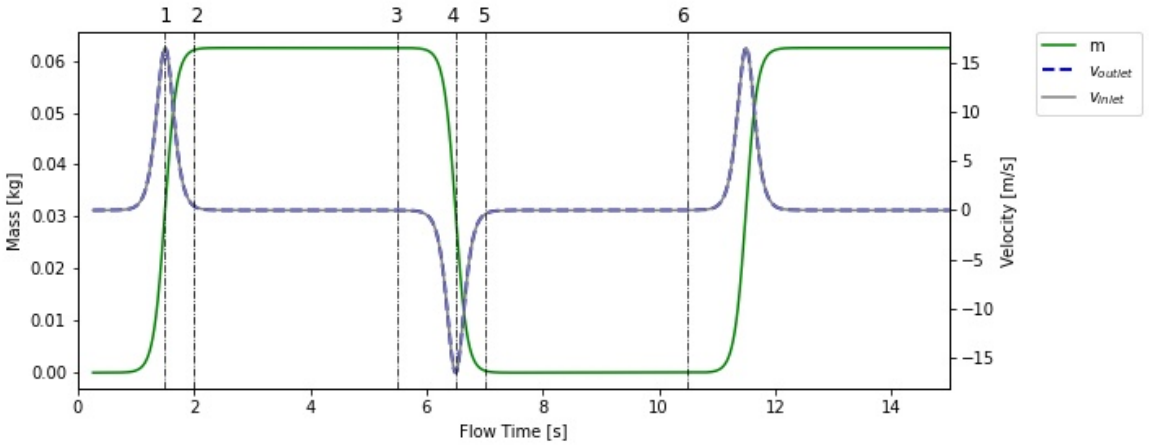


Figure 17: *Time marks for the low frequency function results. The horizontal lines indicate at which point in time the contour plot was created and how high the velocity was at that point in time.*

at the right side, marked with an arrow.

Both contour plots during the pressure ramp show velocities in one direction only, that is a flow into the lung at 1, marked in red, and a flow out of the lung at 4 marked in blue. After 2 seconds (graph 2) there is still a fast gas flow in the direction of the lungs. This is indicated again by the red color, but the velocity already decreases on the initial side of the tube, indicated in light green. The counterpart to this can be seen after 7 seconds (graph 5). The gas is still flowing out of the lungs, marked in dark blue, and the velocity on the other side is already slowing down. When the pressure is kept constant for some time (graph 3 and 6), the representation does not change too much compared to the beginning (graph 2 and 5). In the core, the velocity is present in the current flow direction, while a flow in the opposite direction occurs close to the wall. It should be noted, however, that the numerical values in the legend become smaller and smaller over time. Therefore it can be said that at the end of the pressure plateau there is only a marginally small flow.
In all six representations it can be seen that the velocities in the core of the tube have a different color than at the tube edge. But these colors in the contour plots do not always represent the same velocity value. From the legend it can be seen that the blue color always has smaller values than the red color. This means either that the flow in the blue area is slower, comes to a standstill or flows in the opposite direction. In Graph 1 for example, the velocity at the tube wall is zero, where as in graph 2 there is a negative gas flow in the opposite direction.

The last test for the low frequency function is to verify if there is a change in the mass or in the outlet velocity when the pressure is kept constant at a high level. For this purpose, only the first pressure ramp was generated and then the pressure was kept constant for more than 20 seconds at a high pressure plateau. Figure 18 shows no change in mass or velocity. For further verification, a contour plot was generated again, but with fixed limits for the velocities. From the figures in Figure 21, it can be seen that the difference in velocity disappears after a few seconds and the velocities stagnate in the tube.

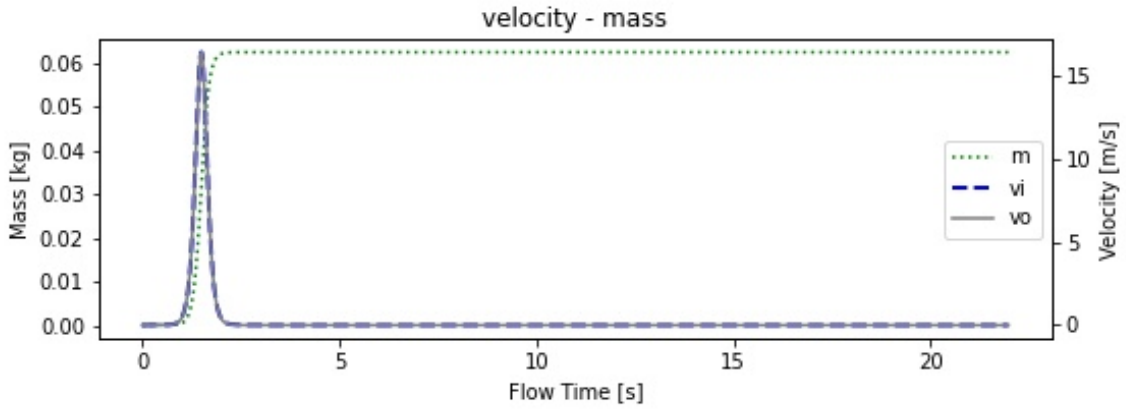


Figure 18: *The mass and velocity curve indicate that a constant pressure results in constant mass and constant velocity.*

### 4.1.2 Adjusting the high frequency jet part

For the high frequency jet gas, the term `(1+amplitude2*sin(2*3.1415926*frequency2*time)` was multiplied to the inlet function of the `pressure_inlet_square` boundary condition. Thus amplitude2 and frequency2 are added as additional variable terms. Since it was already verified that a change in frequency only leads to variability in the number of oscillations, this test was not repeated again. For frequency2 a value of 10 Hz was selected for all experiments which corresponds to 600 cycles per minute.

The first attempt to simulate low freuqency (LF) and high freuqency (HF) together (V015), can be seen in Figure 22. An amplitude2 of 0.03 was chosen for this simulation, which corresponds to a pressure of 1389 Pa. In the left plot, the mass and the inlet and outlet velocities are shown. In the right plot, the pressure is shown instead of the velocity. It can also be seen that the mass correlates with the pressure curve. In all curves of the figure,

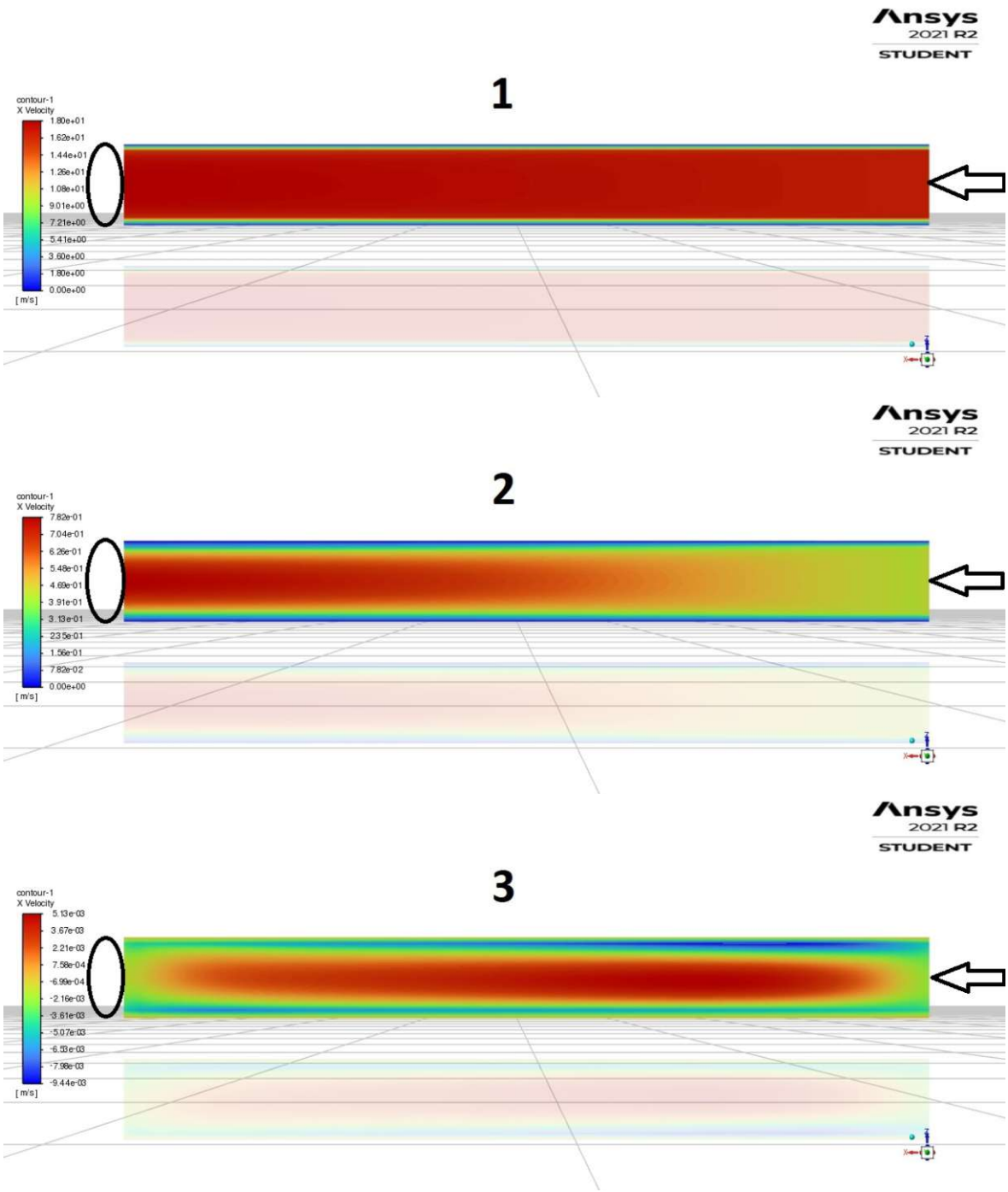


Figure 19: *These three contour plot show the velocities during inspiration and the high pressure plateau. The numbers of the images indicate the time when they were captured. The explanation can be found in the diagram of Fig. 17.*

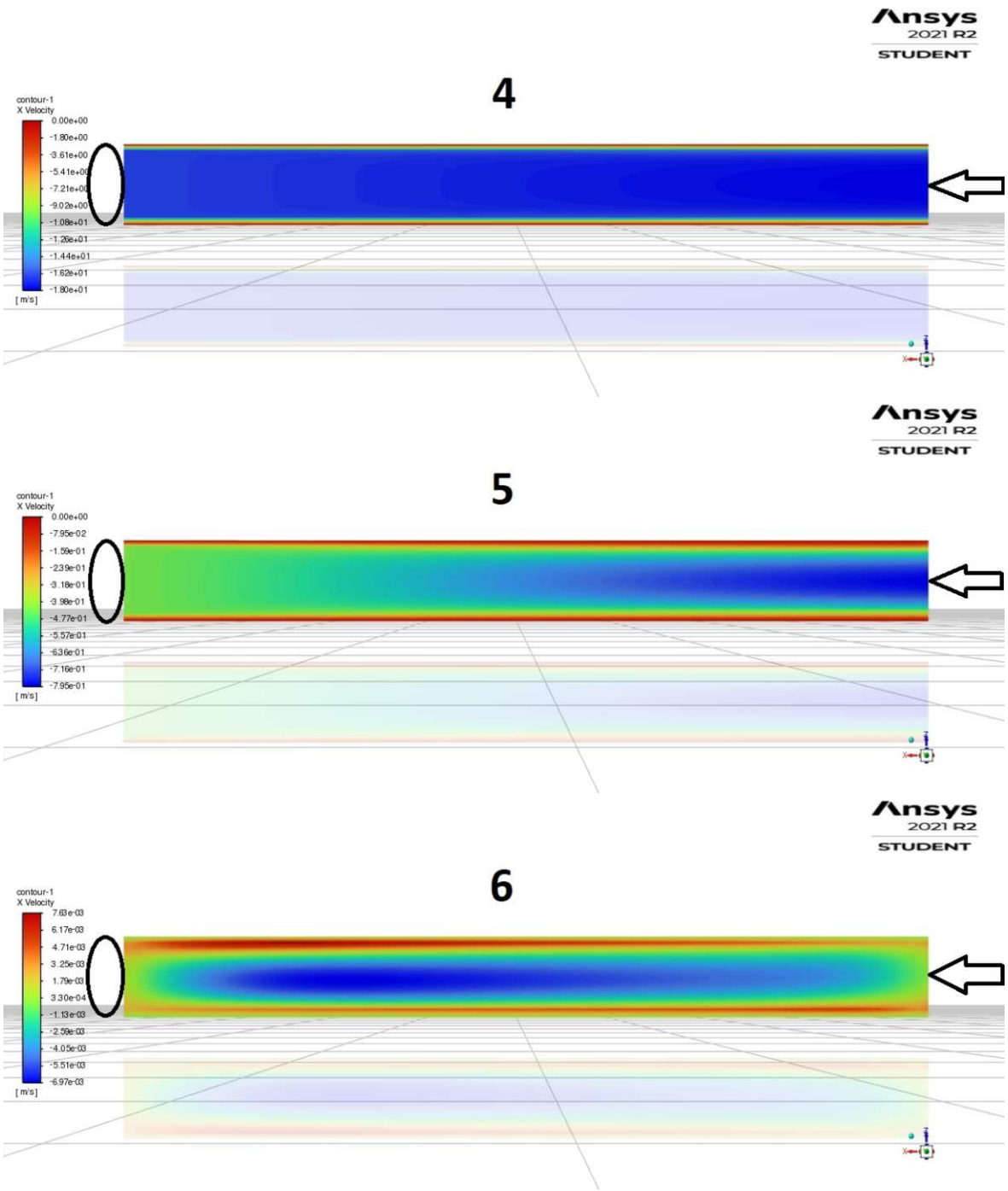


Figure 20: *These three contour plot show the velocities during expiration and the respiration pause. The numbers of the images indicate the time when they were captured. The explanation can be found in the diagram of Fig. 17.*

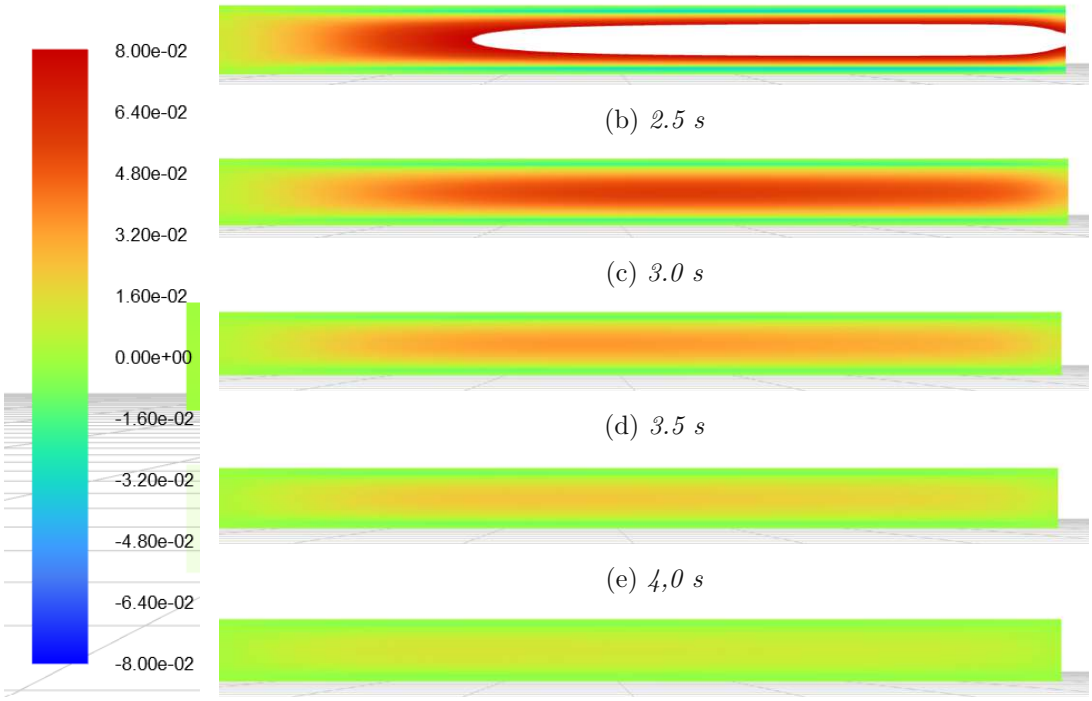


(a) *Legend*

(b) *2.5 s*

(c) *3.0 s*

(d) *3.5 s*

(e) *4,0 s*

(f) *5,0 s*

Figure 21: *Progression of velocities at constant pressure of 50000 Pa within 2.5 seconds.*

Table 7 *Preliminary test parameter for low and high frequency terms*

| name | pressure $[Pa]$ | A1 NF | A2 HF | time step $[s]$ | rate ts $[s]$ | notes |
|---|---|---|---|---|---|---|
| V015 | 24000 | 46300.0 | 0.03 | 0.001 | 10 | A2 very high |
| V016 | 25000 | 50000.0 | 0.005 | 0.001 | 10 | A2 comparison |
| V017 | 25000 | 50000.0 | 0 | 0.001 | 10 | A2 comparison |
| V018 | 25000 | 50000.0 | 0.0005 | 0.001 | 10 | A2 comparison |
| V019 | 25000 | 50000.0 | 0.00005 | 0.001 | 10 | A2 comparison |
| V021 | 25000 | 50000.0 | 0.00005 | 0.0001 | 10 | V019 different ts |
| V022 | 25000 | 50000.0 | 0.0005 | 0.0001 | 10 | V018 different ts |
| V023 | 25000<br>30000 | 50000.0 | 0.00005 | 0.001 | 10 | PEEP-test |
| V025 | 25000 | 50000.0 | 0.0005 | 0.0006471 | 10 | mesh size, ts |

the HF oscillation is clearly visible. The set amplitude is apparently already sufficient to generate velocities in the tube almost exactly as high as those generated with the low-frequency oscillation. The amplitude of the oscillation was compared with Figure 6 and, on the basis of this, set to a lower value in the further course of the work.
In the pressure mass plot it can generally be seen well that the mass curve follows the set pressure profile. This behavior could already be seen in the LF curves.

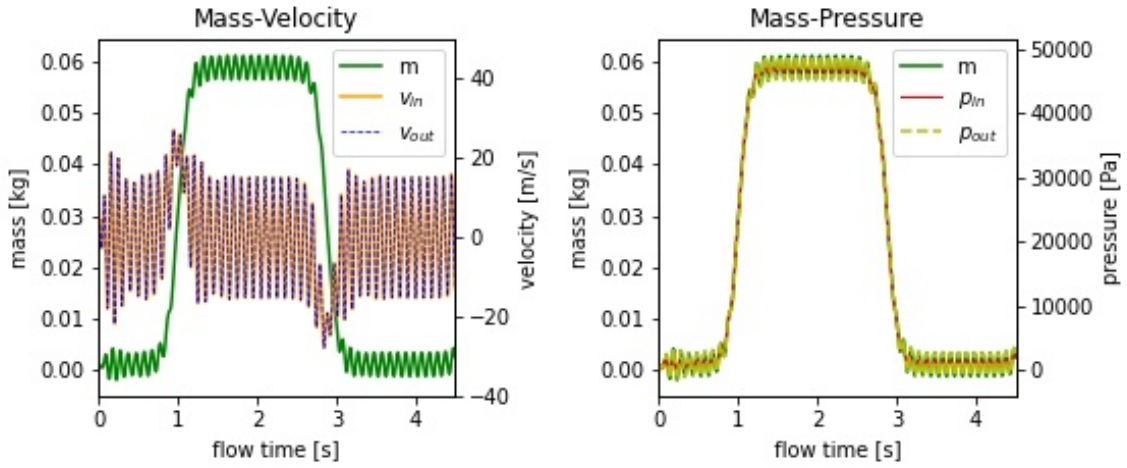


Figure 22: *First test with high and low frequency terms with the effect on velocity and mass. The amplitude for the HF term has a value of 0.03 which corresponds to a pressure of 1389 Pa.*

The next tests were performed with varying the amplitude magnitude (V016-V022). The amplitude of the high frequency can be seen as a percentage of the low frequency flow. Thus, at an amplitude of 0 the gas has no additional pressure due to the HF, at A 0.00005 the amplitude maximum has a value of 2.5 Pa, at A 0.0005 one of 25 Pa and at A 0.005 250 Pa are reached. In this case, A 0.0005 and A 0.00005, as seen in Figure 23, produce an oscillation that is hardly noticeable in the mass and and slightly more noticeable in the velocity diagrams. This is evident when looking at amplitude2 in comparison to amplitude1 in table 7. In relation to 50000 Pa, 25 Pa and 2.5 Pa are very small. In the plot of A 0.005 (bottom right) a pressure peak of 250 Pa is generated, whereby the oscillation is already clearly visible. The effect of the high frequency is thus visible in the mass curve as well as the velocity curve. Based on the velocity curve, it is easy to see that this high-frequency flow consistently generates a sinusoidal flow in the direction of the lungs, even if there is no pressure from the low-frequency jet.

A critical parameter in CFD simulations are the scaled residuals, which are used to control the convergence of the calculation. In order to improve this, the time step must be reduced, which was done in V021 and V022 in comparison to V019 and V018.

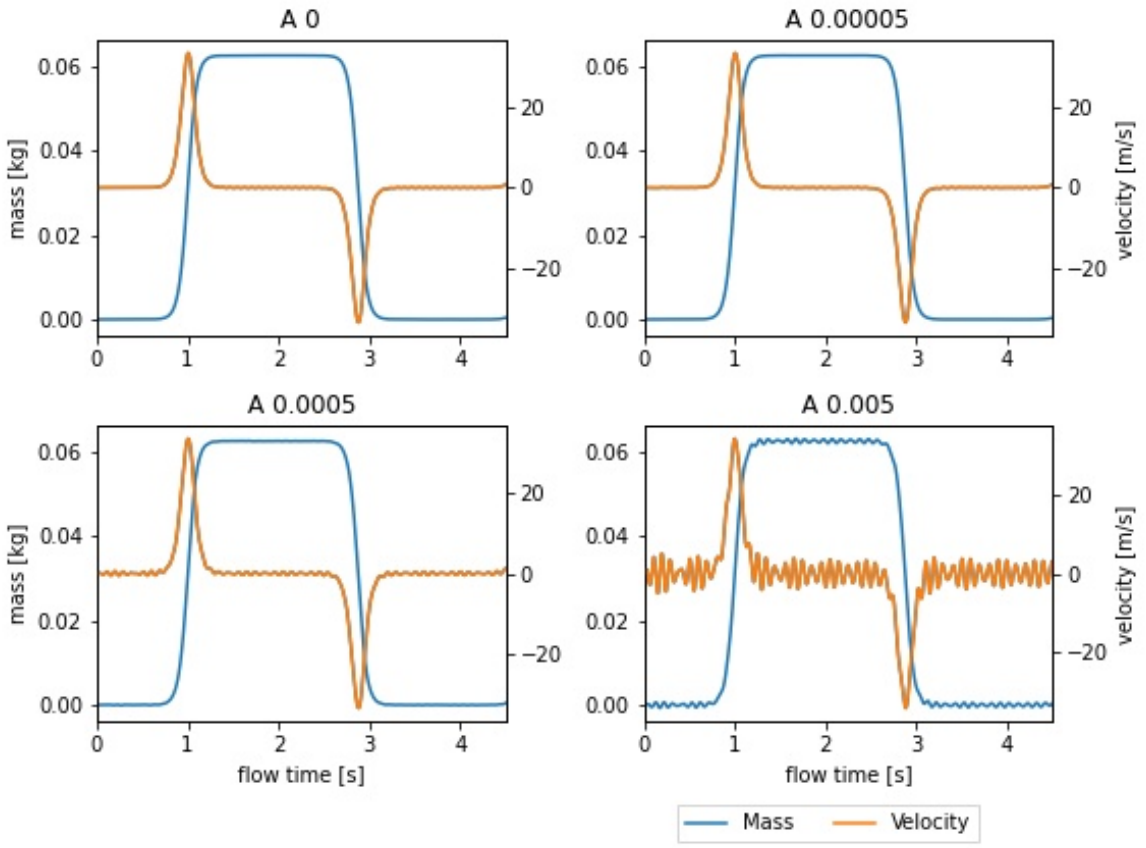


Figure 23: *Within these diagrams the only parameter changes is the amplitude of the high frequency term. The HF is seen best in A 0.005 (bottom right) in the mass and velocity curve. In contrary, the plot A 0 in the upper left position shows the graph with no HF oscillation.*

In the next step, the positive end-expiratory pressure (PEEP) was integrated into the curve of V023. For this purpose, starting with the second if argument of the `pressure_inlet_square` boundary condition, the initial pressure was increased and additionally the divisor of the the tangent hyperbolic argument was increased from 2 to 2.5. These changes were compared to V018 and Figure 24 (right plot) shows that the new function only affects the lower pressure level and thus produces a PEEP at 10000 Pa.

Next, a finer mesh was created for the tube and verified that the previously used mesh was

accurate enough for the calculations. When comparing meshes, it is important to note that the time step must also be changed in percentage, otherwise the relationship between time step and mesh size will no longer be correct. The left plot in Figure 24 shows the comparison of V018 and V025 on basis of the mass. It can be seen, that there is no significant difference between the mass curves due to the mesh size.

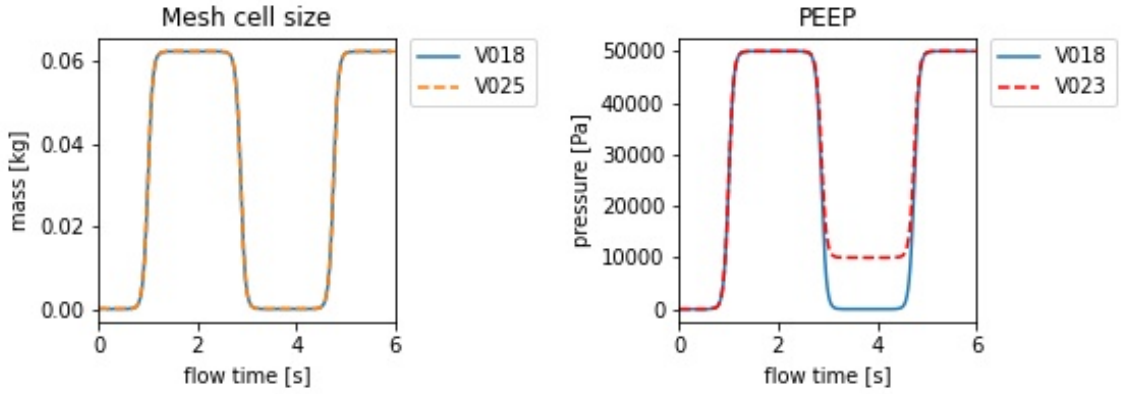


Figure 24: *The right image shows that the difference between the two networks is not significant. The left image shows that the described changes to the function only have an influence on the lower pressure level.*

The results of the high- and low-frequency pressure curves are again analyzed using contour plots. In Figure 25, the times at which the contour plots were created were again marked with horizontal lines. In order to see the influence of the high frequency, not only two points on the plateaus were selected, but four closely spaced time points. The bottom plot in this figure shows the high frequency curve in detail to see exactly which phase the oscillation is in and which contour plot depicts that moment. This graph shows the magnitude of the velocity, which can be seen by the fact that both velocity peaks point in the same direction. This graph shows the magnitude of the velocity, which can be seen from the fact that both velocity peaks point in the same direction. Since in the more complex lung geometries the outputs no longer look in one direction, the magnitude of the velocity was chosen for plotting the results. To ensure that the results are comparable, the magnitude of the velocity was selected for this and the following diagrams instead of the velocity in the x-direction.

Inspriation (1) and expiration (2), respectively, are shown in Figure 26 and depict the same picture as in the low-frequency plot (Fig. 19, plot 1 and Fig. 20, plot 4). A flow velocity in one direction is present throughout the tube. Into the lung is shown in red and out of

the lung in blue. For both, the flow velocity at the wall is zero. If the legend is examined more closely and compared with that of Fig. 19 or 20, it is noticeable that the maximum speed is slightly reduced in both the positive and negative directions. This is due to the superposition of the two waves. Considering the velocity magnitude curve of Fig. 25, one can see an overlapping oscillating profile even with the largest increase in velocity. Amplifications as well as cancellations of the amplitudes occur, which then results in a slightly higher or also a slightly lower maximum velocity than with the plain low-frequency curve.

Since the low-frequency flow on the pressure plateaus has a constant amplitude, there is no longer any superposition. Thus, the velocity in the tube is exclusively dependent on the high-frequency flow, Fig. 27 and 28. If the high frequency curve rises or falls, the velocity mapping is the same as during inspiration or expiration. However, the maximum and minimum velocity is much lower (approx. 3 m/s (plot 3) instead of 13 m/s (plot 1)). At the high point and low point there is a change of direction in the tube. This can be seen in plot 4, 6 and 10. At the high point and low point there is a change of direction in the tube. This can be seen in plots 4, 6 and 10. As already described for the low-frequency contour plots, the flow in the center of the tube remains in the direction for the longest time, while a flow in the opposite direction occurs at the edge. However, the velocity difference between the two flows is smaller here than in the LF plot.

### 4.1.3 Adapting the system to the lung geometry

The previous tests until this point were all performed on a tube with 0.1 m in diameter and a length of 1 m. However, the lung geometry is much smaller (18 cm in diameter at the inlet) and consequently the system must be scaled down. The tests were carried out both with the scaled tubes from the preliminary tests and with a simplified lung geometry. The simplified lung geometry refers only to the trachea (Gen0) in the initial tests.

In the first scaling tests, the resulting curves did not behave as in the other tests. The high inlet pressure of 50000 Pa was identified as the cause of problem after some trials and a lower pressure of 500 Pa was selected for the smaller system. The tests were first calculated only with the low-frequency term and only after verification of the results the high-frequency term was added.
ANSYS Fluent offers the possibility to change the geometry directly in the program. To see

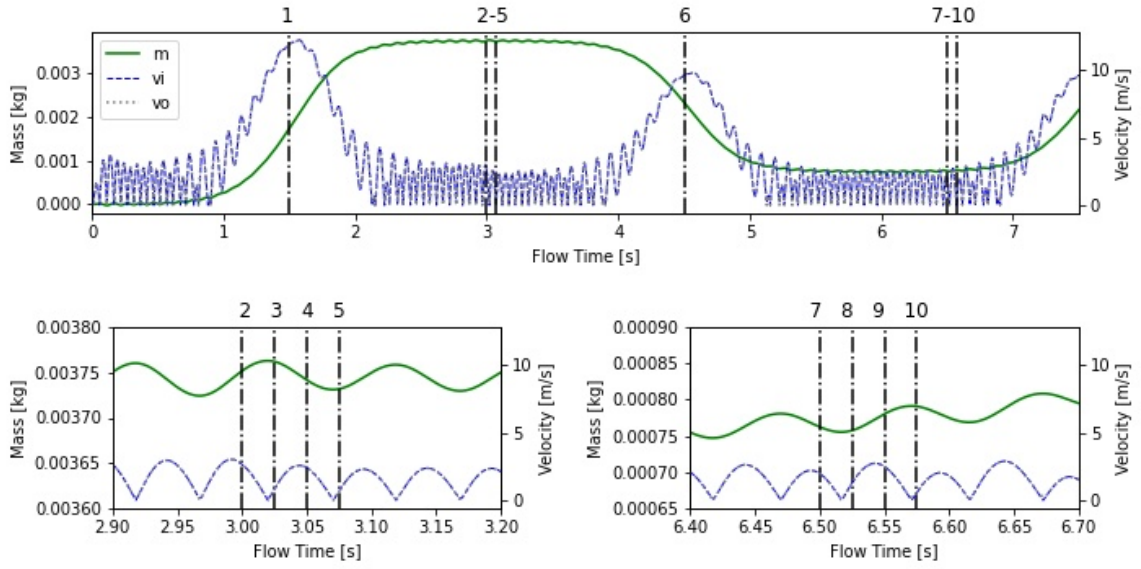


Figure 25: *Time marks for the high and low frequency function results. The horizontal lines indicate at which point in time the contour plot was created and how high the velocity magnitude was at that point in time.*

the influence of scaling, the simulations were performed once with the original tube size and once with reduced tube size.Because the reduced tube in V028 was redrawn with a factor in Fluent, it was only approximated to the trachea and did not exactly match the trachea dimensions. The dimensions of the tube in V028 were a diameter of 20 cm and a length of 12 cm. As expected, Figure 29 shows that at the same pressure at the inlet, the velocity in the small tube is much higher than in the large one.

In transferring these parameters to the lung geometry, it was noticed that the residuals became very high during the pressure rise. As a result, the time steps were reduced in version Lung_V009, but this did not result in any improvement. Next, the ramp of the tangent hyperbolic function was adjusted by reducing the rate. This reduced the increase in the residuals. However, as can be seen in Figure 30, the rate cannot be decreased arbitrarily. At small values, the increase took a very long time and the desired pressure could not be achieved in the time specified by the frequency. This caused a step between the consecutive functions in the UDF, which in turn caused oscillations in the velocity and mass curves. Therefore, the frequency was slowly increased during the tests and a value of 3.5 proved to be a good compromise.

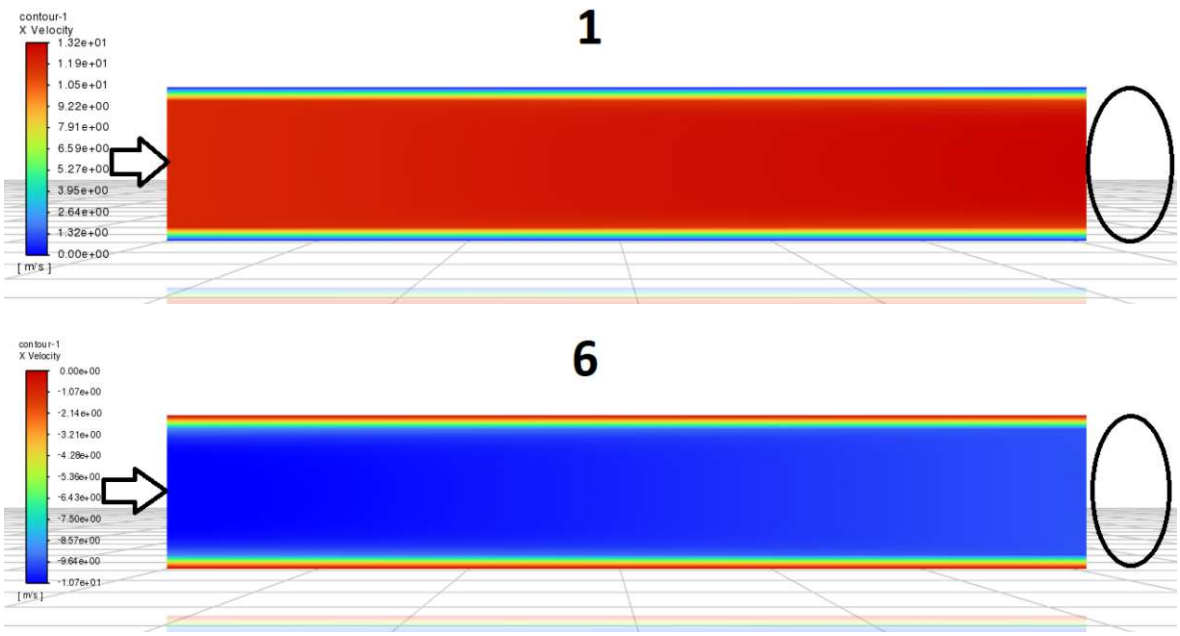


Figure 26: *The two contour plots for inhalation (top) and exhalation (bottom) show the same behavior as in the low-frequency-only plot. The numbers of the images indicate the time when they were captured. The explanation can be found in the upper diagram of Fig. 25.*

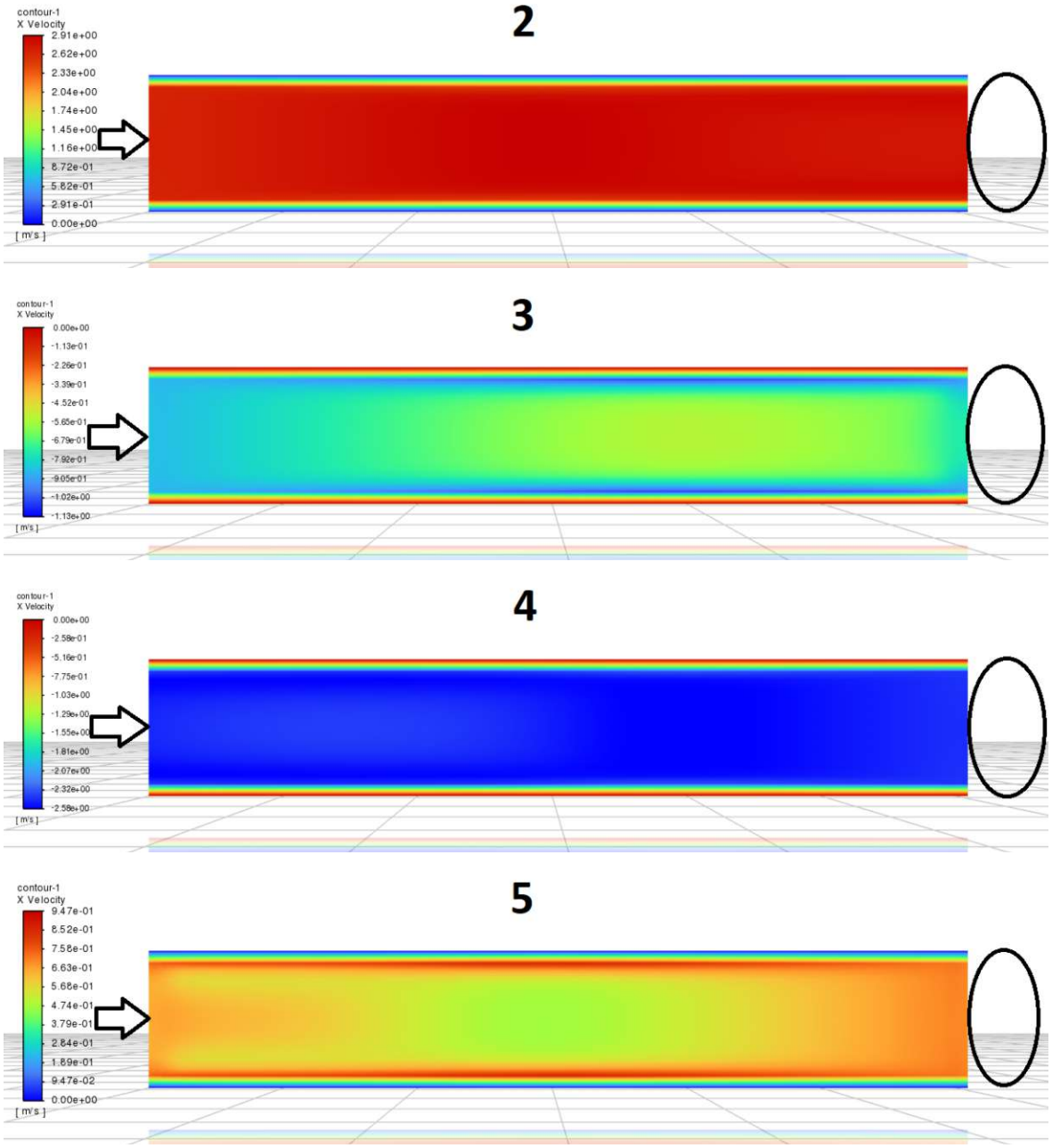


Figure 27: *In these four images, the influence of the high-frequency flow during the phase of the high-pressure plateau can be seen. Depending on which phase of high frequency the image is made, the gas either has a velocity toward the lungs (2), out of the lungs (4), or several different velocities occur (3 & 5). The numbers of the images indicate the time when they were captured. The explanation can be found in the diagram bottom left of Fig. 25.*

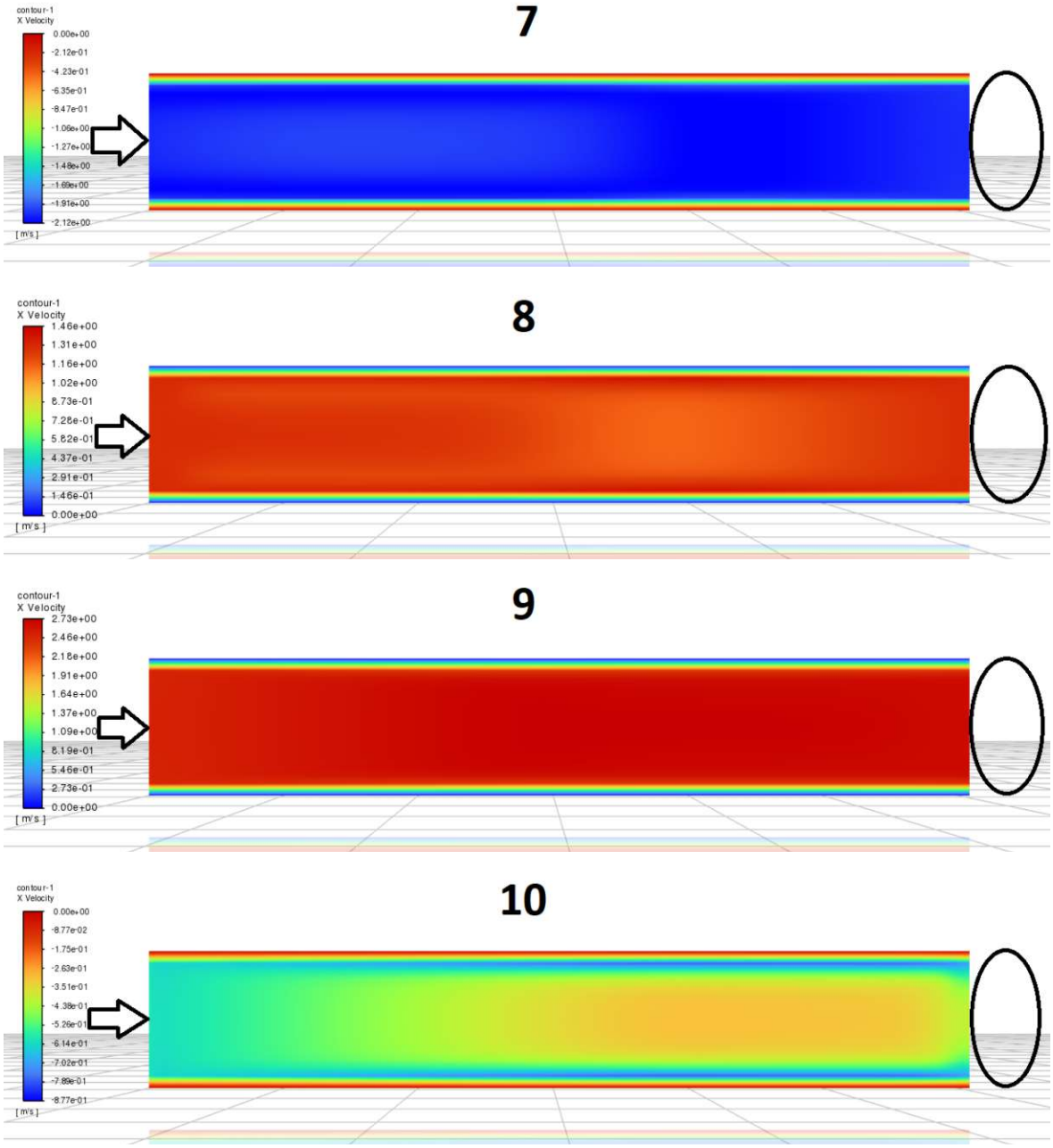


Figure 28: *There is also high frequency flow at the PEEP level. The velocities on the flow images depend on the position of the HF oscillation. The numbers of the images indicate the time when they were captured. The explanation can be found in the diagram bottom right of Fig. 25.*

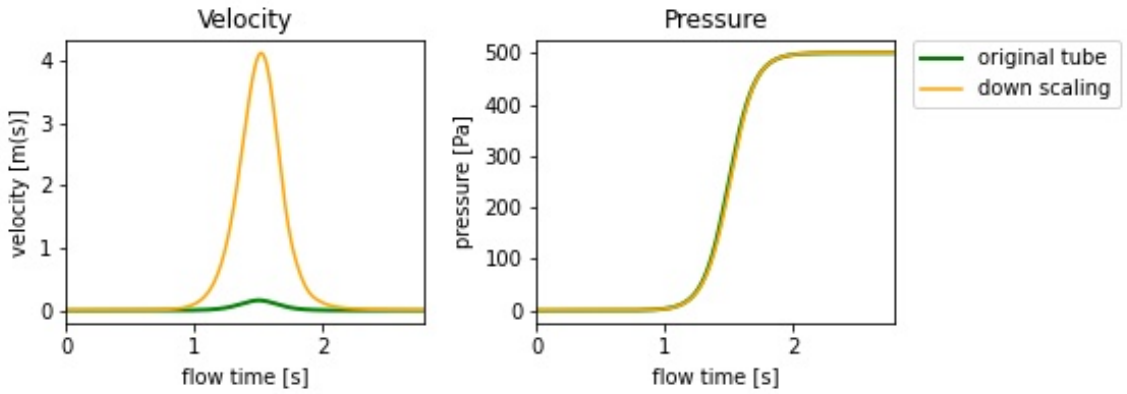


Figure 29: *The effect of scaling can be seen here. The same pressure curve results in different velocities if the tube diameter varies. For a bigger tube the velocity is much lower than for a smaller tube.*

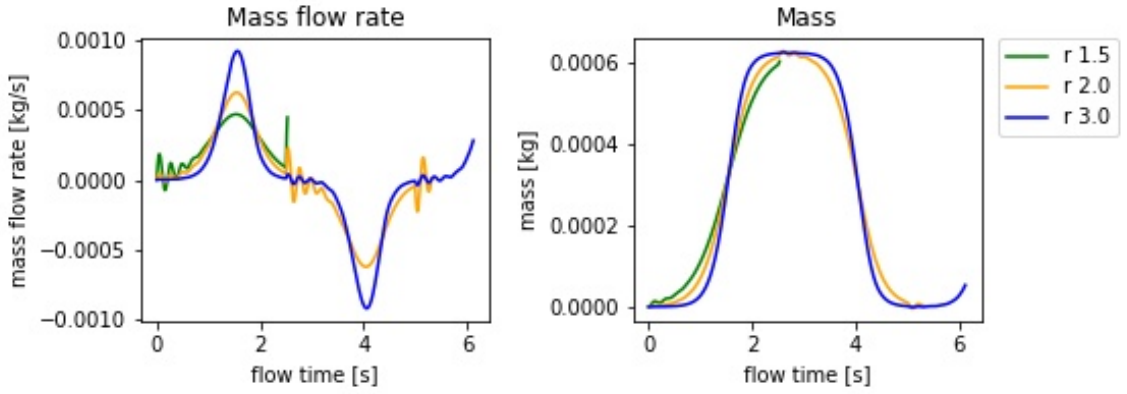


Figure 30: *If the rate is too low, the specified pressure will not be reached in the desired time and will result in a step between the contiguous functions in the UDF. This causes the unwanted oscillations in the graphs.*

Table 8 *Preliminary tests to adapt the parameters to the lung geometry*

| name | pressure $[Pa]$ | A1 NF | A2 HF | time step $[s]$ | rate ts $[s]$ | notes |
|---|---|---|---|---|---|---|
| V027 | 250 | 500 | – | 0.0005 | 5 | not scaled |
| V028 | 250 | 500 | – | 0.0005 | 5 | scaled |
| V030 | 250<br>300 | 500 | 0.005 | 0.0005 | 2.5 | LF+HF+PEEP |
| V031 | 1498<br>1800 | 3000 | 0.01 | 0.0005 | 2.5 | real values |
| Lung_V009 | 250 | 500 | – | variable | 5.0 | different time steps |
| Lung_V010 | 244.5 | 500 | – | 0.0001 | 1.5 | Gen0 6438 |
| Lung_V011 | 250 | 500 | – | 0.0001 | 2.0 | Gen0 6438 |
| Lung_V012 | 250 | 500 | – | 0.0001 | 3.0 | Gen0 6438 |
| Lung_V013 | 1500<br>1800 | 3000 | 0.01 | 0.00008 | 3.5 | real values<br>factor tests |
| Lung_V014 | 1500<br>1800 | 3000 | 0.01 | 0.00008 | 3.5 | Density test |

As soon as the results with the low inlet pressure were comparable again with the previous preliminary tests, the parameters were adjusted to reality. Although the gas comes out of the nozzle of the converter of the ventilator with a pressure of 0.5 bar, this pressure decreases significantly in the tubes and has a pressure of only a few millibars at the inlet of the trachea. [3] In Carl Reiner's high frequency superimpose jet ventilator, the airway pressure is measured at the beginning of the endotracheal tube, see the red line in Figure 7. These pressure values can be seen in the diagram of Figure 6 and served as a template for the simulation parameters. The modified parameters of these tests are summarized in Table 8.

Table 9 *Pre-tests on the compliance and changing symmetry axis*

| Name | Gen0 | Sym. axis | $p_{out}$ | Compliance | Vol [L] |
|---|---|---|---|---|---|
| Lung_V013d | half | 1 | 800543.*mass | 0.2 | 6 |
| Lung_V013f | quarter | 2 | 800543.*2.*mass | 0.2 | 6 |
| Lung_V013g | whole | 0 | 800543.*mass | 0.1 | 3 |
| Lung_V013h | quarter | 2 | 800543.*4.*mass | 0.1 | 3 |
| Lung_V013i | half | 1 | 800543.*2.*mass | 0.1 | 3 |
| Lung_V013j | whole | 0 | 800543./2.*mass | 0.2 | 6 |
| Lung_V013k | quarter | 2 | 800543.*20.*mass | 0.02 | 0.61 |
| Lung_V013l | quarter | 2 | 800543.*10.*mass | 0.04 | 1.25 |

As already mentioned in chapter 3.1, symmetry axes were created in the geometry in order to be able to design the lung model larger. However, this also changes the factor of the pressure boundary condition at the outlet.

In this preliminary tests, various factors were tested on multiple Gen0 geometries. The whole tube without a symmetry axis, a half tube with a symmetry axis and a quarter tube with two symmetry axes were used for this purpose. For the variation of the compliances, the term 800543*factor was changed in the pressure outlet boundary condition. Since the compliance correlates with the lung volume, the volume was calculated with $V = m/\rho * 1000 * symmetry$ for the evaluation of the results and are illustrated in graph 31. It can be seen, that a compliance of 0.1 results in a lung volume of 3 L, whereas 6 L are achieved at a value of 0.2. Furthermore, it can be seen that the factor must additionally be adapted to the geometry. Thus, for a compliance of 0.1, the quarter tube must be multiplied by a factor of 4 and the half tube by a factor of 2 to obtain the same result for the whole tube without a factor. For the main simulations, the factor was chosen so that a maximum of 6 L of air is blown into the lung.

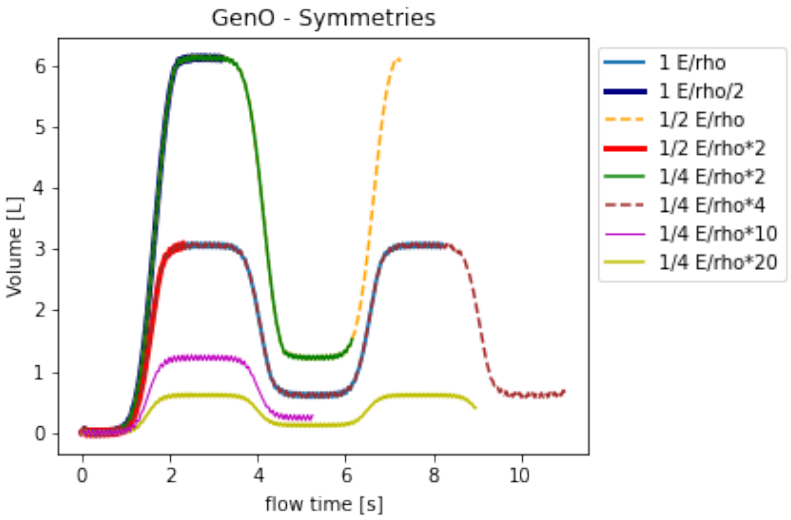


Figure 31: *This diagram shows all generation 0 geometries. Number 1 refers to the whole tube, 1/2 to half of the tube and 1/4 to a quarter tube. By varying the term 800543*factor, the compliance and also the lung volume can thus be adjusted. A compliance of 0.1 results in a volume of 3 L whereas 6 L are achieved at 0.2.*

At the concluding stage of the pre-test, the dependence of the results on density was verified. All previous tests were calculated with an air density of 1,225 kg/m³ at 15°C. For the comparative calculation, a value of 1.1839 kg/m³ at 25°C was chosen. Figure 32 clearly shows that there is no deviation of the results due to the density and therefore this parameter does not have to be considered in the further course.

The results of these pre-tests were primarily an information for the adjustment of the parameters. The selected setting of the parameters for the low and high frequency curves, which are applied in the following tests, is summarized again in Table 10.

Since the following tests were performed with more complex geometries, a mesh dependence check was performed again for Gen4. Therefore, three different tight meshes were created. A coarse mesh with 41248, a medium mesh with 67503 and a fine mesh with 113359 nodes. The figures of the three meshes can be seen in chapter 3.2 in Fig. 5. In Figure 33, the coarse and fine meshes are compared to each other and no deviations can be found in terms of mass and mass flow rate but also in terms of pressure and velocity. Based on this evaluation, the medium mesh size was used to create the meshes for generation 0, 1, 2 and 3.
Each lung geometry used for the main simulation was tested in advance with a simulation at

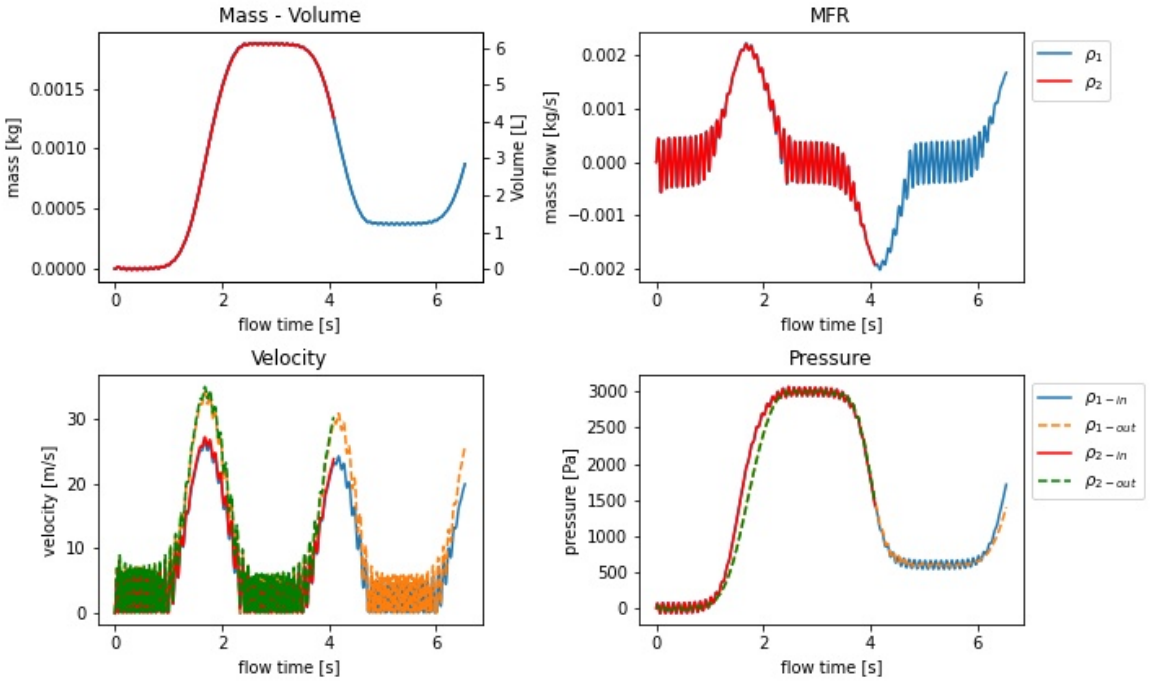


Figure 32: *Changing the air density in the calculations does not affect the results. The air densities at 15 °C (ρ=1.225 kg/m³) and at 25 °C (ρ=1.1839 kg/m³) were compared.*

Table 10 *Final Parameter for the user defined function*

| Parameter | name | Value |
|---|---|---|
| High pressure plateau | Amplitude1 | 3000 |
| Low pressure plateau | Amplitude2 | 0.01 |
| Low Frequency | frequency1 | 10 |
| High Frequency | frequency2 | 10 |
| Starting point | pressure1 | 1500 |
| PEEP level | pressure2 | 1800 |
| | offset | 1.5 |
| | rate | 3.5 |

constant pressure and/or constant velocity to see if there were any errors or if the geometry was ready for use.

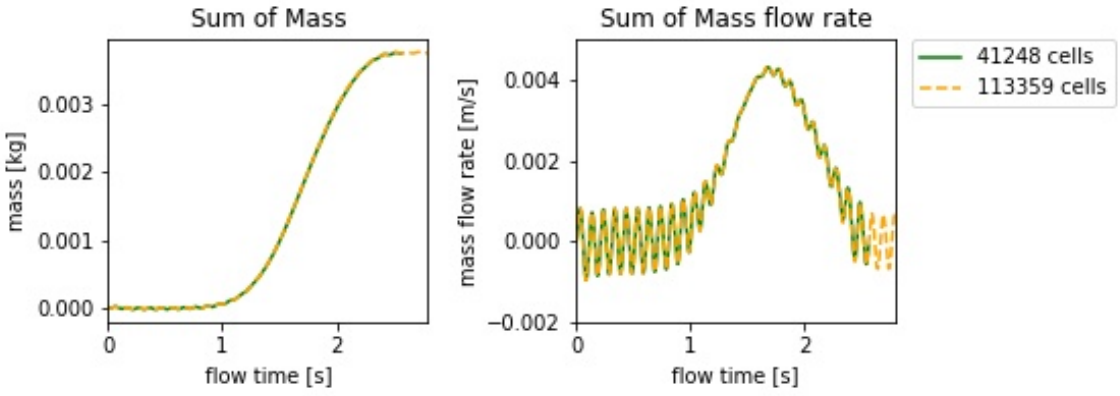


Figure 33: *The mesh dependence was tested again for Gen4. No deviations can be seen in either the mass or the mass flow rate.*

### 4.1.4 Discussion of preliminary tests

When a simulation system is set up, many parameters must be verified to produce reliable data. Only single parameters may be changed for new simulations to see the corresponding effect of the changed parameter as for example in figure 14. Since not all parameters of a real systems are given for simulations, assumptions have to be made repeatedly or, in the ideal case, the results can be compared with existing data. For example, the test of different pressure rates in figure 15 showed that this parameter has a large influence on the velocities in the system. However, this could only be estimated and would have to be verified with experimental tests. In this work, due to the lack of comparable data, the rate for example was chosen in such a way that the residuals in the CFD simulation do not increase abruptly and at the same time the desired curve remains. Thus, however, they can only be seen as guide values.

For the low frequency part, the most noticeable result is the gas flow inside the tube when the pressure is kept constant. The results of figure 19 can probably be explained by looking at the pressure gradient. The system is programmed so that the mechanical ventilator initiates a fixed pressure at the inlet, which follows a pressure profile, while there is no pressure at the outlet, thus in the lungs. The gas flows into the lungs and a counter pressure builds up

there. As soon as the gas pressure at the inlet is kept constant, the excess pressure that is likely to be present in the lungs at this time, can flow in the opposite direction. In this way, a equilibrium between inlet and outlet is established over time, as shown in Fig. 21. The same effect can also be observed after the pressure drops from the high pressure plateau either to zero, Figure 20, or to a positive end expiratory pressure level (PEEP). Another effect can be seen in the contour plot, right before the beginning and end of the tube. The velocities in diagrams 3 and 6 of Fig. 19 and 20 are nearly zero, highlighted in orange (inspiration) or green (expiration). At these location points, the positive and negative flows probably cancel each other out.

As soon as the high-frequency component is added as a sinusoidal oscillation, the constant state on the pressure plateau just described no longer occurs. How strong the influence of the high frequency is depends on the amplitude level as can be seen in Fig. 22 and 23. Already 3% of the curve pressure means that the velocity maximum of the low-frequency part is not significantly higher than the velocities of the individual HF oscillations. This would possibly be a setting for a patient with a very stiff lung, but for the simulations in this work, an amplitude between 0.5 and 1 % of the pressure was chosen to be able to distinguish the high-frequency from the low-frequency part and because these are typical values from the clinic.
The contour plots, Figure 26 to 28, show in comparison to those of the low frequency that the directions of the flow change continuously. Since there is no inertia term or anything else in the programmed user defined function that keeps the flow in the lungs longer during the simulation, the system reacts immediately to any change. At each positive and negative peak there is a turnover of the flow. Probably the same happens as with the LF, that there is a parallel flow in the tube for a short time and the flows extinguish each other before there is a flow in the opposite direction. However, since it happens much faster, it cannot be reconstructed more accurately in the available figures.

When working with symmetry axes, as was done with the lung geometry then, there are again several points to consider. The advantage of it is that the element number of the cells and thus the computation time can be reduced, however it leads to a further deviation from reality, since an idealized geometry is assumed. The parameters must be adapted to the corresponding symmetry of the geometry, which increases the error susceptibility again. As can be seen in Figure 31, the factor must be in accordance with the symmetry axis to obtain adequate results.

## 4.2 Main simulations

To perform calculations across multiple generations, the data from the paper by Jagan and Jayalalitha [51] are considered in more detail. Since only the tube systems up to the beginning of the alveoli are considered below, the data are analyzed up to the $17^{th}$ generation. In figure 34 on the upper left, it can be seen that the number of tubes increases with each generation and shows an exponential growth. The graph of diameter, upper right, correspondingly decreases with each new generation and an exponential decrease can be seen. The individual areas of the tube outlets, middle left, behave in the same way. As the diameter of the tubes gets smaller, the outlet area also gets smaller. However, as the number of tubes increases strongly, the sum of all outlet areas, center right, increases exponentially. The diagrams in the bottom row show a similar picture as before. On the left is the ratio of outlet to inlet, with the percentage again decreasing exponentially. For the calculation, the area at the beginning of the trachea (d = 18 cm) was always taken as the inlet and the end area of the respective generation as the outlet. On the right is the reverse picture again. The curve increases exponentially when the outlet area of a tube is multiplied by the number of tubes per generation and again related to the inlet of the trachea.
What is not seen in this last graph is that the sum of the outlets relative to the inlet decreases over the first three generations, and only becomes greater than the inlet from the fourth generation on.

All experiments considered in this section are summarized in Table 11. Either geometries with one axis of symmetry or with two axes of symmetry were used. The number of outlets corresponds to the geometry actually used. For example, in Gen0, the outlet with two axes of symmetry is only a quarter of the original size. Gen1 has also two symmetry axes, so the outlet is split in half. To obtain the amount of outlets in the real lung, the values in the table must be calculated times 2 for each symmetry axis. The pressure output summarizes the reset pressure used in each simulation and the compliance that was applied to it. Finally, the volume used for ventilation is noted.

The tests with a small number of tubes were primarily to see how the system behaved as the lungs progressed and to be able to draw conclusions about deeper regions.
The observation made from Fig. 34 is also reflected in the velocity diagram, Fig. 35. Due to the fact that the sum of the outlet area is smaller than that of the inlet, the velocity increases during inspiration from generation 0 up to the $3^{rd}$ generation. After that, the value for the

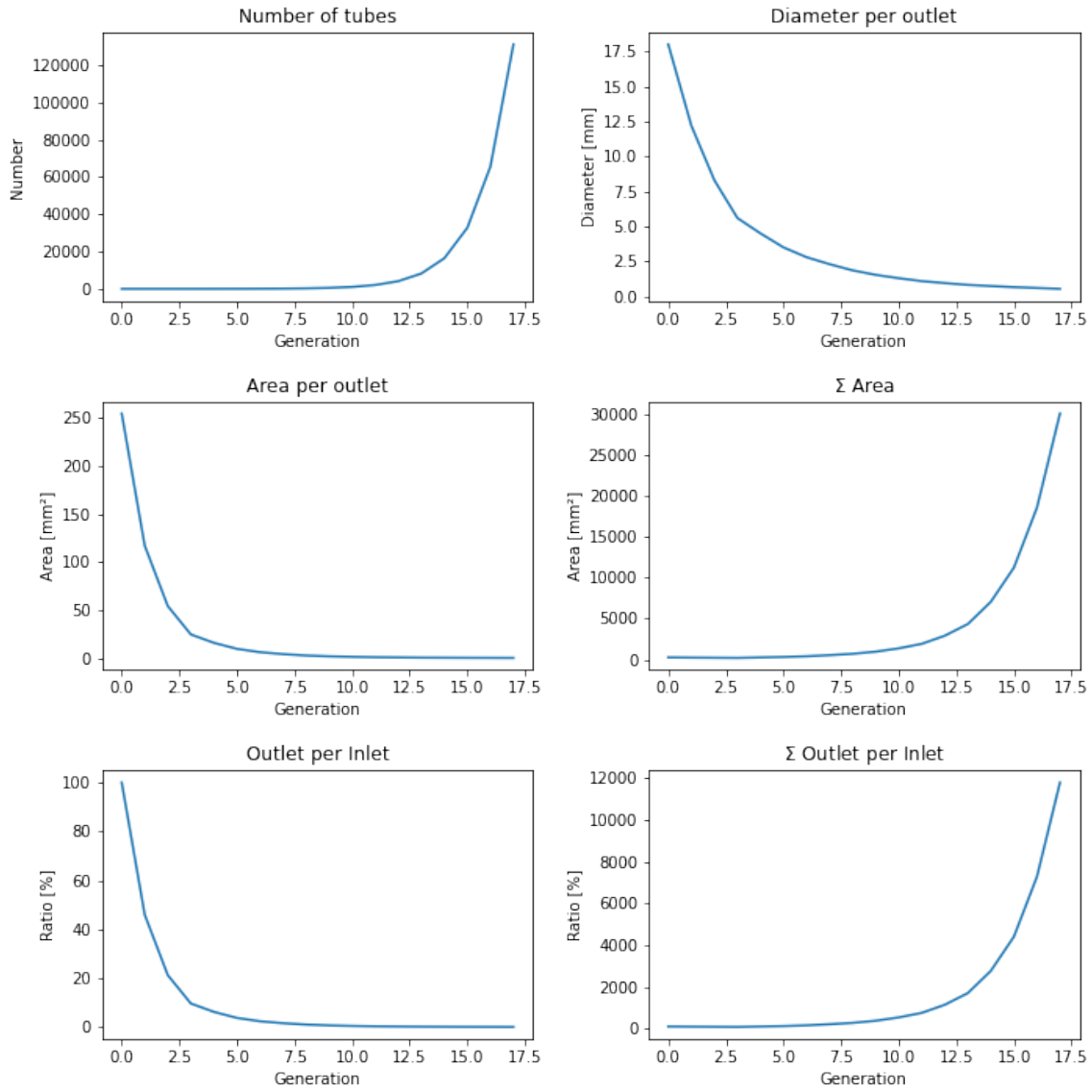


Figure 34: *These six diagrams serve to illustrate how the quantities in the title behave over 17 generations.*

Table 11 *Overview of the main simulations*

| Geometry | Sym. | Outlets | $p_{out}$ | Comp. | Vol [L] | Notes |
|---|---|---|---|---|---|---|
| Gen0 | 2 | 1/4 | 800543*2*m | 0.2 | 6.1 | |
| Gen1 | 2 | 1/2 | 800543*2*m | 0.2 | 6.1 | |
| Gen2 | 2 | 1 | 800543*2*m | 0.2 | 6.1 | |
| Gen3 | 2 | 2 | 800543*4*m | 0.2 | 6.1 | |
| Gen4 | 1 | 8 | 800543*8*m | 0.2 | 6.1 | 41248 nod. |
| Gen4 | 1 | 8 | 800543*8*m | 0.2 | 6.1 | 113359 nod. |
| Gen8 | 2 | 64 | 800543*128*m | 0.2 | 6.1 | |
| Gen8 | 2 | 64 | 8005429*128*m | 0.02 | 0.6 | |
| Gen8 | 2 | 64 | 800543*128*m<br>8005429*128*m | 0.2 | 6.1 | |
| Gen8 | 2 | 64 | 800543*128*m | 0.2 | 1.6 | HFO<br>$p_{in}$=785 Pa |

maximum velocity decreases for the $4^{th}$ generation and even more for the $8^{th}$ generation. A different picture emerges for the high frequency velocities. Generation 0 shows the highest speed. Generations 1 to 3 have very similar velocities, except for the first peak on the high-pressure plateau. However, they are all smaller than that of Gen0. For Gen4 and Gen8, the velocities are even lower.

Based on the information for generation 0 to 4 as well as generation 8, an average inlet velocity can be calculated. The approximate outlet velocities can be calculated via the ratio of the outlet totals to the inlet and result in the curve of figure 36. This curve shows that the velocity of the air decreases continuously, which is consistent with the literature that there is both turbulent and laminar flow in the lung. In this graph, it can be seen again that the velocity is highest at generation 3, because, as already discussed, the inlet area is larger than the sum of the outlet areas.

It is also interesting to note that the pressure curve flattens towards the outlets. As the pressure increases, the curve is flattest at Gen3, and little difference can be seen between Gen2 and Gen8. On the other hand, when the pressure curve drops, a different behavior of the system can be observed. There is a pressure delay that only becomes visible from Gen4 on wards. Since air is first blown into the entire lung system during the first inspiration

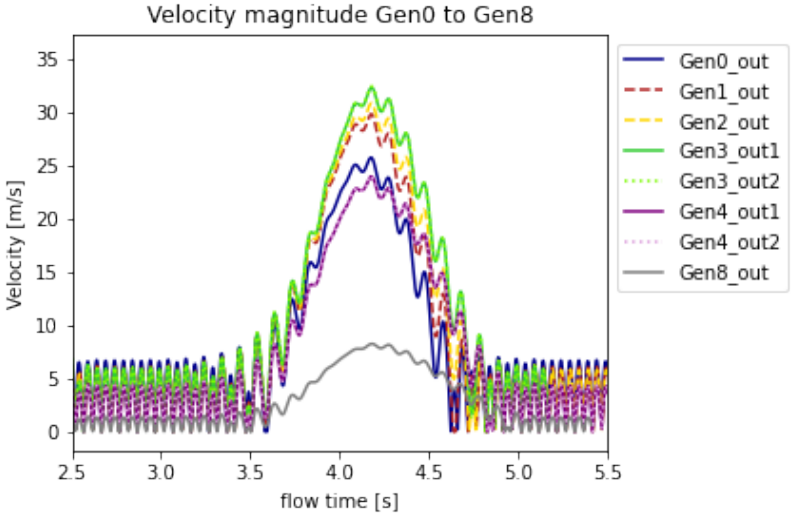


Figure 35: *The magnitude of the velocity is plotted across the outlets of the generations. It can be seen that, compared to generation 0, the velocities increase up to generation 3 and decrease thereafter.*

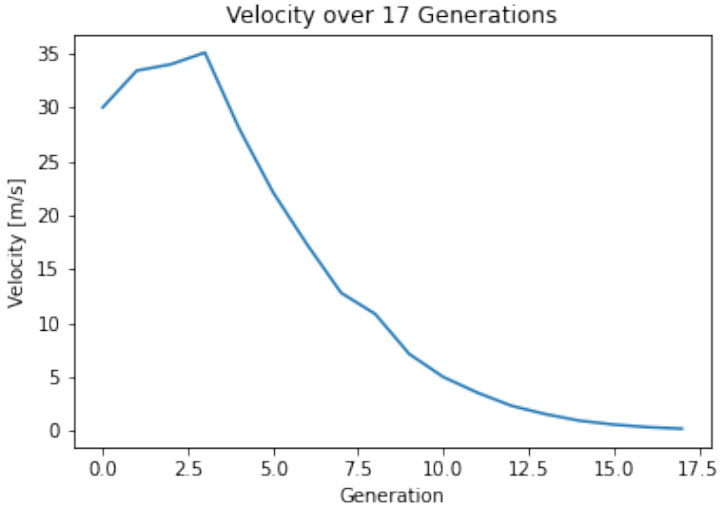


Figure 36: *This graph shows the estimated maximum velocity values for the first peak across 17 generations during expiration. The highest velocity is seen at generation 3 and after that they decrease exponentially.*

phase, the system probably reacts much faster. During the pressure drop at expiration, on the other hand, the air must first escape slowly, starting with the trachea, Gen0, through each generation. Therefore, the pressure drop in Gen8 occurs much later than in the others.

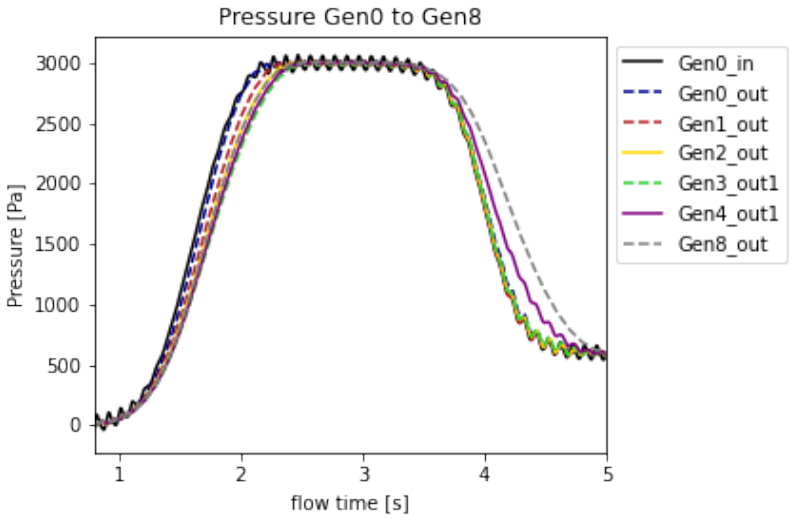


Figure 37: *There is a delayed pressure response of the pulmonary system during both inspiration and expiration. During expiration, the effect is more pronounced because the system must continuously reduce pressure over the generations.*

For further calculations, the velocity normal to the outlet was used instead of the magnitude of the velocity. Thus, the velocity becomes smaller by the amount of velocities pointing in different directions. Another difference is that the normal velocity indicates the direction of the flow with its sign, which is omitted for the magnitude of the velocity. The normal velocity is calculated from the mass flow rate, equation 9, divided by the area and density of the medium. As area A, the single outlet area or the sum of all outlet areas in the lung can be used.

$$v_n = \frac{mfr}{\rho * A} \tag{9}$$

Figure 38 shows all normal velocities at the outlets of Gen8. It can be seen that the velocities are not all the same, but vary between the individual outlets, especially for the inspiration phase. During expiration, on the other hand, the deviations are much smaller. However, in the case of the high-frequency part, no shifts can be seen. Only the amplitude height varies at the positive peak values.

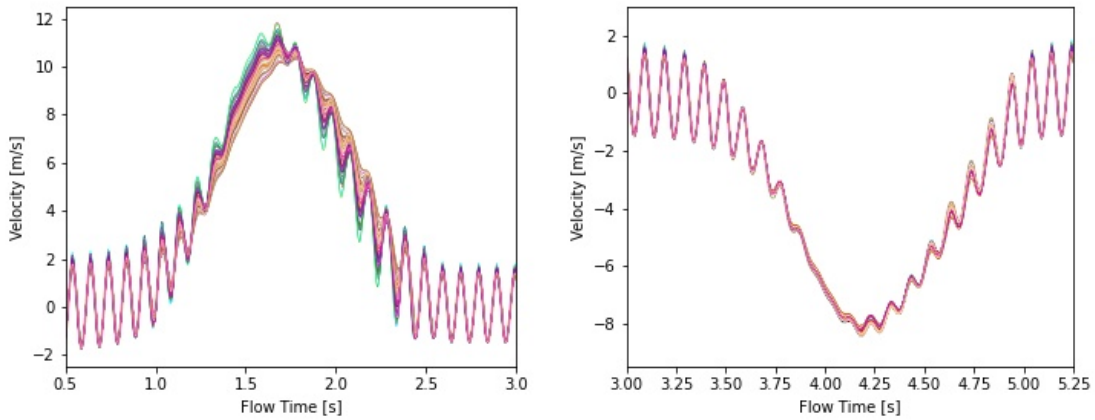


Figure 38: *The normal velocity curves of all outlets of the Gen8 are shown in these diagrams. It can be seen that as the curves increase, there is a shift in the individual curves. However, this shift is barely visible in the negative curve.*

### 4.2.1 Kinetic Energy

To determine the kinetic energy at the outlet of Gen8, equation 11, the mass change and normal velocity for each outlet, as well as the sum of all outlets were calculated. Since, the standard deviation of the mean mass of all Generation 8 outlets is very small (in the range of $10^{-7}$, which can be seen in Fig. 39), the change in mean mass of all outlets was used for the calculation. This is obtained by the following formula 10.

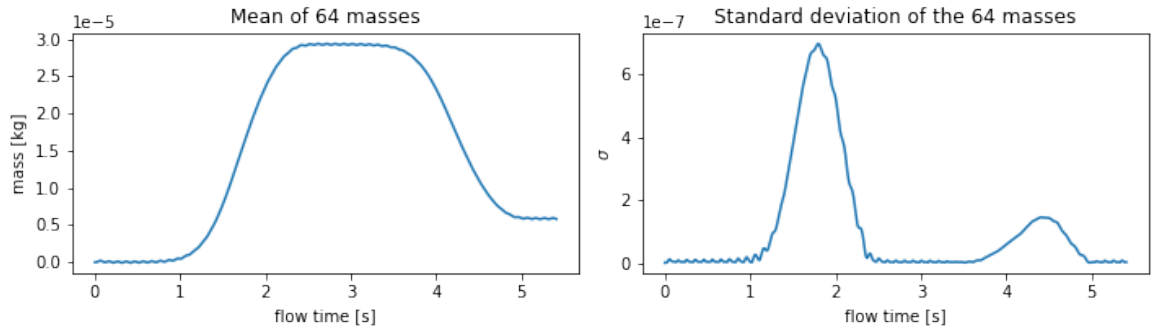


Figure 39: *In this diagram, the mean mass over all outlets of Gen8 and the standard deviation thereof were calculated.*

$$\overline{m} = \frac{m_n - m_{n-1}}{ts} \tag{10}$$

$$E_{kin} = \frac{\Delta\overline{m} * v_n^2}{2} \tag{11}$$

A comparison was made between the low-frequency flow and the superimposed flow in terms of kinetic energy, see Fig. 40. The left graph shows the sum of the kinetic energy over all outlets and the right graph shows the integral of the kinetic energy. It is easy to see that the peak receives several higher energy peaks due to the HF component. These lead to more kinetic energy flow into the system, as can be seen from the integral diagram. This may allow more kinetic energy to be conserved in the system over time, which might favor alveolar opening.
The low frequency simulation was calculated for a longer period than the superimposed one. In the left image, the LF curve shows that the second positive peak is much smaller than the first. This effect is due to the step between the two pressure plateaus and the resulting different velocities. In the first ramp, the system ramps up from 0 Pa to 3000 Pa to simulate switching on the ventilator. After the first high pressure plateau, a PEEP level of 800 Pa is established. The second ramp thus goes up from 800 to 3000 Pa, reducing the resulting velocity. The negative peaks have the same magnitude, being larger than the second positive peak. This reduces the integral of the kinetic energy. Probably the system settles at certain values, but no definite statement can be made. This would require a longer simulation and a recalculation of the kinetic energy.

Figure 41 shows the kinetic energy curve for multiple generations during the simulation (upper) for one mean outlet on the one hand and for the sum of all outlets on the other hand. As expected, the kinetic energy of the sum of all outlets is larger than that of the single outlet. Most of the kinetic energy flowing into the lungs is during the inhalation phase for both diagrams. The proportion of high-frequency flow is also clearly visible in this curve due to the jagged profile. The amount of kinetic energy for the upper diagrams is between 0.2 and 400 $\mu$J. The mean kinetic energy runs according to the generations. It is highest in Gen1 and lowest in Gen8. The sum of the kinetic energy over all outlets shows a similar picture to the velocities in Figure 35. Gen2 and Gen3 have both the highest velocity and the highest kinetic energy. Gen1 has a high velocity, but the change in mass is much smaller, so even Gen4 has more kinetic energy. Gen8 again has the lowest kinetic energy.
During the pressure plateau, the high-frequency part of the kinetic energy can be seen in the bottom diagrams only for generation 8. The kinetic energy of the high frequency for a single outlet is in the range of 0.4 nJ and for the outlet sum up to 200 nJ.

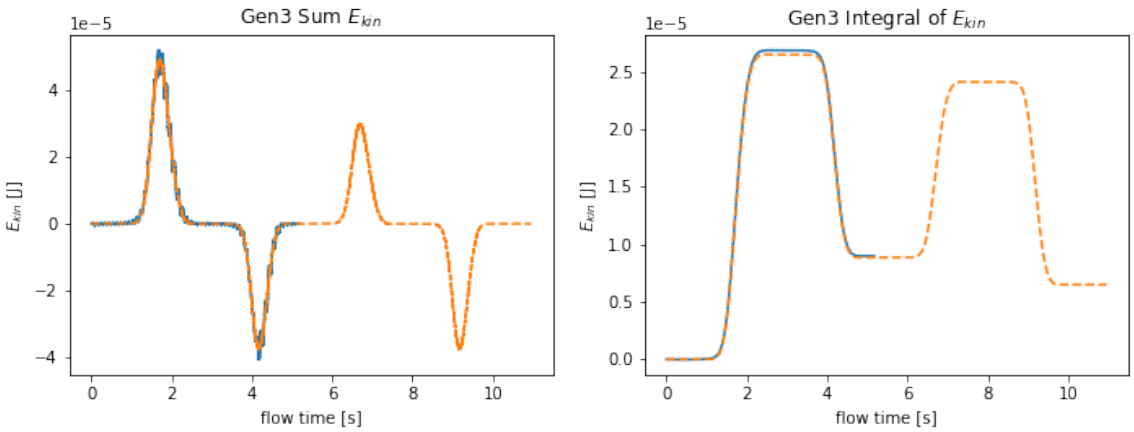


Figure 40: *The difference of the kinetic energy for low frequency (orange) and for the superimposed flow (blue) is shown for the sum of the kinetic energies and the integral of the energy. It becomes apparent that the additional high frequency jet leads to higher values of kinetic energy.*

### 4.2.2 High-frequency oscillatory ventilation

To compare superimposed high frequency jet ventilation with a second ventilation method, the UDF was reprogrammed to mimic high frequency oscillatory ventilation. A ramp was added at the beginning to simulate the machine ramping up. Then a mean airway pressure of 8cm $H_20$ (= 785 Pa) was set, around which the high frequency oscillation is imitated with a sinusoidal oscillation. The pressure profile as well as the velocity profile can be found in figure 42.

If the HF curves of the SHFJV and the HFOV are compared to each other in Fig. 43, it can be seen immediately that the SHFJV curve has faster velocity values. However, this is due to the programming of the curve, as in both cases the HF amplitude should be 5% of the maximum pressure. Since the pressure in the SHFJV is much greater at 3000 Pa than in the HFOV at 785 Pa, the pressure amplitude for the SHFJV is greater and higher velocities are obtained.
The splitting of the outlets can be seen as another distinguishing feature. These can be seen at the positive peak in the SHFJV (left) and not in the HFOV (right). Since the only difference in the programming of the two curves is the amplitude, the splitting is likely to occur only above a certain pressure amplitude.

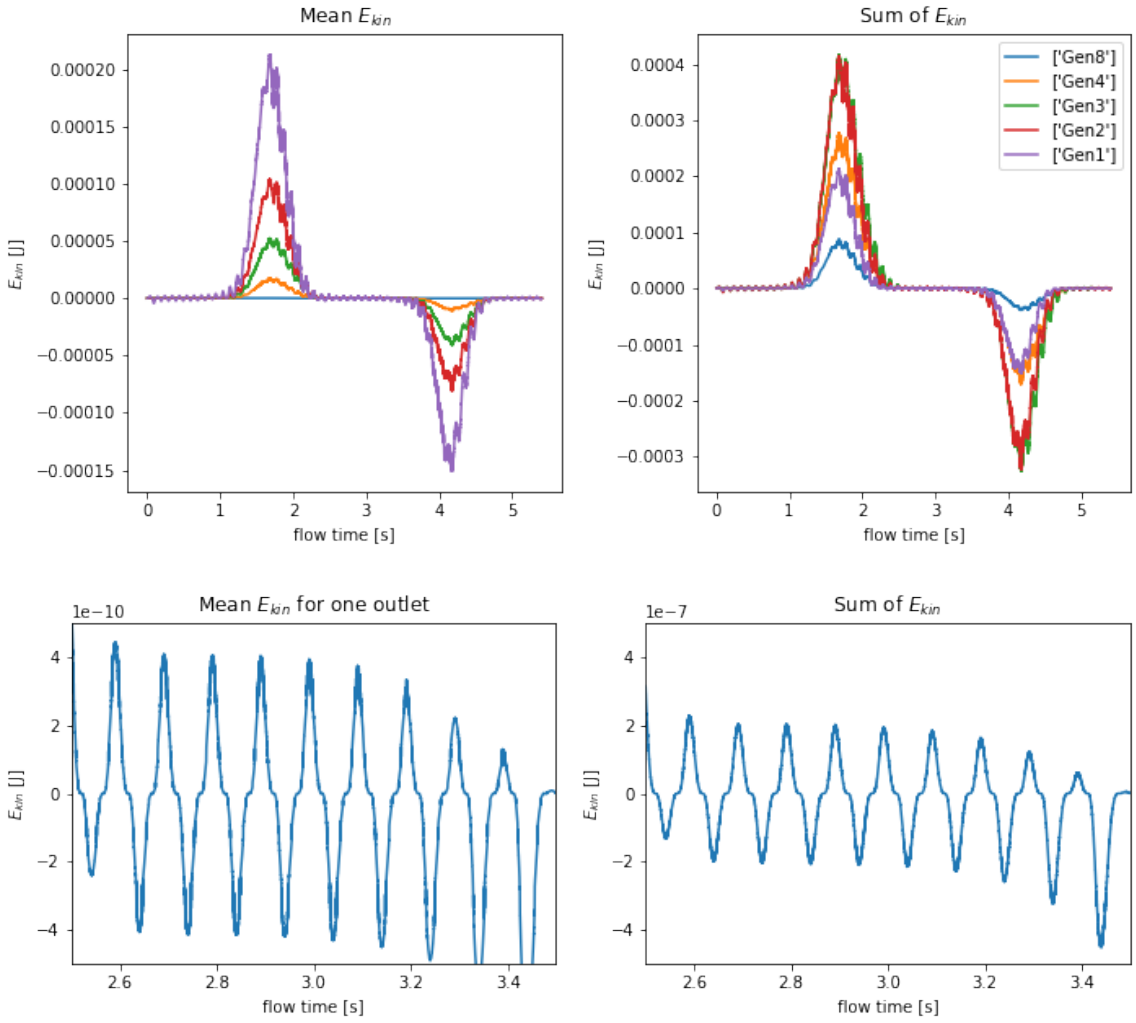


Figure 41: *Kinetic energy was calculated for both the individual outlet and the sum of all outlets for multiple generations. The top image shows the progression of kinetic energy over the entire simulation time for the single outlets (top left) and for the sum of all outlets (top right). In contrast, the lower images show the kinetic energy during the plateau phase only of generation 8.*

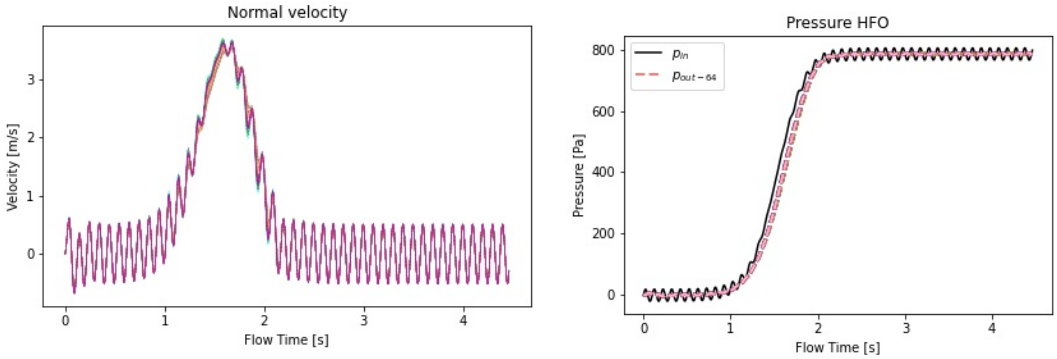


Figure 42: *For high-frequency oscillatory ventilation, the pressure curve was programmed to activate the system at the beginning and oscillate a high-frequency curve at 785 Pa. Thus, the velocity peaks as the pressure rises and then oscillates between -0.5 and 0.5.*

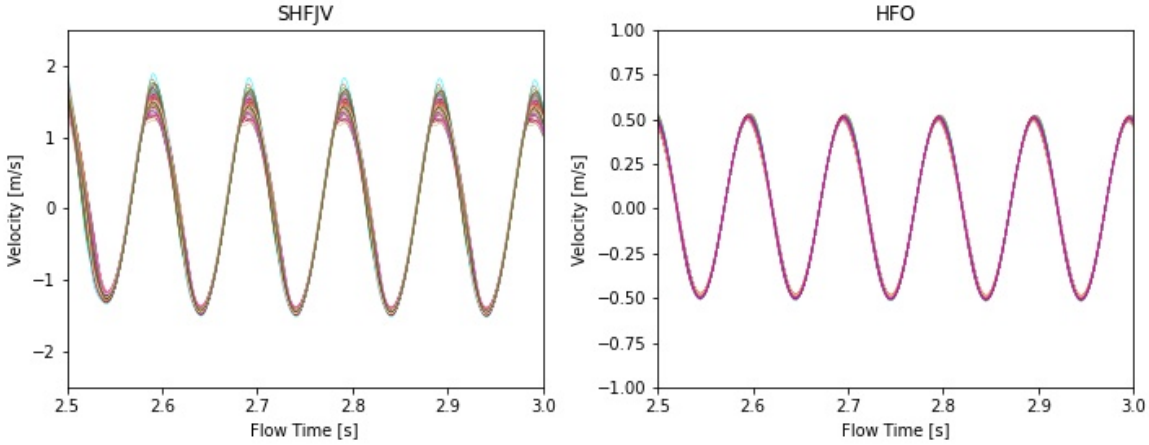


Figure 43: *These two plots show the high frequency curve during SHFJV and HFO. Since the mean airway pressure during HFO is lower than the pressure during SHFJV, the amplitude of the HF curve is different for both.*

### 4.2.3 Womersley number and tidal volume

In the case of lung diseases or conventional mechanical ventilation, the alveoli regularly collapse. As a result, oxygen exchange is only possible to a limited extent. The high-frequency component of SHFJV is intended to counteract this effect. One parameter who indicates the opening of the alveoli is the Womersley number $\alpha$. This is a dimensionless number composed of the frequency f in relation to the kinematic viscosity $\nu$ according to the formula 12. dt stands for the diameter of the tube. Bauer and Brücker [59] have shown in their study with a membrane bubble that a value greater than 10 in the trachea leads to the recrudescence of collapsed alveoli. A second parameter considered in this context is the tidal volume, equation 13, where $v_{max}$ is the maximum peak velocity, A the outlet area and f the frequency. Makris et al. [60] confirms in his paper that the tidal volume decreases as frequency increases.

$$\alpha = \frac{d_t}{2} * \sqrt{\frac{2 * \pi * f}{\nu_f}} \tag{12}$$

$$V_T = \frac{v_{max} * A}{\pi * f} \tag{13}$$

All calculated quantities are summarized in table 12. Several information can be derived from the values. It can be seen that the Womersley number decreases significantly in deeper lung areas, as it is related to the tube diameter. Since frequency also enters into the formula, it is reasonable that the number is much lower at low frequency than at high frequency. Ventilation frequency is considered an important parameter for alveolar recruitment. [59]
The kinematic viscosity is a temperature-dependent variable. Although it has been shown in Figure 32 that no difference in velocity is seen when the temperature and thus the air density is changed, it still has a small effect on the Womersley number. At 10 °C temperature difference, there is a deviation in the first decimal number.
The tidal volume of the high frequency part of the SHFJV has a value of 55 mL at the inlet in the trachea which corresponds to that of the HFOV. [61, 62] Again, it can be seen that along the bronchial tree the tidal volume decreases progressively, so that in the $8^{th}$ generation only 0.1 mL is present.

Table 12 *Summary of Womersley number and tidal volume for LF and HF for the main simulation geometries.*

| Name | Diameter | Womersley NF | | Womersley HF | | Tidal volume |
|---|---|---|---|---|---|---|
| | [mm] | T=15 °C | T=25 °C | T=15 °C | T=25 °C | HF [mL] |
| Gen0 | 18 | 2.4021 | 2.3259 | 18.6069 | 18.0160 | 55.1745 |
| Gen1 | 12.2 | 1.6281 | 1.5764 | 12.6113 | 12.2109 | 23.3138 |
| Gen2 | 8.3 | 1.1077 | 1.0725 | 8.5798 | 8.3074 | 10.4346 |
| Gen3 | 5.6 | 0.7473 | 0.7236 | 5.7888 | 5.6050 | 5.30570 |
| Gen4 | 4.5 | 0.6005 | 0.5815 | 4.6517 | 4.5040 | 2.54071 |
| Gen8 | 1.86 | 0.2482 | 0.2403 | 1.9227 | 1.8617 | 0.1443 |

### 4.2.4 Graphical evaluation of Gen8 simulations

In the following, the flows in the Generation 8 bifurcation geometry are represented by pathlines. Representations of the velocity magnitude, the static pressure as well as the turbulent kinetic energy were chosen. The explanation of the color coding of the pictures can be taken from the legend in each image. Three different simulations were made with the Generation 8 geometry. One had a compliance of 0.2 $\frac{L}{cmH_2O}$, the next a compliance of 0.02 $\frac{L}{cmH_2O}$ and during the third simulation one eighth of the lungs outlets had a worse compliance than the rest. To see larger effects in the lungs, the images during inspiration (at 1.5 seconds) and during expiration (at 4.2 seconds) are evaluated and compared.

Figure 44 and 45 show the course of static pressure for inspiration and expiration. With good compliance of 0.2 $\frac{L}{cmH_2O}$, Fig. 44 top, the lung is very elastic which leads to a larger variability of static pressure. In the trachea, pressures of about 1.18 kPa are reached while in generation 8 about 0.78 kPa are present. It can be seen that the pressure at each branching between the two new branches is higher than in other locations. The highest values are obtained at the first branch division from the trachea (Gen0) to Gen1. This is due to the fact that the highest pressures generally prevail in the middle of the trachea and the flow splits at this point. The lowest pressure is always at the edge just prior to the next branch. It is also noticeable that the pressure loss is highest up to the $3^{rd}$ generation. From the this generation on, only a small local pressure difference can be seen. Since the flow takes the path of least resistance, the branches that run straighter than the others have higher static pressures.

The lower image of the same figure shows the same lung system with a poor compliance of 0.02 $\frac{L}{cmH_2O}$. Although the inlet pressure of the trachea is similar to that of the upper lung,

the color coding shows a difference of only 40 Pa. Thus, it can be clearly seen that due to a stiff lung only little pressure change can occur.

During expiration, Figure 45, the pressure from the lobes of the lungs is returned to the trachea. Thus, the pressure is highest at the end of Gen8. The legend shows that with good compliance, the static pressure in the thin tubes is greater than it was in the thicker tubes during inspiration. The largest pressure drop in this direction is between the sixth and the third generation. When the airflow from two branches is merged into one, there is another local increase in pressure, which is slightly broader than in the opposite direction.
In reality, the alveoli do not collapse in the entire lung but in individual areas. This should be imitated with this experiment of partially stiff lung branches. Due to the two axes of symmetry in the geometry, the pulmonary branches were also mirrored, which is why both the right and the left lung are affected. The air flow can not distribute regularly due to locally stiff branches. The neighboring branches of the stiff ones exhibit less static pressure as branches where all the outlets have the same compliance. Until generation 5, the stiff areas show a constant pressure of about 1.40 kJ. From there back to the trachea no further differences can be seen.

Figure 46 shows the magnitude of velocity for a flexible lung as well as a lung with partially stiff branches during inspiration. For the elastic lung (upper image), velocities are higher in the middle of the tube than near the wall. As indicated in earlier velocity figures, the velocity between Gen2 and Gen4 is higher than in the other regions. The highest velocities are seen along the tube between two branching areas on the side facing to the other branch. At this point the air jets hit the tube after splitting. Since there is less turbulence along the tube the flows do not reduce each other by overlapping. This effect can be seen on the outside of the tube of the branching region. Since the walls in the lung geometry were defined as rigid, the reduction in velocity is mainly due to flow effects. The slowest value can be seen in the $8^{th}$ generation.
In the lower image, it can be seen that there is no flow in the stiffer branches, marked with dark blue. It is not until generation 6 that a slight flow begins to occur. In addition, it can be observed that stiffer areas have also an effect on the velocities of the neighboring branches and the higher positioned branches. In generation 5 and 4, faster velocities can already be seen who lead to the affected branches, but these values are still lower than in branches at the same level with good compliance. This picture clearly shows that the flow travels to where there is the least resistance.

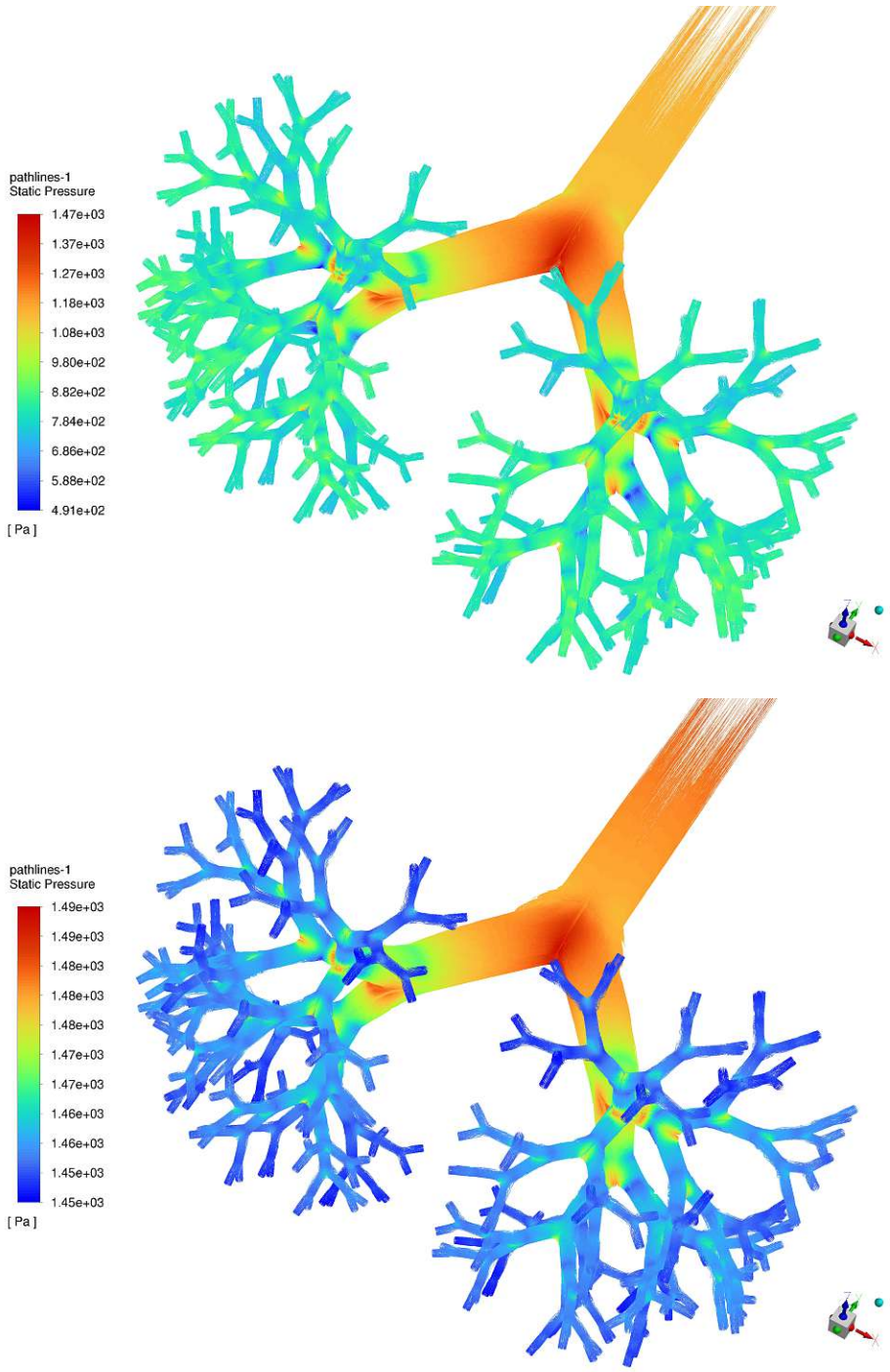


Figure 44: *These images show the static pressure at a flow time of 1.5 seconds in the pulmonary branches at a good compliance of 0.2* $\frac{L}{cmH_2O}$ *(top) and at a poor compliance of 0.02* $\frac{L}{cmH_2O}$ *(bottom). It can be seen, that the static pressure varies in the flexible lung, but stays rather constant in a stiff lung.*

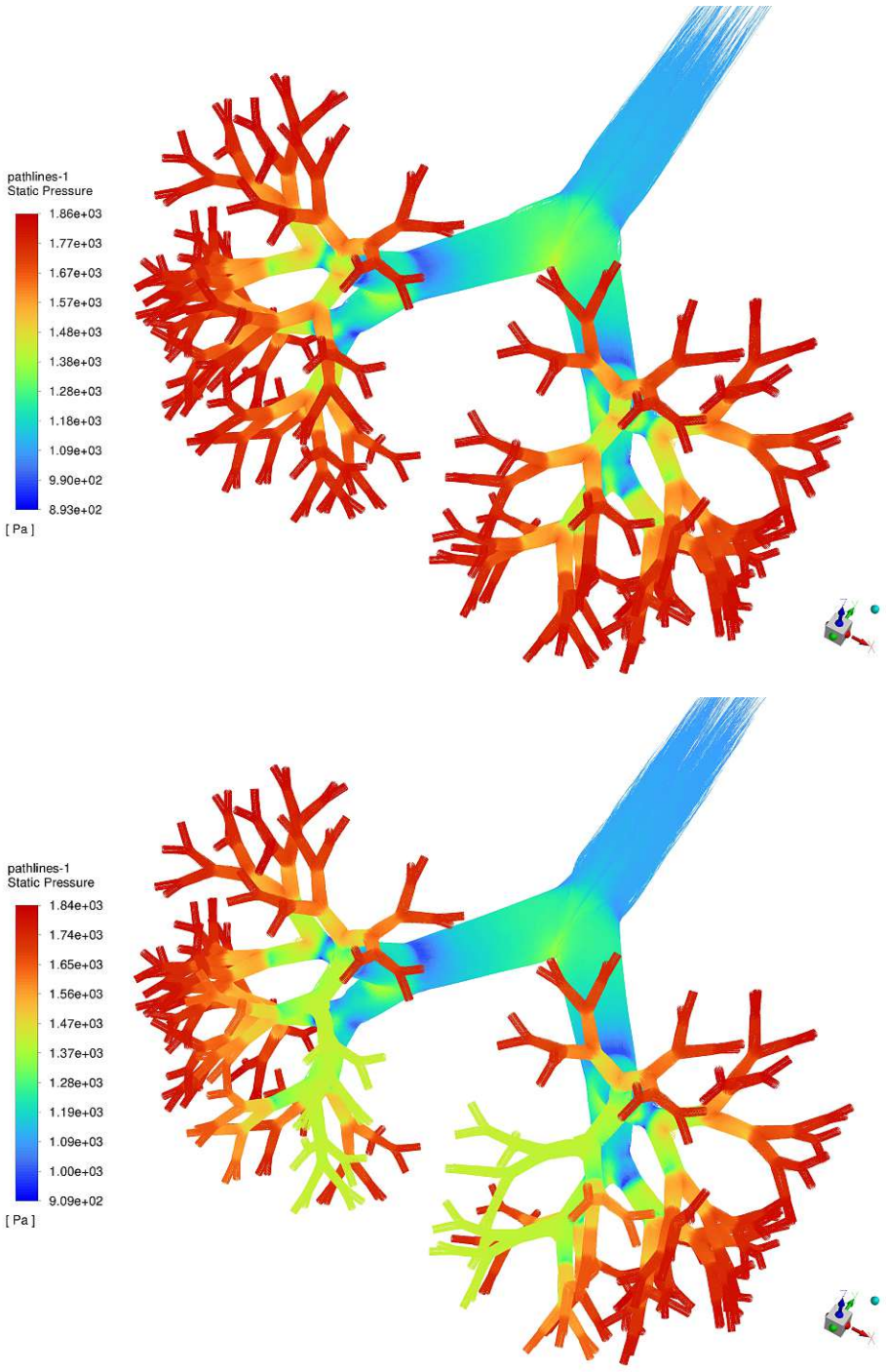


Figure 45: *During expiration (at 4.2 s), the air flows from the lobes of the lung back to the trachea. As a result, the pressure in the outer lung branches is higher. The pressure profile of an elastic lung is shown at the top and one with partially stiff branches at the bottom.*

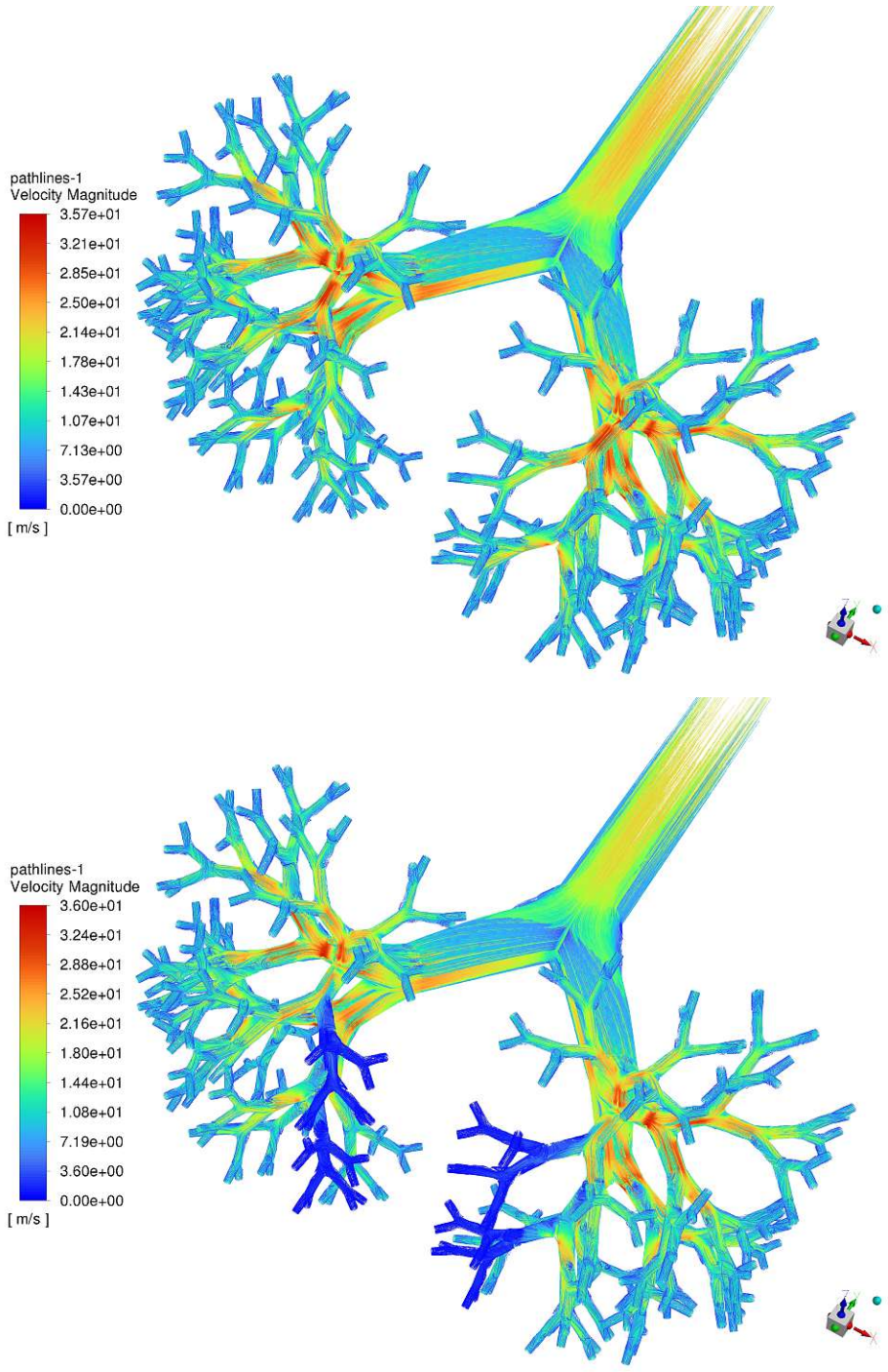


Figure 46: *The magnitude of velocity for a flexible lung (C=0.2 $\frac{L}{cmH_2O}$, top) and a lung with partially stiff branches (bottom) during inspiration is depicted. Generally slow velocities are seen near the wall and fast velocities are seen in the middle of the tube. In the stiff branches, however, there is no air flow.*

The turbulent kinetic energy shows those areas, where the mixing of velocities occurs. An elastic lung is again compared to a stiff lung, as for the static pressure, Fig. 44. The upper image shows a lung with C = 0.2 $\frac{L}{cmH_2O}$ and the lower one a lung with C = 0.02 $\frac{L}{cmH_2O}$, both during expiration. It can be seen that during exhalation in a flexible lung the highest turbulent kinetic energy occurs between the first and fourth generation. It is also good to see that local energy maxima occur at the edge of the tube. In a stiff lung, the areas of velocity mixing shift mainly to Gen1 or into the trachea. In deeper lung areas the turbulent kinetic energy is negligible small. This indicates that the compliance shifts the turbulence along the lung branches.

In high-frequency oscillatory ventilation, there is only one major pressure ramp. After that, the curve oscillates around 785 Pa. The upper image in Fig. 48 shows a very similar picture to Fig. 46. However, the velocities are reduced by approx. 40 % due to the lower pressure. After 4.2 seconds only high frequency oscillation effects can be seen at the HFOV, in the lower figure. At this point, the high frequency curve is close to its maximum and thus air flows into the lungs also in this figure. It can be seen immediately that the number of slow areas have increased, especially at the edge of the tube. It looks as if the higher velocities are to be found in the interior of the tube and above all between $4^{th}$ and $6^{th}$ generation. However, a legend comparison between the two figures shows that the maximum velocity is now only 2 m/s instead of 13 m/s.

To further observe the pathlines of the flows, detailed images were taken with a reduced number of lines in Figure 49 and 50. Both of them show again the inspiration, thus the gas flow into the lungs for the lungs with two different compliances. That branch with the darkes shade of blue in the turbulent kinetic energy graph, Fig. 49, is one with higher compliance. It can be seen that turbulences occur rather in the branches to the right, which are less strongly distributed to the previous generations. Furthermore, it can be seen that the turbulent kinetic energy is highest between Gen3 and Gen5 and higher near the wall regions. The deeper the branches are positioned in the lung, the more eddies the pathlines make.
When mapping the velocity magnitude in detail, Fig. 50, eddies can be seen on the surface near branches. However, these locations have only slow velocities. The highest velocities are on the inside of the leg of the daughter branches and just before the division of the gas flow. It can also be seen that the branches that are more bent across the branches have slower velocities than those that are less bent.

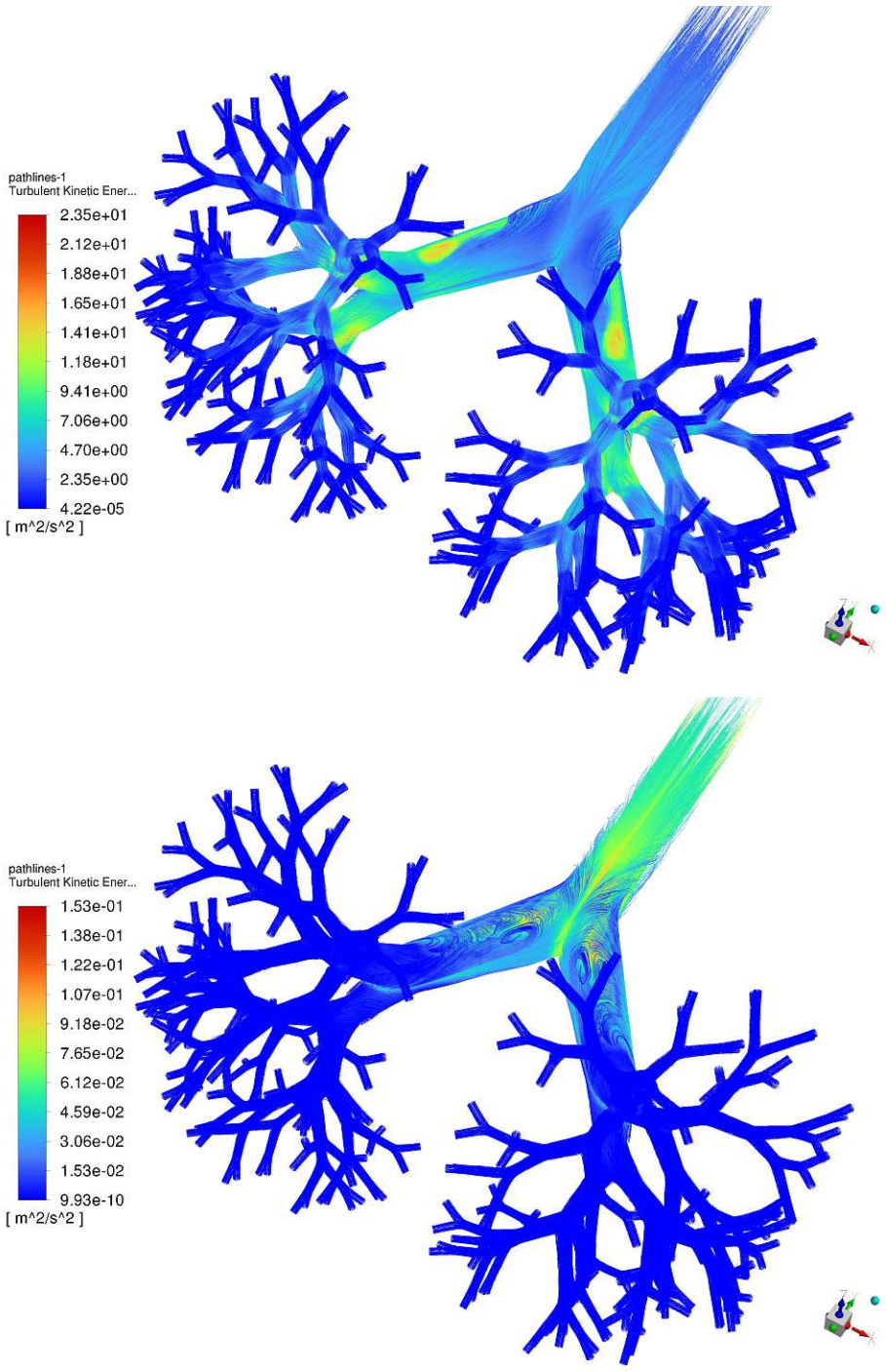


Figure 47: *The upper image shows the turbulent kinetic energy at a compliance of 0.2* $\frac{L}{cmH_2O}$ *and the lower image that during expiration at a compliance of 0.02* $\frac{L}{cmH_2O}$.

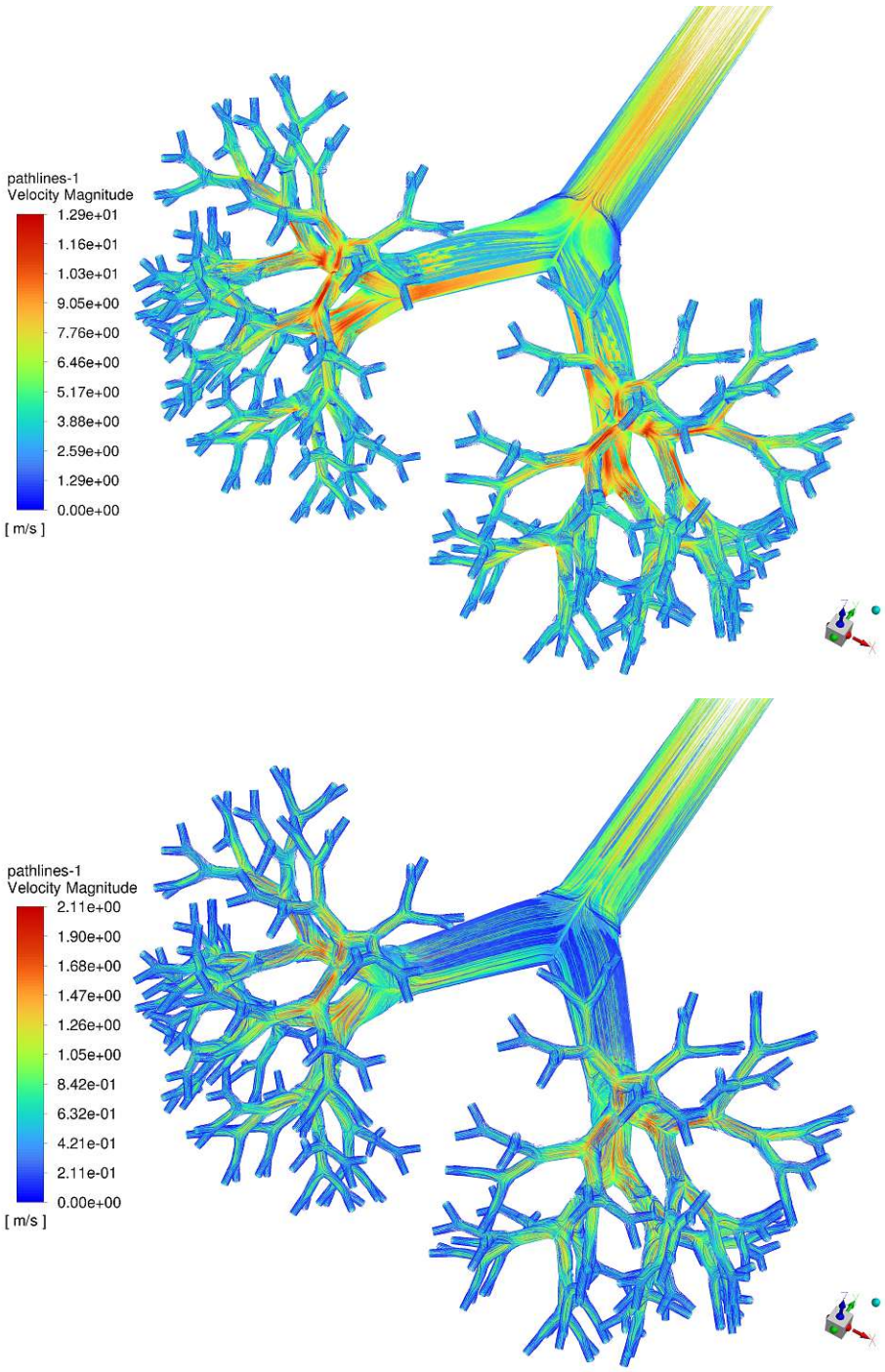


Figure 48: *During Inspiration at 1.5 s the high frequency oscillation image (upper) shows a similarities to the upper image of Fig. 46, but with lower velocities due to the reduced inlet pressure of 785 Pa. At 4.2 s (lower), on the other hand, only slight velocity variations can be seen due to the oscillation of the high frequency.*

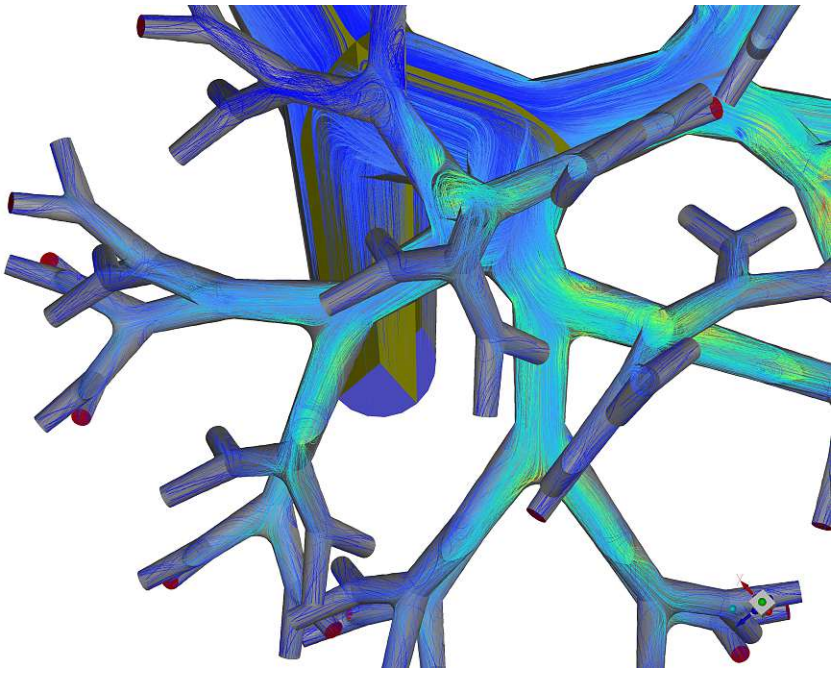

Figure 49: *Detailed view of turbulent kinetic energy with partially stiff branches during inspiration. Between Gen3 and Gen5 most of the turbulence occur near the wall.*

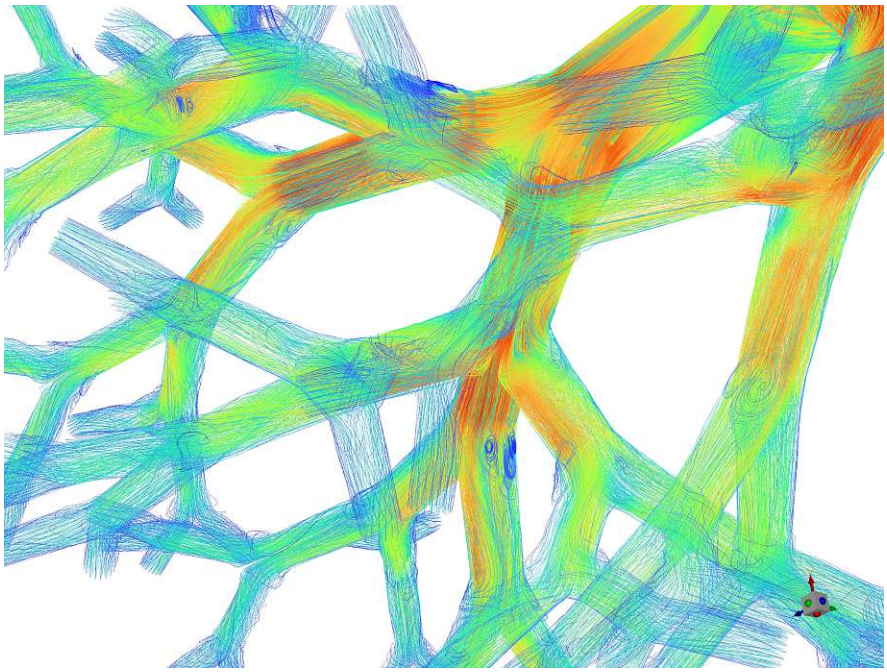

Figure 50: *Detailed view of velocity magnitude with partially stiff branches during inspiration. The highest velocity can be seen at the inside of the daughter's leg.*

### 4.2.5 Discussion of main simulations

Because the simulations for this study were limited in time and scope, the various lung geometries were created and the simulations were run with them. This allows estimates of velocities in deeper lung regions to be made based on multi-generation results and area ratios, as done in Fig. 36. According to this calculation, a maximum velocity of 0.23 m/s is present in the $17^{th}$ generation during inspiration. At this velocity, a Reynolds number of 245 is obtained, which clearly shows that laminar flow is present in this region. With the given parameters in chapter 4, a critical Reynolds number is reached at a velocity of 1.9 m/s, which indicates the transition between laminar and turbulent flow. This value is reached approximately between the 12th and 13th generation during the first velocity peak.

Since the preliminary tests showed that the curve kept repeating uniformly for inspiration and expiration, the simulations were mostly stopped after about 5s. However, it was realized very late that the pressure difference with a PEEP level is much smaller than the first ramp and thus the velocity of the second inspiration peak has lower values than the first one. In diagram of the comparison between low frequency and the super imposed flow, figure 40 it is clear that the second peak in positive direction is also lower for the kinetic energy. The difference between the two kinetic energy peaks is about 40 %. The normal velocity has a deviation of about 15 % and the deviation of the magnitude of velocity for the expiration peak and the second inspiration peak is down to 7 %. Consequently, the results shown in this thesis are the maximum inspiration values for a pressure difference of 3000 Pa.

Choi et al. [63] has already established in his study that kinetic energy is a key parameter for differences in airway resistance. However, in that study, the kinetic energy coefficient was calculated based on the pressure difference, while here the kinetic energy was calculated using the mass and normal velocity. There is a suggestion that kinetic energy is the driving force for alveolar opening, but there are no accurate studies on this yet. Based on the Reynolds number, a quasi-steady state is assumed in the alveolar region. However, Li and Kleinstreuer [64] doubt this theory because they observed scattered streamline patterns in their study. Presumably the kinetic energy induces these streamlines.

High-frequency oscillatory ventilation has already been studied by many research groups. [19, 60, 61]. This ventilation method is considered efficient for opening the alveoli. Bauer and Brücker [59] showed that the opening of stiffer membranes positioned at the distal end

of a lung model, which were designed to mimic collapsed alveoli, was possible at higher frequencies. The Womersley number for higher frequencies is larger as shown in table 12 and also higher velocities are being induced thereof, which is important to keep the alveoli open. Since comparable frequencies are set in superimposed high-frequency jet ventilation, this indicates that this method also leads to better opening of the alveoli. The only difference found when comparing the two methods was even higher velocities with SHFJV but since both ventilation methods were programmed with the same frequency, the same Womersley number is obtained for HFOV and SHFJV.

Among the experiments with different compliance, the most interesting are those in which individual branches show worsened compliance as in Figure 45, 46, 49 and 50. It can be clearly seen that the flow of the affected branches, but also that of the neighboring branches, are varied. As compliance is reduced, the pressure at the affected branches increases. This creates a counterpressure during inspiration, which makes it more difficult for the airflow to reach these areas. Depending on the magnitude of this pressure, more or less back generations are affected. In that generation, in this case Gen5, where a healthy and a diseased branch meet, the flow is slowed down by the back pressure and also less air flows into the healthy neighboring branches. This effect can be seen well in figure 45 and 46.

# 5 Conclusion

In this thesis, the flow behavior generated by a superimposed high-frequency jet ventilator was investigated in several symmetrical single-bifurcation geometries with up to eight generations using a computer fluid dynamic simulation. The focus was on mapping the flows that occur during SHFJ ventilation for the first time and taking into account the influence of compliance on the flow patterns in the lung model. The experiments showed that poorer lung compliance causes higher pressure in the lungs, making them inflexible. If only local areas are affected by deterioration, this also has an impact on the healthy neighboring areas.

In addition, the influence of kinetic energy was considered. It was shown that, compared to conventional low-frequency ventilation, the kinetic energy is higher with superimposed high-frequency jet ventilation. Furthermore, it was found that the kinetic energy is lower in deeper lung areas.

In order to evaluate the ventilation method against an already well researched method, the behavior of a high-frequency oscillatory ventilation was simulated and compared to the SHFJV. It was shown that higher velocities result at the same ventilation frequency.

To be able to perform further simulations in deeper lung areas, a possible approach for the future would be to map only a single branch. This would reduce the number of mesh cells which would also result in shorter simulation times. However, it must be kept in mind that a resistance is set at each outlet that remains free in order to imitate the theoretical branch systems that is attached to it. This can be done, for example, with the help of a porous membrane.

By creating a geometry without a symmetry axis, an asymmetric compliance could be set in another experiment, which on the one hand is more in line with reality and on the other hand probably better clarifies the flow effects.

Another interesting approach for further studies would be to adjust the system so that the reset pressure is not linear, but includes an inertia term. This would dampen the flow in the lungs, making the simulation more realistic.

In the simulations, which were carried out in this work, a compromise between computation

time and computation accuracy was made. At a flow of 25 m/s, the flow travels a distance of 25 m in one second. If a time step of $8 * 10^{-5}$ s is used, as it was done in this work for the large calculations, this means that 125000 time steps per second are needed. From this results that a time step covers a distance of 2 mm. Since the mesh of the lung geometry was finer, this can cause problems for the simulator. Thus, in a further step, the calculation could be verified with a smaller time step, which, however, would result in significantly longer computation times.

# References

[1] Tài Pham, Laurent J. Brochard, and Arthur S. Slutsky. Mechanical ventilation: State of the art. *Mayo Clinic Proceedings*, 92(9):1382–1400, 2017. ISSN 0025-6196. doi: https://doi.org/10.1016/j.mayocp.2017.05.004. URL `https://www.sciencedirect.com/science/article/pii/S0025619617303245`.

[2] Paul L. Marino, Götz Geldner, and Tilmann (Eds.) Müller-Wolff. *Das ICU-Buch. Praktische Intensivmedizin*. Urban & Fischer, 5th edition edition, 2017. ISBN 9783437170324; 3437170325. URL `libgen.li/file.php?md5=6afc7e2871cb762649f5d18e285062e8`.

[3] Alexander Aloy. *Moderne Beatmungstechniken in der Intensivmedizin*. Scriptum TU Wien, 2020. URL `https://www.aloy.at/wp-content/uploads/2021/01/Scriptum-TU-Wien-2019.pdf`.

[4] Alexander Aloy, Simon Hell, Andreas Nowak, and Matthaeus Grasl. Cfd analysis of flow characteristics in a jet laryngoscope and the different application forms of superimposed jet ventilation. In Serdar Küçük and Abdullah Erdem Canda, editors, *Medical Robotics*, chapter 2. IntechOpen, Rijeka, 2020. doi: 10.5772/intechopen.85535. URL `https://doi.org/10.5772/intechopen.85535`.

[5] Rüdiger Schwarze. *CFD-Modellierung*. Springer-Verlag, 2013. ISBN 978-3-642-24377-6. doi: https://doi.org/10.1007/978-3-642-24378-3.

[6] Fotis Sotiropoulos. Computational fluid dynamics for medical device design and evaluation: Are we there yet? *Cardiovascular Engineering and Technology*, 3(2):137–138, 2012. doi: https://doi.org/10.1007/s13239-012-0095-5.

[7] Georg Kleiser. Einführung in die strömungslehre. `https://d-nb.info/1143711688/34`, 2017. Accessed: 2022-04-26.

[8] Wolfgang Kümmel. *Technische Strömungsmechanik*. Teubner Verlag, 2007. ISBN 978-3-8351-0141-8.

[9] Reza Tabe, Roohollah Rafee, Mohammad Sadegh Valipour, and Goodarz Ahmadi. Investigation of airflow at different activity conditions in a realistic model of human upper res-

piratory tract. *Computer Methods in Biomechanics and Biomedical Engineering*, 24(2): 173–187, 2021. doi: 10.1080/10255842.2020.1819256. URL https://www.tandfonline.com/doi/epub/10.1080/10255842.2020.1819256?needAccess=true. PMID: 32940084.

[10] Andrew Davies and Carl Moores. *Atmungssystem*. Organsysteme verstehen. Urban und Fischer in Elsevier, 2017. ISBN 978-3-437-41257-8.

[11] Andres L. Mora Carpio and Jorge I. Mora. *Ventilator Management*. StatPearls Publishing, 2022.

[12] Ewald Weibel and D.M. Gomez. Architecture of the human lung. *Science*, 137:577–585, 01 1962.

[13] U. Koehler, O. Hildebrandt, N. Koehler, and K. Sohrabi. Are small airways the key to understanding pathophysiology and treatment efficacy in chronic obstructive pulmonary diseases? *Pneumologie*, 72:790–796, 2018. ISSN 0934-8387. doi: 10.1055/a-0707-5826. URL https://www.thieme-connect.com/products/ejournals/pdf/10.1055/a-0707-5826.pdf.

[14] John R. Fitz-Clarke. Mechanics of airway and alveolar collapse in human breath-hold diving. *Respiratory Physiology & Neurobiology*, 159(2):202–210, 2007. ISSN 1569-9048. doi: https://doi.org/10.1016/j.resp.2007.07.006. URL https://www.sciencedirect.com/science/article/pii/S1569904807002078.

[15] Biljana Drašković and Goran Rakić. Complications of mechanical ventilation. *Srpski arhiv za celokupno lekarstvo*, 139(9-10):685–692, 2011. doi: https://doi.org/10.2298/sarh1110685d.

[16] Göran Hedenstierna. Alveolar collapse and closure of airways: regular effects of anaesthesia. *Clinical Physiology and Functional Imaging*, 23(3):123–129, 2003. doi: https://doi.org/10.1046/j.1475-097X.2003.00483.x.

[17] Marcin Karcz, Alisa Vitkus, Peter J. Papadakos, David Schwaiberger, and Burkhard Lachmann. State-of-the-art mechanical ventilation. *Journal of Cardiothoracic and Vascular Anesthesia*, 26(3):486–506, 2012. ISSN 1053-0770. doi: https://doi.org/10.1053/j.jvca.2011.03.010. URL https://www.sciencedirect.com/science/article/pii/S1053077011001364.

[18] Thomas Bein and Ulrich von Hintzenstern. *Praxisbuch Beatmung*. Urban & Fischer, 6. auflage edition, 2015. ISBN 9783437234132; 3437234137; 9783437187315; 3437187317. URL libgen.li/file.php?md5=b65d10be8483dfae4fefd73ba3a61201.

[19] Jiwoong Choi, Guohua Xia, Merryn H Tawhai, Eric A Hoffman, and Ching-Long Lin. Numerical study of high-frequency oscillatory air flow and convective mixing in a ct-based human airway model. *Annals of biomedical engineering*, 38(12):3550–3571, 2010. doi: 10.1007/s10439-010-0110-7.

[20] Sujen K. Kunugiyama and Christine S. Schulman. High-frequency percussive ventilation using the vdr-4 ventilator: an effective strategy for patients with refractory hypoxemia. *AACN advanced critical care*, 23(4):370–380, 2012. doi: https://doi.org/10.1097/NCI.0b013e31826e9031. URL https://pubmed.ncbi.nlm.nih.gov/23095962/.

[21] Yu-Xiong Guo, Zhao-Ni Wang, Ya-Ting Li, Li Pan, Li-Fen Yang, Yan Hu, Yue-Yu Sun, Liang-Ming Cai, and Zhuang-Gui Chen. High-frequency oscillatory ventilation is an effective treatment for severe pediatric acute respiratory distress syndrome with refractory hypoxemia. *Therapeutics and clinical risk management*, 12, 2016. doi: doi:10.2147/TCRM.S115884.

[22] U Lucangelo, L Fontanesi, V Antonaglia, T Pellis, G Berlot, G Liguori, F M Bird, and A Gullo. High frequency percussive ventilation (hfpv). principles and technique. *Minerva anestesiologica*, 69(11):841–851, 2003.

[23] Ivan Wong, Berhane Worku, Jeremy A. Weingarten, Alexander Ivanov, Feli Khusid, Ashwa Afzal, Robert F. Tranbaugh, and Iosif Gulkarov. High-frequency percussive ventilation in cardiac surgery patients. *Interactive cardiovascular and thoracic surgery*, 25 (6):937–941, 2017. ISSN 0761-8425. doi: https://doi.org/10.1093/icvts/ivx237. URL https://pubmed.ncbi.nlm.nih.gov/29049534/.

[24] Duncan Young, Sarah E. Lamb, Sanjoy Shah, Iain MacKenzie, William Tunnicliffe, Ranjit Lall, Kathy Rowan, and Brian H. Cuthbertson. High-frequency oscillation for acute respiratory distress syndrome. *New England Journal of Medicine*, 368(9):806–813, 2013. doi: 10.1056/NEJMoa1215716. URL https://doi.org/10.1056/NEJMoa1215716. PMID: 23339638.

[25] David N Hager, Jerry A Krishnan, Douglas L Hayden, and Roy G Brower. Tidal

volume reduction in patients with acute lung injury when plateau pressures are not high. *American journal of respiratory and critical care medicine*, 172(10), 2005. doi: 10.1164/rccm.200501-048CP.

[26] N. González-Pacheco, M. Sánchez-Luna, C. Ramos-Navarro, N. Navarro-Patiño, and A R-S de la Blanca. Using very high frequencies with very low lung volumes during high-frequency oscillatory ventilation to protect the immature lung. a pilot study. *Journal of Perinatology*, 36(4), 2016. doi: https://doi.org/10.1038/jp.2015.197.

[27] Henry E Fessler, Stephen Derdak, Niall D Ferguson, David N Hager, Robert M Kacmarek, B Taylor Thompson, and Roy G Brower. A protocol for high-frequency oscillatory ventilation in adults: results from a roundtable discussion. *Critical care medicine*, 35, 2007. doi: 0.1097/01.CCM.0000269026.40739.2E.

[28] Anatoliy Korzhuk, Ashwad Afzal, Ivan Wong, Felix Khusid, Berhane Worku, and Iosif Gulkarov. High-frequency percussive ventilation rescue therapy in morbidly obese patients failing conventional mechanical ventilation. *Journal of intensive care medicine*, 35(6):583–587, 2020. doi: https://doi.org/10.1177/0885066618769596. URL `https://pubmed.ncbi.nlm.nih.gov/29683055/`.

[29] Courtney M Rowan, Ashley Loomis, Jennifer McArthur, Lincoln S Smith, Shira J Gertz, Julie C Fitzgerald, Mara E Nitu, Elizabeth As Moser, Deyin D Hsing, Christine N Duncan, Kris M Mahadeo, Jerelyn Moffet, Mark W Hall, Emily L Pinos, Robert F Tamburro, and Ira M Cheifetz. High-frequency oscillatory ventilation use and severe pediatric ards in the pediatric hematopoietic cell transplant recipient. *Respiratory care*, 63(4), 2018. doi: 10.4187/respcare.05765.

[30] Daniel S. Tawfik, Tellen D. Bennett, Brent Welch, and W. Bradley Poss. Use of high-frequency ventilation in the pediatric intensive care unit. *Journal of pediatric intensive care*, 5(1):12–20, 2016. doi: https://doi.org/10.1055/s-0035-1568160. URL `https://pubmed.ncbi.nlm.nih.gov/31110877/`.

[31] H. K. Chang. Mechanisms of gas transport during ventilation by high-frequency oscillation. *Journal of applied physiology: respiratory, environmental and exercise physiology*, 56(3):553–563, 1984. doi: https://doi.org/10.1007/s00134-003-1828-6. URL `https://pubmed.ncbi.nlm.nih.gov/11056732/`.

[32] Martin A. Nagels and John E. Cater. Large eddy simulation of high frequency oscillating flow in an asymmetric branching airway model. *Medical Engineering & Physics*, 31(9):1148–1153, 2009. ISSN 1350-4533. doi: https://doi.org/10.1016/j.medengphy.2009.07.013. URL https://www.sciencedirect.com/science/article/pii/S135045330900157X.

[33] Paul Kraincuk, Günther Körmöczi, Mathias Prokop, Gerald Ihra, and Alexander Aloy. Alveolar recruitment of atelectasis under combined high-frequency jet ventilation: a computed tomography study. *Intensive care medicine*, 29(8):1265–1272, 2003. doi: https://doi.org/10.1007/s00134-003-1828-6. URL http://www.ncbi.nlm.nih.gov/pubmed/12879246.

[34] R. Sütterlin, R. Priori, A. Larsson, A. LoMauro, P. Frykholm, and A. Aliverti. Frequency dependence of lung volume changes during superimposed high-frequency jet ventilation and high-frequency jet ventilation. *British Journal of Anaesthesia*, 112 (1):141–149, 2014. ISSN 0007-0912. doi: https://doi.org/10.1093/bja/aet260. URL https://www.sciencedirect.com/science/article/pii/S0007091217319803.

[35] S. Sehati, J.D. Young, M.K. Sykes, and C.N. McLeod. Monitoring of end-tidal carbon dioxide partial pressure during high frequency jet ventilation. *British Journal of Anaesthesia*, 63(7, Supplement 1):47S–52S, 1989. ISSN 0007-0912. doi: https://doi.org/10.1093/bja/63.7.47. URL https://www.sciencedirect.com/science/article/pii/S0007091217499387.

[36] P. Kraincuk, A. Kepka, G. Ihra, C. Schabernig, and A. Aloy. A new prototype of an electronic jet-ventilator and its humidification system. *Critical care (London, England)*, 3(4):101–110, 1999. doi: https://doi.org/10.1186/cc351. URL https://pubmed.ncbi.nlm.nih.gov/11056732/.

[37] G. Riffard and M. Toussaint. Indications de la ventilation à percussions intrapulmonaires (vpi) : revue de la littérature. *Revue des Maladies Respiratoires*, 29(2):178–190, 2012. ISSN 0761-8425. doi: https://doi.org/10.1016/j.rmr.2011.12.005. URL https://www.sciencedirect.com/science/article/pii/S0761842511015609.

[38] P. F. Allan, J. R. Thurlby, and G. A. Naworol. Measurement of pulsatile tidal volume, pressure amplitude, and gas flow during high-frequency percussive ventilation,

with and without partial cuff deflation. *Respiratory care*, 52(1):45–49, 2007. URL https://pubmed.ncbi.nlm.nih.gov/17194317/.

[39] Margaret Starnes-Roubaud, Elizabeth A. Bales, Alex Williams-Resnick, Philip D. Lumb, Joe A. Escudero, Linda S. Chan, and Warren L. Garner. High frequency percussive ventilation and low fio(2). *Burns : journal of the International Society for Burn Injuries*, 38(7):984–991, 2012. doi: https://doi.org/10.1016/j.burns.2012.05.026. URL https://pubmed.ncbi.nlm.nih.gov/22766403/.

[40] Kevin K. Chung, Steven E. Wolf, Evan M. Renz, Patrick F. Allan, James K. Aden, Gerald A. Merrill, Mehdi C. Shelhamer, Booker T. King, Christopher E. White, David G. Bell, Martin G. Schwacha, Sandra M. Wanek, Charles E. Wade, John B. Holcomb, Lorne H. Blackbourne, and Leopoldo C. Cancio. High-frequency percussive ventilation and low tidal volume ventilation in burns: a randomized controlled trial. *Critical care medicine*, 38(10):1970–1977, 2010. doi: https://doi.org/10.1097/CCM.0b013e3181eb9d0b. URL https://pubmed.ncbi.nlm.nih.gov/20639746/.

[41] Thomas Godet, Matthieu Jabaudon, Raïko Blondonnet, Aymeric Tremblay, Jules Audard, Benjamin Rieu, Bruno Pereira, Jean-Marc Garcier, Emmanuel Futier, and Jean-Michel Constantin. High frequency percussive ventilation increases alveolar recruitment in early acute respiratory distress syndrome: an experimental, physiological and ct scan study. *Critical care (London, England)*, 22(1):3, 2018. doi: https://doi.org/10.1186/s13054-017-1924-6. URL https://pubmed.ncbi.nlm.nih.gov/29325586/.

[42] Sergey P. Marchenko, Ecaterina Scarlatescu, Paul Robert Vogt, Alexey Naumov, and Sergey Bognenko. Intermittent high-frequency percussive ventilation therapy in 3 patients with severe covid-19 pneumonia. *The American journal of case reports*, 22:e928421, 2021. doi: https://doi.org/10.12659/AJCR.928421. URL https://pubmed.ncbi.nlm.nih.gov/33542171/.

[43] E. Schragl, A. Donner, A. Kashanipour, and A. Ullrich, R.and Aloy. Superponierte hochfrequenz jetventilation (shfjv) unter verwendung von no. *Der Anaesthesist*, 44:843–849, 1995. doi: https://doi.org/10.1007/s001010050220.

[44] Thomas Luecke, Peter Herrmann, Paul Kraincuk, and Paolo Pelosi. Computed tomography scan assessment of lung volume and recruitment during high-frequency oscillatory

ventilation. *Critical care medicine*, 33:155–162, 2005. doi: 10.1097/01.ccm.0000155916.47455.df.

[45] R. Leiter, A. Aliverti, R. Priori, P. Staun, A. Lo Mauro, A. Larsson, and P. Frykholm. Comparison of superimposed high-frequency jet ventilation with conventional jet ventilation for laryngeal surgery. *British Journal of Anaesthesia*, 108(4):690–697, 2012. ISSN 0007-0912. doi: https://doi.org/10.1093/bja/aer460. URL `https://www.sciencedirect.com/science/article/pii/S0007091217322791`.

[46] Stefan Lecheler. *Numerische Strömungsberechnung*. Springer Vieweg Wiesbaden, 2014. ISBN 978-3-658-05201-0. doi: https://doi.org/10.1007/978-3-658-05201-0.

[47] Herbert Oertel jr., Martin Böhle, and Thomas Reviol. *Numerische Strömungsberechnung*. Springer Vieweg+Teubner Verlag, 2014. ISBN 978-3-658-07785-3. doi: https://doi.org/10.1007/978-3-658-07786-0.

[48] ANSYS Inc. *UDF Manual*, 2009.

[49] D. Wenger. Luft. `https://stoffdaten-online.de/fluide/luft/`, 2019. Accessed: 2022-04-28.

[50] Bela Soni and Shahrouz Aliabadi. Large-scale cfd simulations of airflow and particle deposition in lung airway. *Computers & Fluids*, 88:804–812, 2013. ISSN 0045-7930. doi: https://doi.org/10.1016/j.compfluid.2013.06.015. URL `https://www.sciencedirect.com/science/article/pii/S0045793013002387`.

[51] G Jagan and Gopalakrishnan Jayalalitha. Fractal approach to identify airways of lungs using weibel's model. *Journal of interdisciplinary cycle research*, XI:556–564, 11 2019.

[52] ANSYS Inc. `https://www.ansys.com/academic/students/ansys-student`, 2022. Accessed: 2022-06-07.

[53] Carl Reiner. *Bedienungsanleitung-TwinStream™ ICU*. Carl Reiner GmbH, 2020.

[54] Kenichiro Atsumi, Yoshinobu Saito, Toru Tanaka, Takeru Kashiwada, Hiroki Hayashi, Koichiro Kamio, Masahiro Seike, Rie Osaki, Kazuhiro Sakai, Shinya Kurosawa, Akihiko Gemma, and Arata Azuma. A possible, non-invasive method of measuring dynamic

lung compliance in patients with interstitial lung disease using photoplethysmography. *Journal of Nippon Medical School = Nippon Ika Daigaku zasshi*, 88(4):326–334, 2021. doi: https://doi.org/10.1272/jnms.JNMS.2021_88-411. URL https://www.sciencedirect.com/science/article/pii/S0025619617303245.

[55] Bruce A Koeppen, Bruce M.;Stanton. *Berne & Levy physiology*. Elsevier, 7th ed edition, 2018. ISBN 9780323393942; 0323393942; 9780323443388; 0323443389. URL libgen.li/file.php?md5=ce8b19b0a494b721a83c040b52a12566.

[56] P.G. Koullapis, P. Hofemeier, J. Sznitman, and S.C. Kassinos. An efficient computational fluid-particle dynamics method to predict deposition in a simplified approximation of the deep lung. *European Journal of Pharmaceutical Sciences*, 113:132–144, 2018. ISSN 0928-0987. doi: https://doi.org/10.1016/j.ejps.2017.09.016. URL https://www.sciencedirect.com/science/article/pii/S0928098717305080. A special issue dedicated to COST Action SimInhale: cross-disciplinary perspective on the current state of the art and challenges in pulmonary drug delivery.

[57] ANSYS Inc. *User's Guide*, 2010.

[58] W.M. Faizal, N.N.N. Ghazali, C.Y. Khor, Irfan Anjum Badruddin, M.Z. Zainon, Aznijar Ahmad Yazid, Norliza Binti Ibrahim, and Roziana Mohd Razi. Computational fluid dynamics modelling of human upper airway: A review. *Computer Methods and Programs in Biomedicine*, 196:105627, 2020. ISSN 0169-2607. doi: https://doi.org/10.1016/j.cmpb.2020.105627. URL https://www.sciencedirect.com/science/article/pii/S0169260720314607.

[59] K. Bauer and Ch. Brücker. The role of ventilation frequency in airway reopening. *Journal of Biomechanics*, 42(8):1108–1113, 2009. doi: 10.1016/j.jbiomech.2009.02.018.

[60] Evangelos Makris, Marika Pilou, Panagiotis Neofytou, Sokrates Tsangaris, and Christos Housiadas. Particle transport and deposition under high-frequency oscillatory ventilation and normal breathing. *Aerosol Science and Technology*, 48(2):150–162, 2014. doi: 10.1080/02786826.2013.865831. URL https://doi.org/10.1080/02786826.2013.865831.

[61] Mohammed Alzahrany, Arindam Banerjee, and Gary Salzman. Flow transport and gas mixing during invasive high frequency oscillatory ventilation. *Medical Engineering & Physics*, 36, 06 2014. doi: 10.1016/j.medengphy.2014.01.010.

[62] Bing Han, Hiroyuki Hirahara, and Sho Yoshizaki. Streaming caused by oscillatory flow in peripheral airways of human lung. *Open Journal of Fluid Dynamics*, 06:242–261, 01 2016. doi: 10.4236/ojfd.2016.63019.

[63] Sanghun Choi, Jiwoong Choi, and Ching-Long Lin. Contributions of kinetic energy and viscous dissipation to airway resistance in pulmonary inspiratory and expiratory airflows in successive symmetric airway models with various bifurcation angles. *Journal of Biomechanical Engineering*, 140, 10 2017. doi: 10.1115/1.4038163.

[64] Z Li and C Kleinstreuer. Airflow analysis in the alveolar region using the lattice-boltzmann method. *Medical & biological engineering & computing*, 49(4):441–451, 2011. doi: 10.1007/s11517-011-0743-1.